Cross-scale coupling of Heliophysics Systems
L'Aquila, 12-16 May 2025

Marco Romoli
Dip. di Fisica e Astronomia
Università di Firenze, Italy

Overview of remote sensing instruments

from space

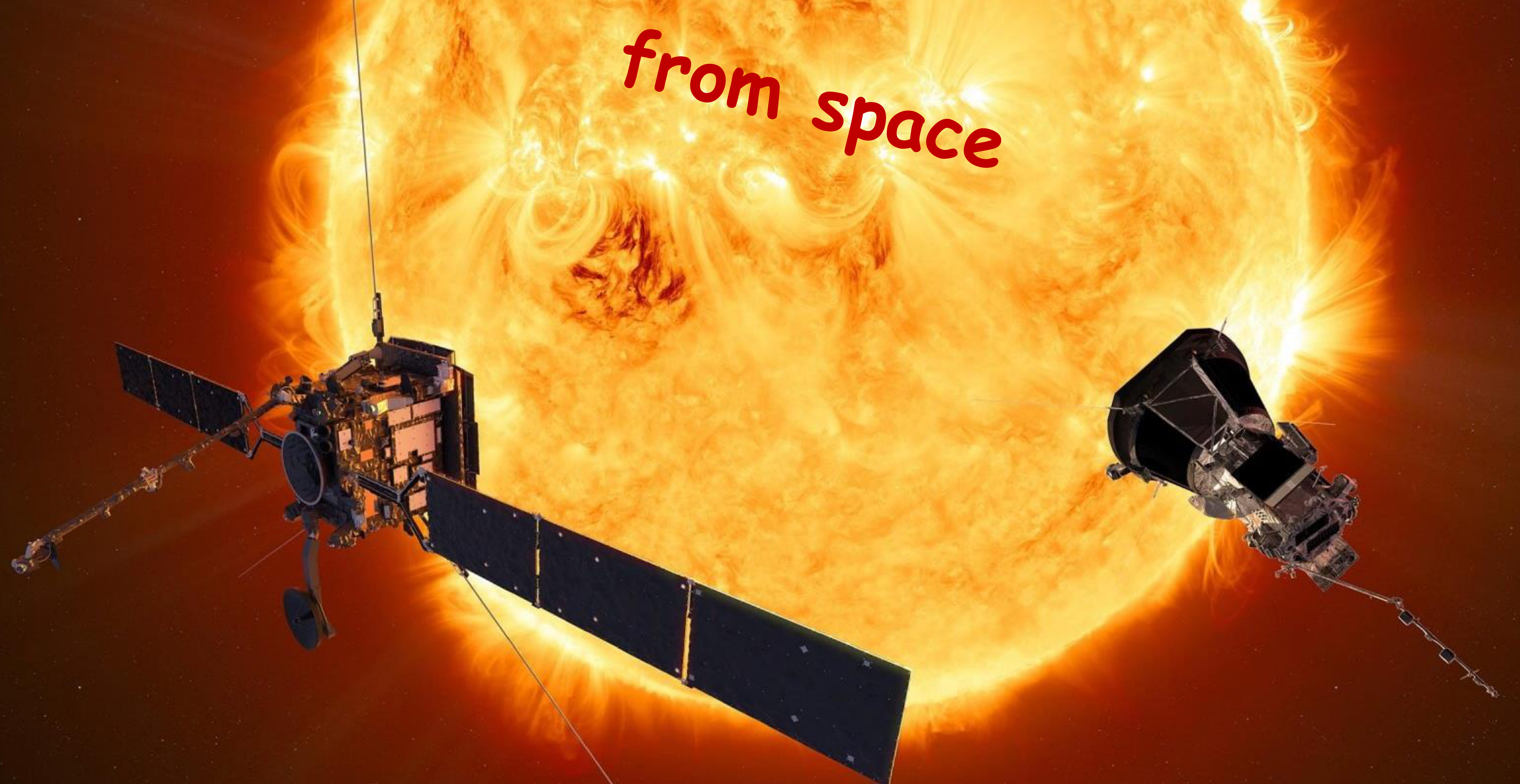

CONSORZIO AREA DI RICERCA IN ASTROGEOFISICA

“We need to be as bold and visionary with our future space missions, in order to acquire the observations that will tell us how nature really works”

Matina Gkioulidou

Summary

- Observing the Sun and the heliosphere today, big questions in solar physics
- Why space based solar observatories?
- Overview of present missions
- The multi-messanger (multi-point of view) decade
- Representative examples of remote sensing instrumentation
- The future

Answering the big questions of solar physics

#1: How and where do the solar wind plasma and magnetic field originate?

Disentangling spatial structures and time evolution requires viewing a given region for more than an active region growth time (~ 10 days)

→ So we need to go closer to the Sun

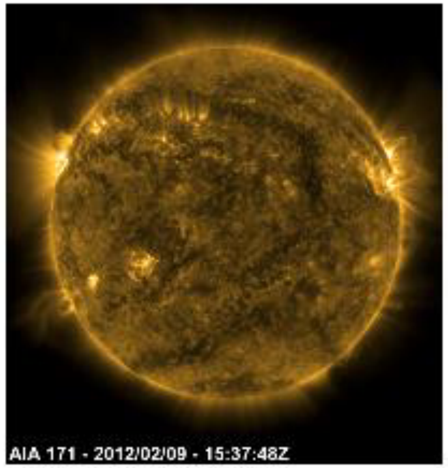

#2: How do solar transients drive heliospheric variability?

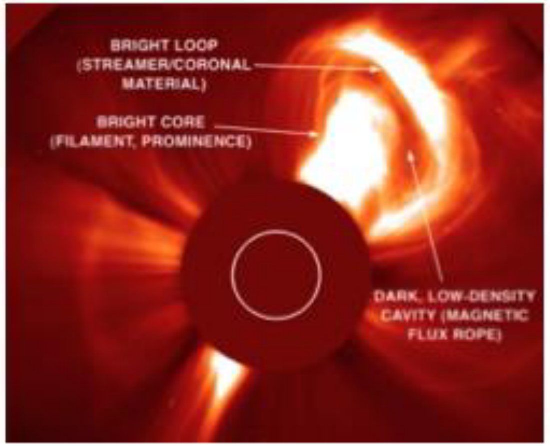

#3: How do solar eruptions produce energetic particle radiation that fills the heliosphere?

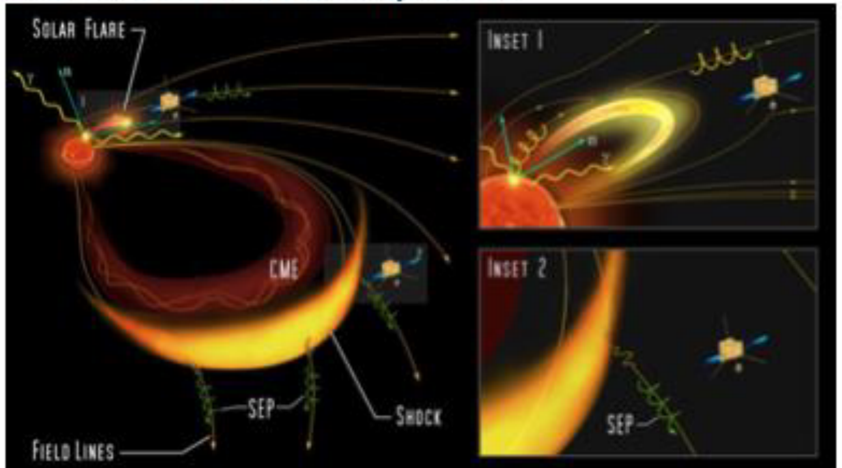

#4: How does the solar dynamo work and drive connections between the Sun and the heliosphere?

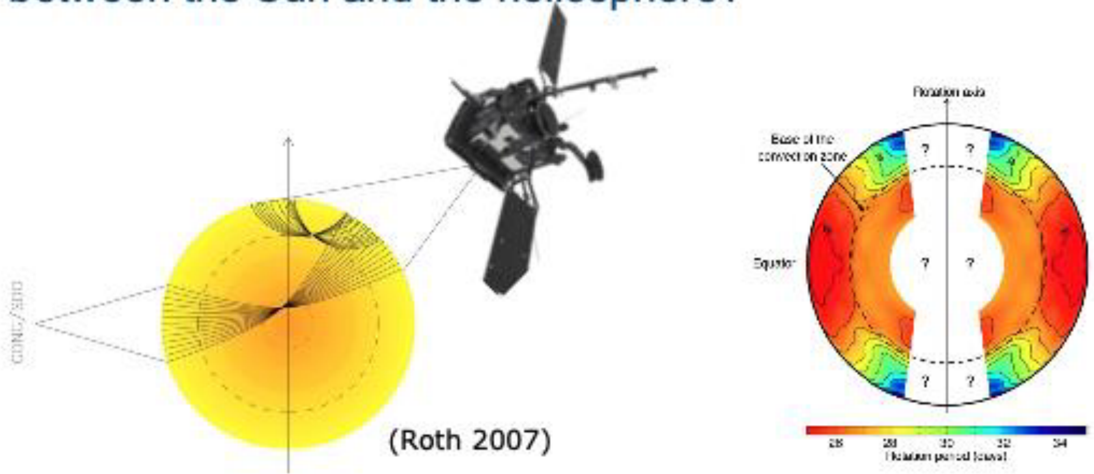

(Roth 2007)

First glimpse of the Sun from space (1946)

- After WWII, captured V2 rockets provided a means for sending scientific instruments above the earth's atmosphere which absorbed UV radiation.
- To study the nature of the atmospheric absorption, and to examine the UV portion of the solar spectrum, a group of the Naval Research Laboratory (NRL), led by Richard Tousey designed a UV solar spectrograph to fly on the V2 warheads.
- The first successful NRL rocket flight was on October 10, 1946. The missile reached an altitude of 173 km and a series of spectra obtained during ascent showed the decrease in UV absorption with altitude and helped set the upper limit to the earth's ozone layer (*Baum+, 1946)*



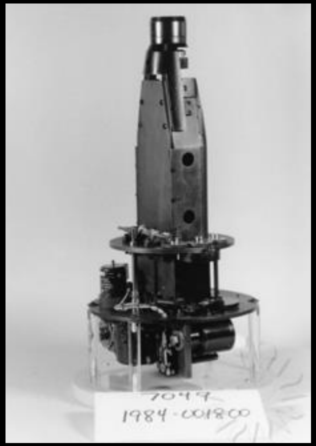

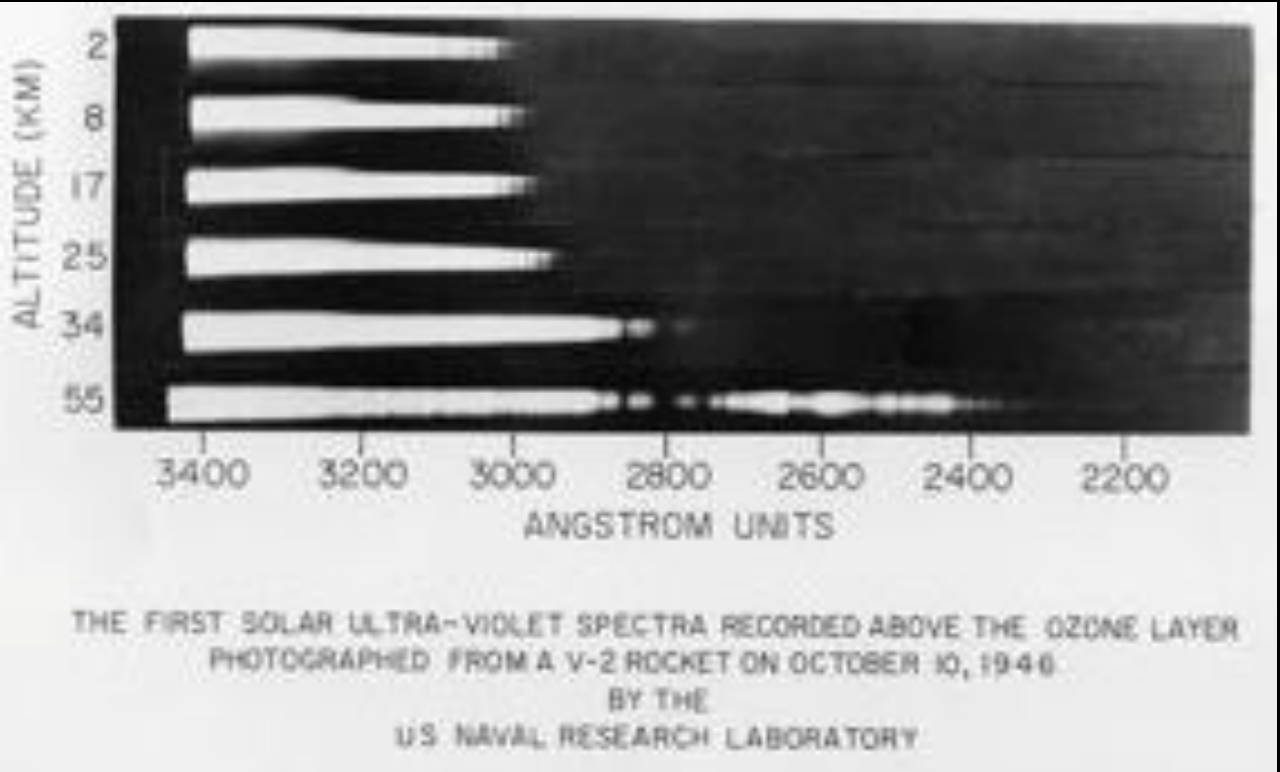

How to observe the Sun

✓ Inner:
Neutrinos, Helioseismology

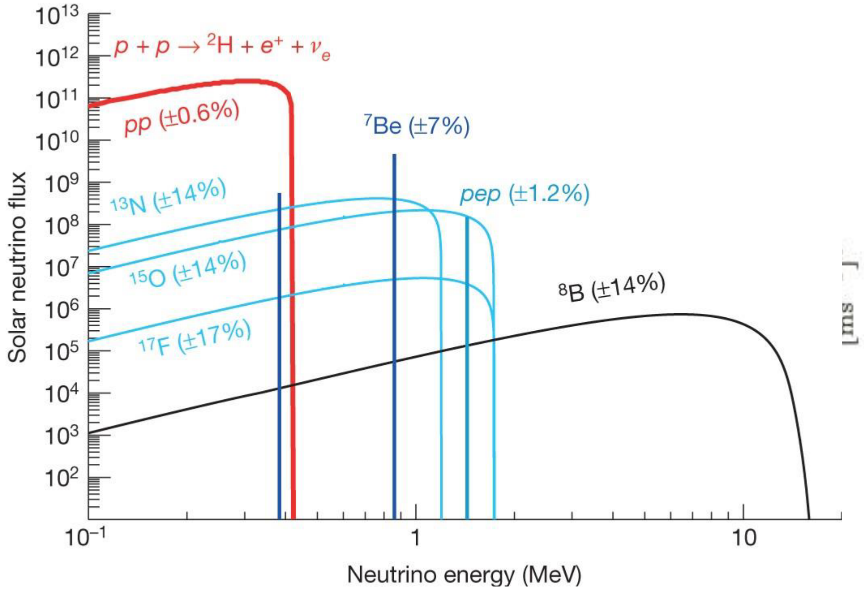

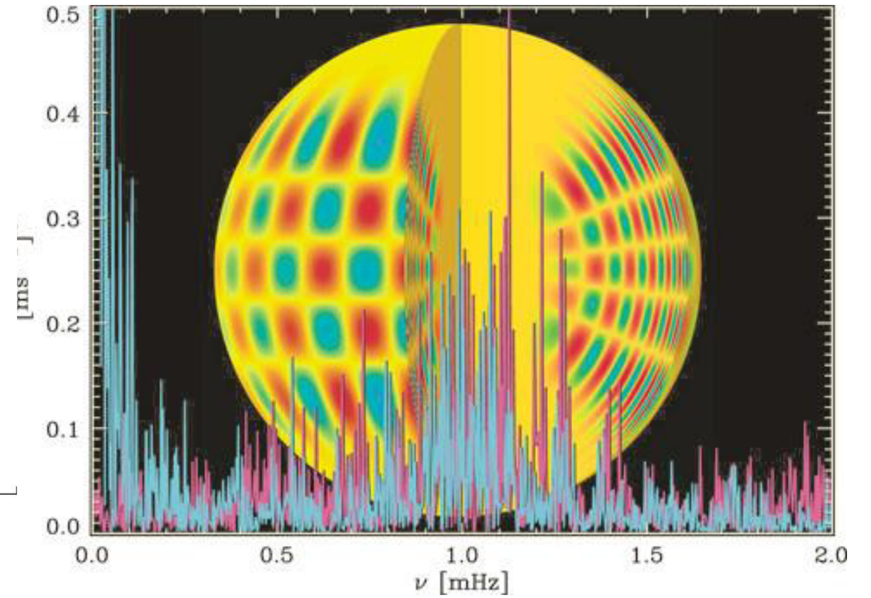

✓ Photosphere and Atmosphere: Remote sensing

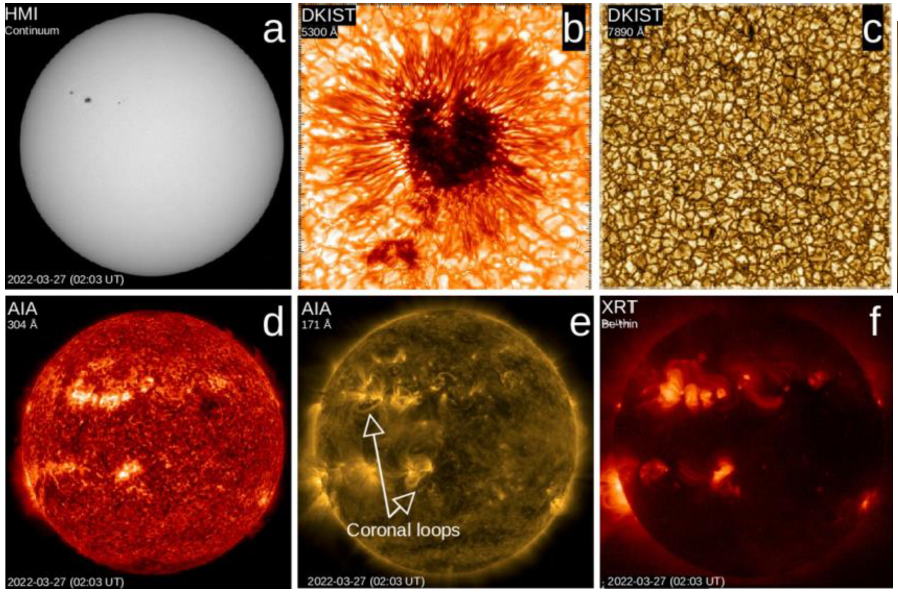

✓ Heliosphere:
"in situ" instrumentation

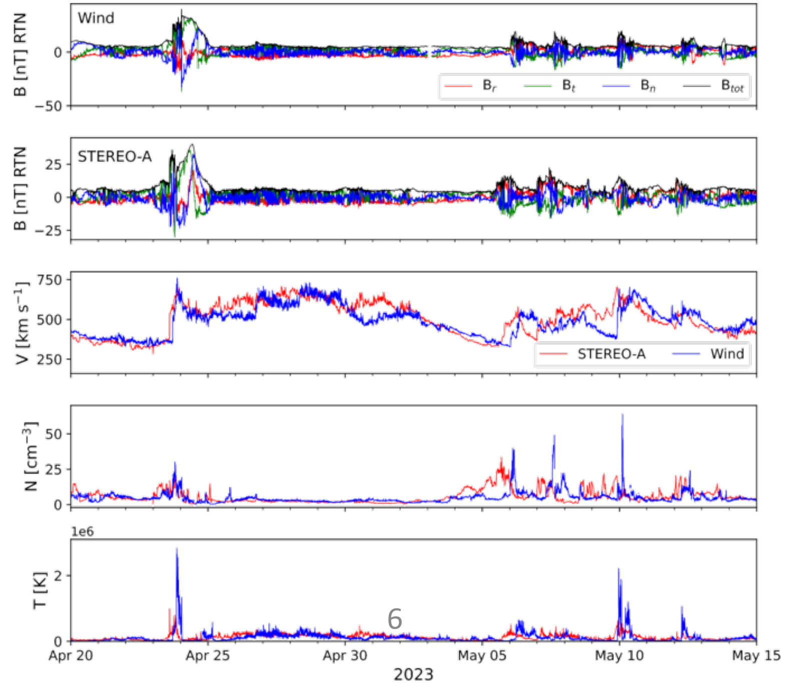

Why from space?

- ✓ Above the atmosphere
  - ✓ UV, X, and γ observations (atmospheric absorption)
  - ✓ Solar corona (sky brightness)
- ✓ Outside the magnetosphere
  - ✓ in situ measurements
- ✓ Uninterrupted observations
  - ✓ Helioseismology
- ✓ Out of ecliptic
  - ✓ Polar imaging
  - ✓ polar wind and CR behavior

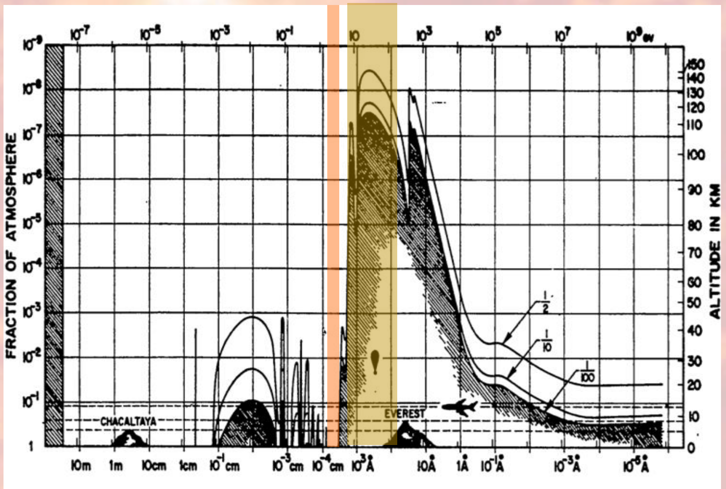

Giacconi, Gursky & van Speybroeck (1968)

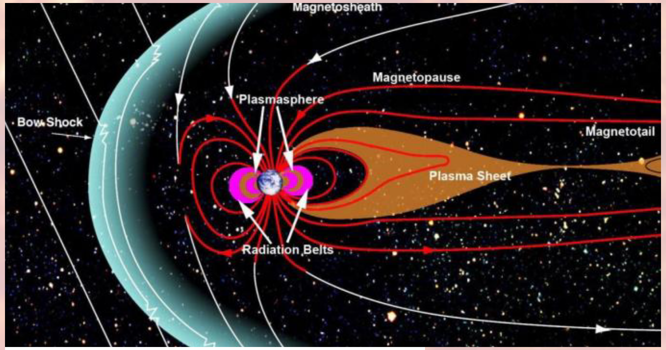

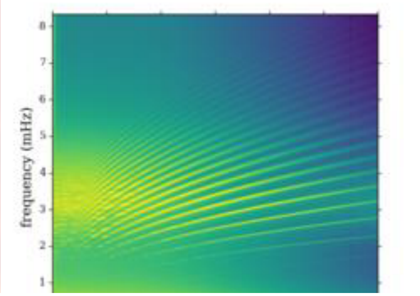

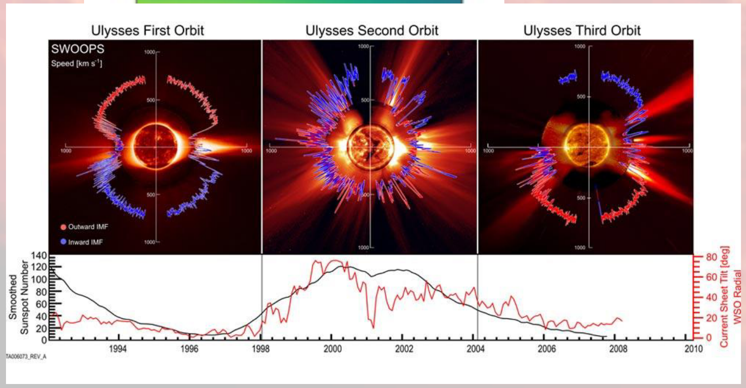

The multi-messanger decade for solar physics

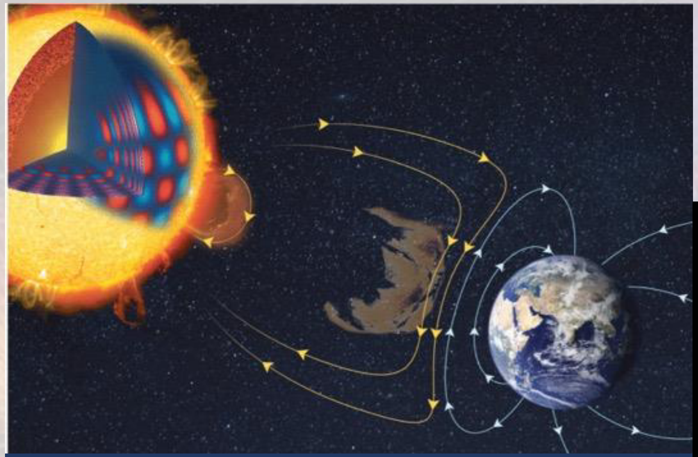
How stars and planets are ......

......magnetically connected

- Ulysses:
  Particles + Magnetic field
- Present days:
  EM radiation + Particles + Magnetic and electric fields
- Multi-point-of-view and multi-wavelength:
  - Ground based (DKIST, etc.)
  - Earth orbit (SOHO, SDO, IRIS, ASO-S, ADITYA-L1)
  - Interplanetary (STEREO-A, PSP, Solar Orbiter)

The multi-messanger decade for solar physics

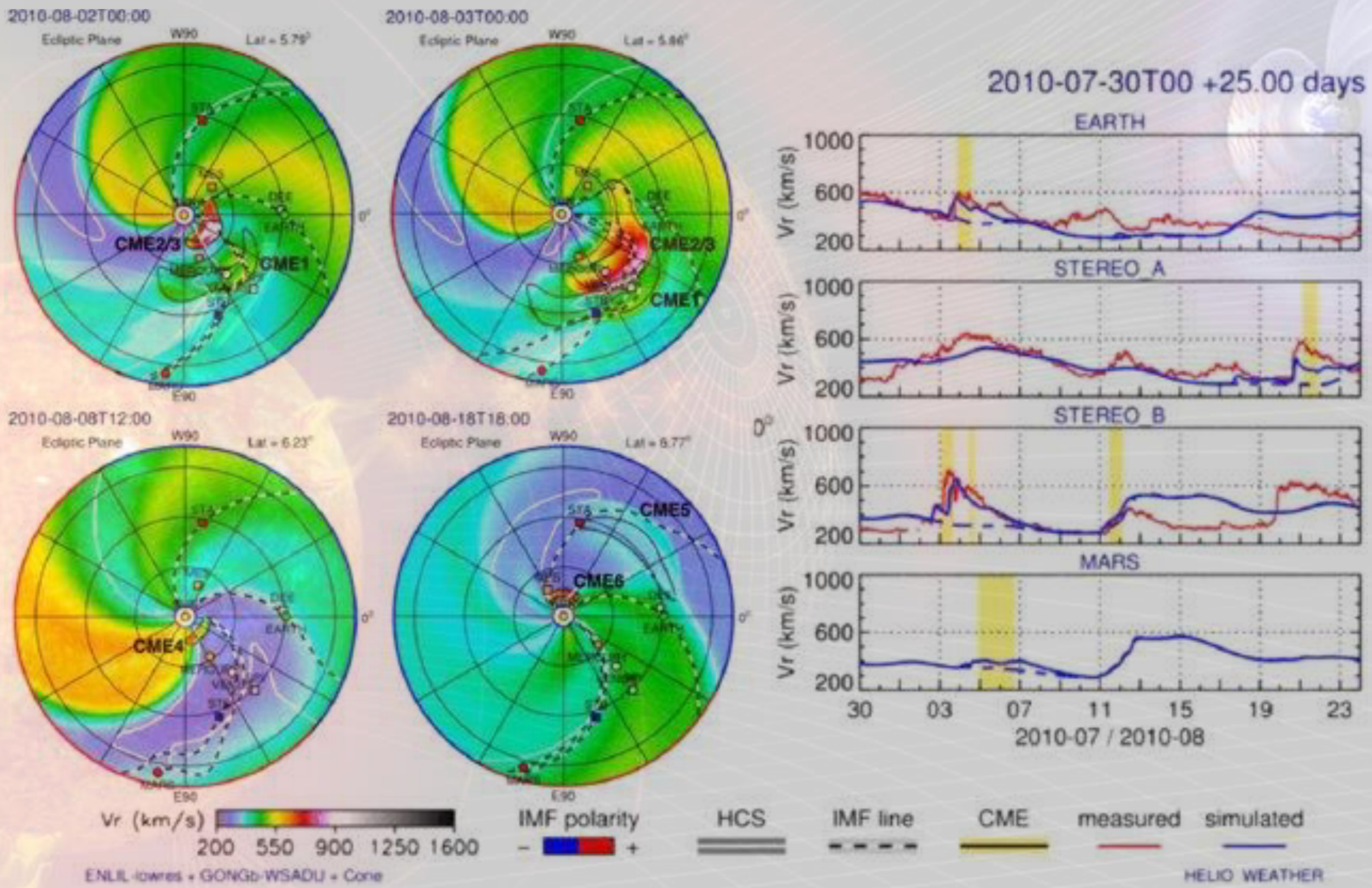

Bain et al. (2016)

http://swelto.oato.inaf.it/parker_spiral.html Biondo+, 2021

HELIOPHYSICS SYSTEM OBSERVATORY

- **20** Operating Missions with **27** Spacecraft
- **13** Missions in Formulation or Implementation
- **1** Under Study

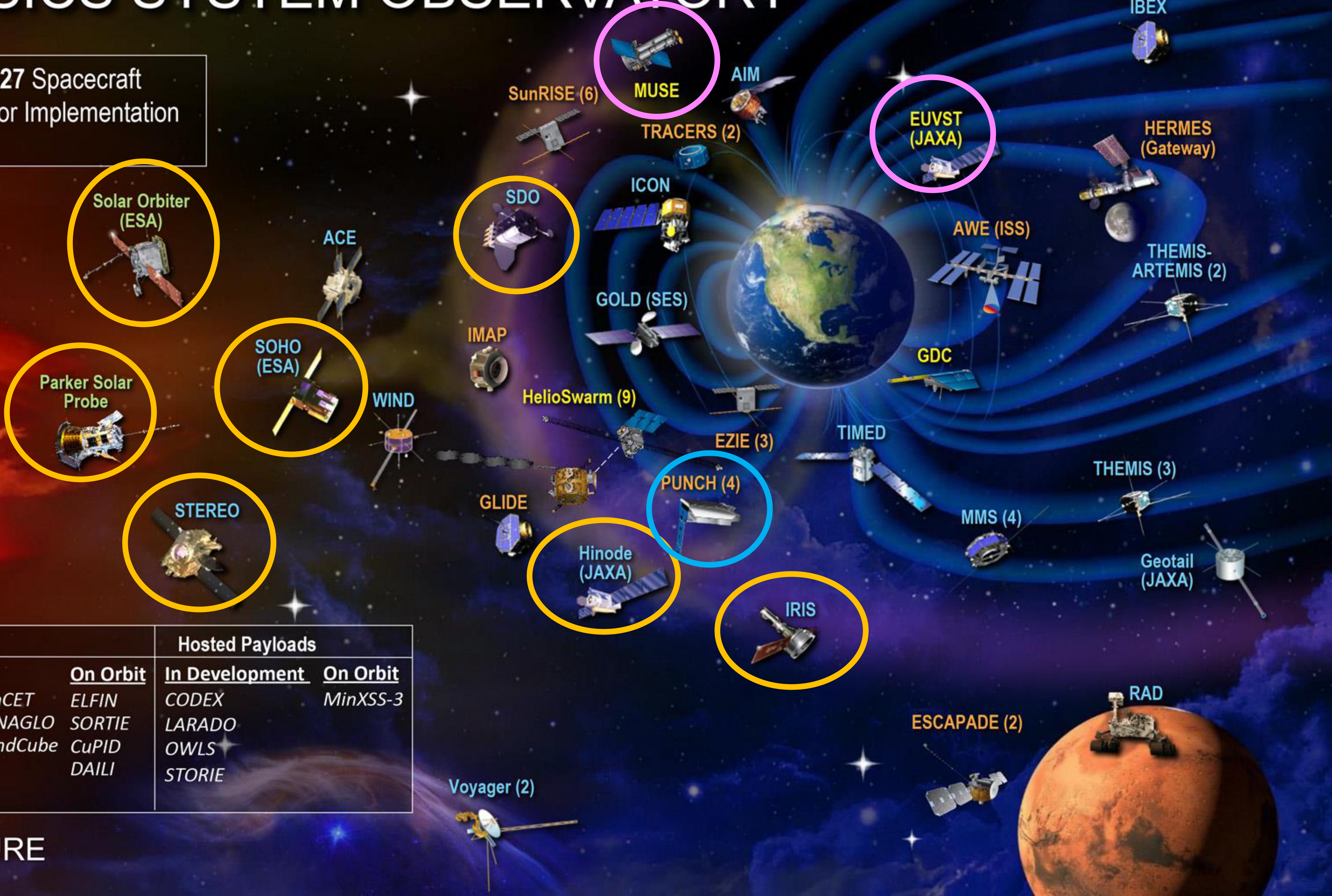

- FORMULATION
- IMPLEMENTATION
- PRIMARY OPS
- EXTENDED OPS

CubeSats					Hosted Payloads	
In Development				**On Orbit**	**In Development**	**On Orbit**
AEPEX	*Dione*	*CubIXSS*	*SunCET*	*ELFIN*	*CODEX*	*MinXSS-3*
AERO / VISTA	*GTOSat*	*petitSat*	*DYNAGLO*	*SORTIE*	*LARADO*	
CIRBE	*ICOVEX*	*REAL*	*WindCube*	*CuPID*	*OWLS*	
CURIE	*LAICE*	*SPORT*		*DAILI*	*STORIE*	
CuSP	*LLITED*	*PADRE*				

OPERATING & FUTURE

Updated August 8, 2022

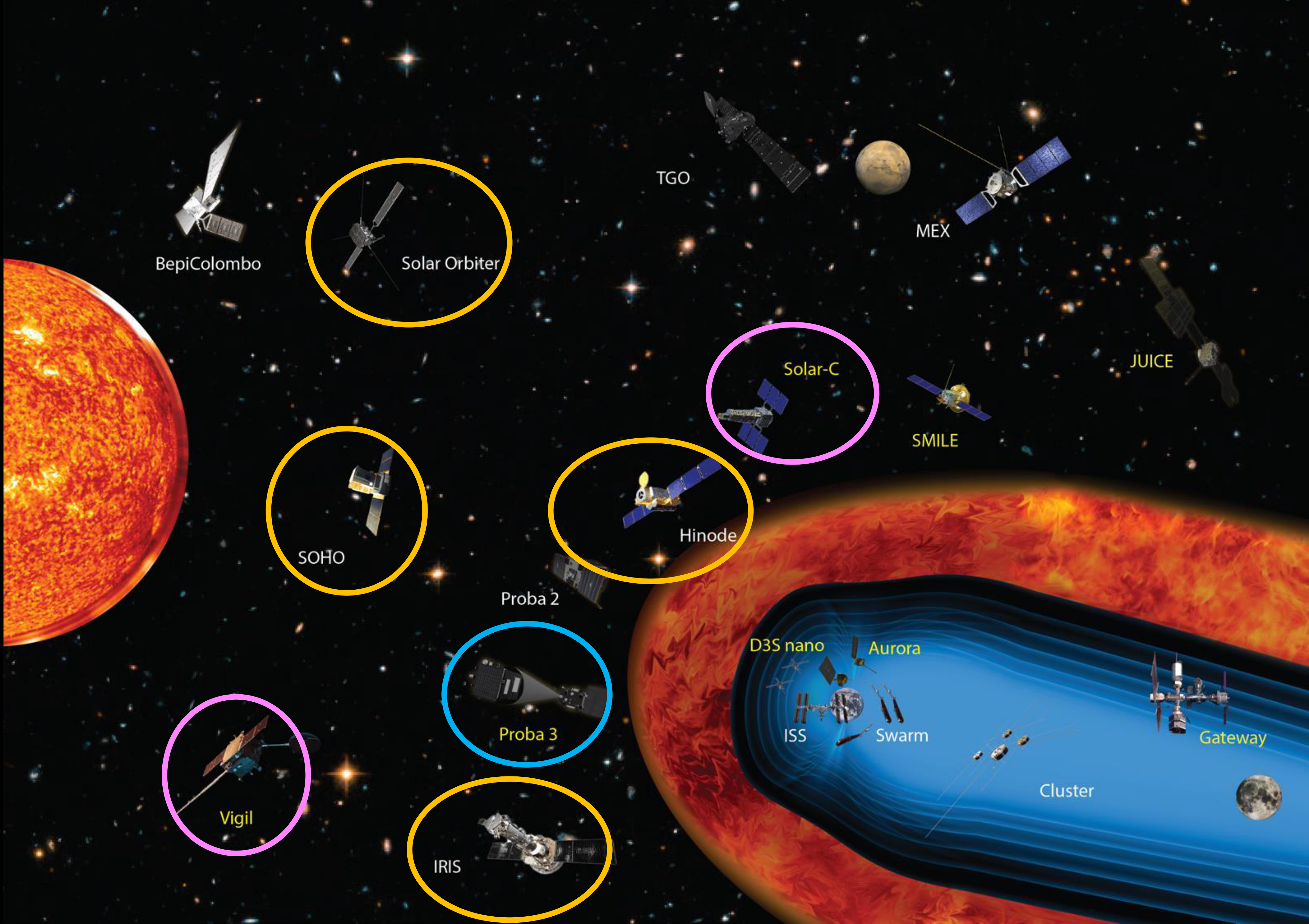

Operational
Implementation

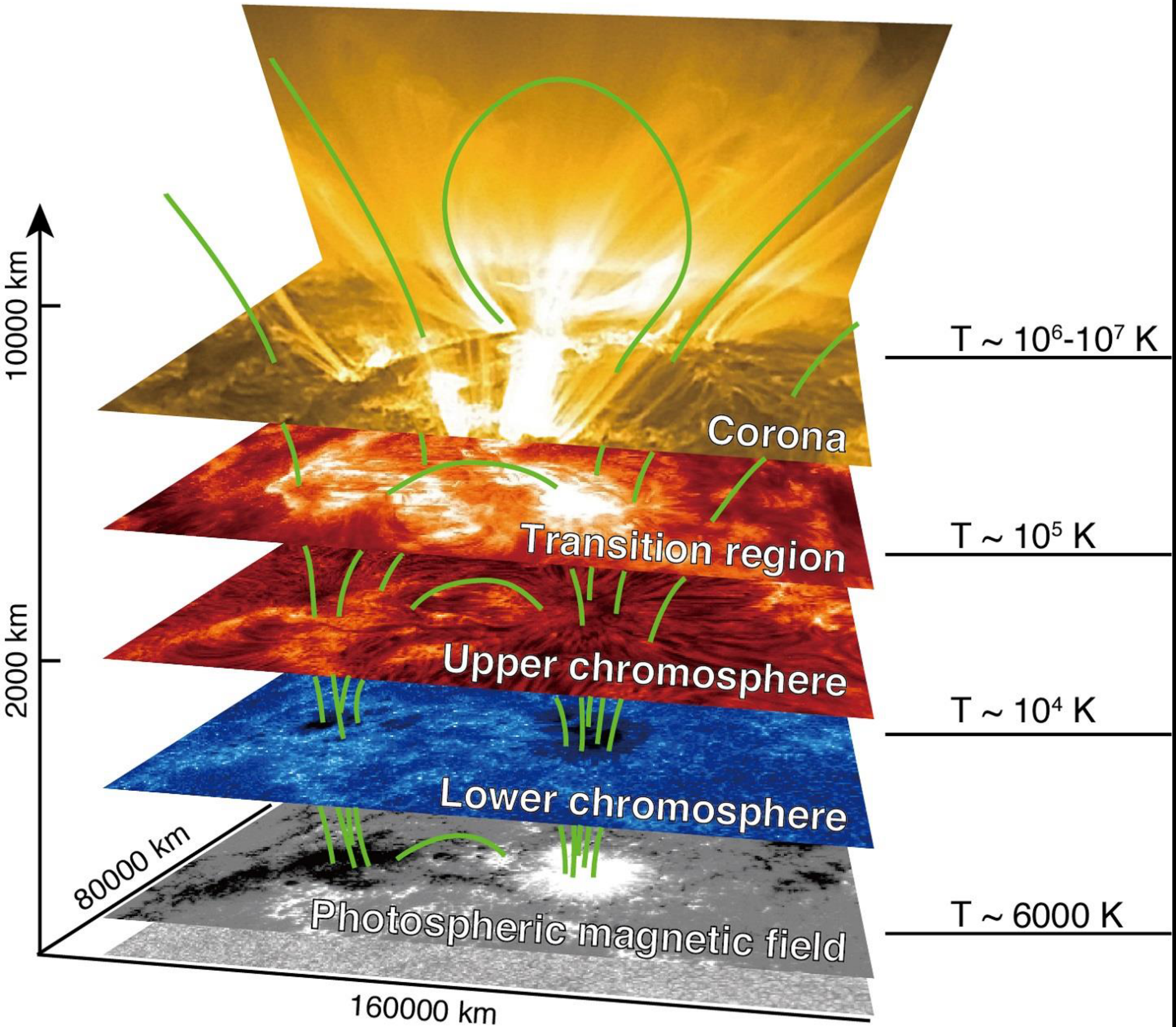

The solar atmosphere and the heliosphere are a system of systems

(N. Viall)

Ground based

Space based

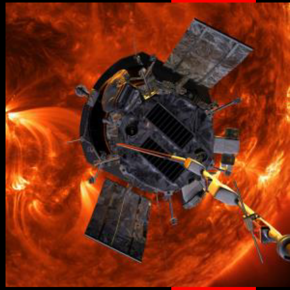

The solar atmosphere is composed of a thin plasma in NLTE equilibrium at temperatures that vary from 4000K to 10MK

- Magnetic fields
- Thermal properties
- Velocities
- Abundances

Plasma temperature

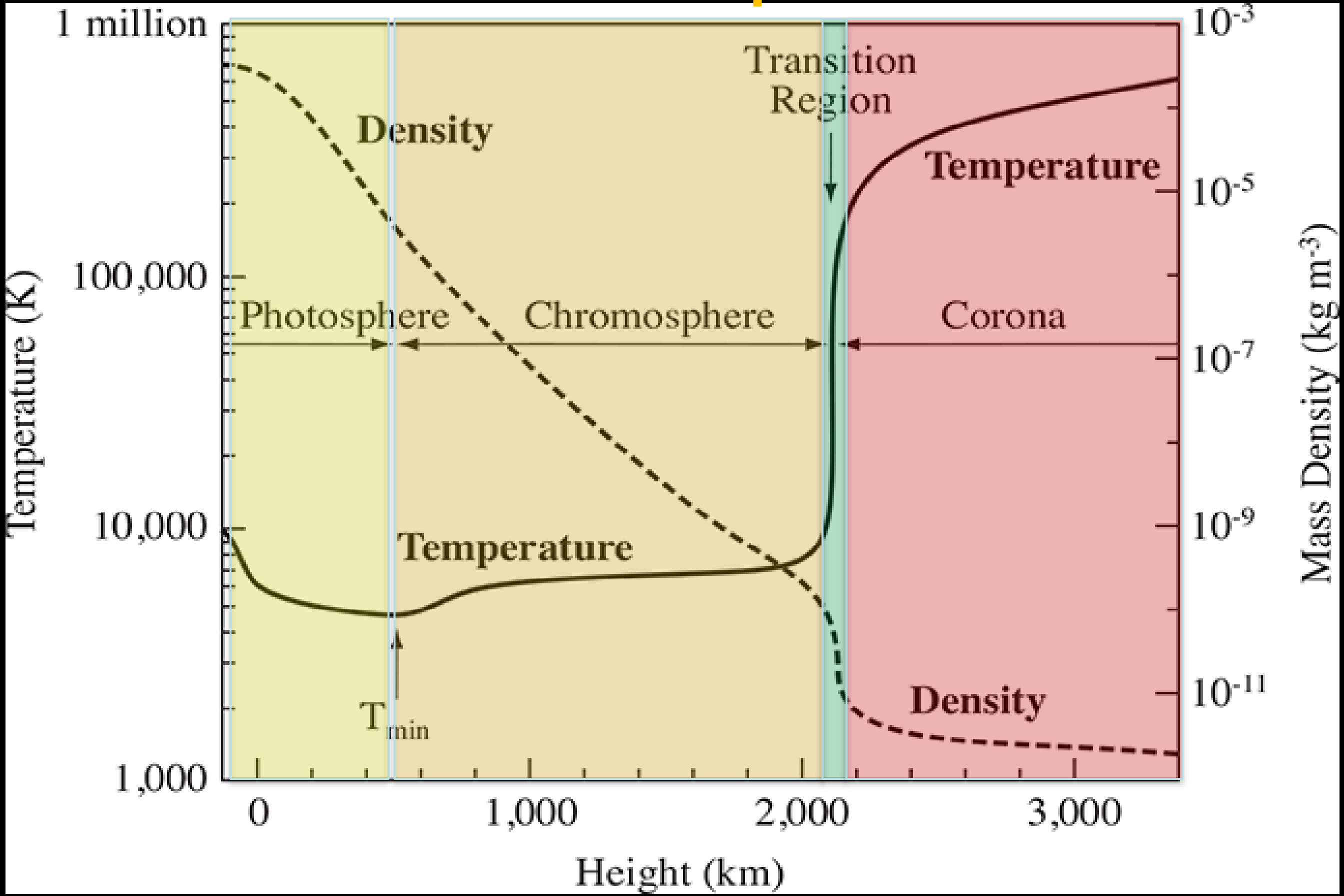

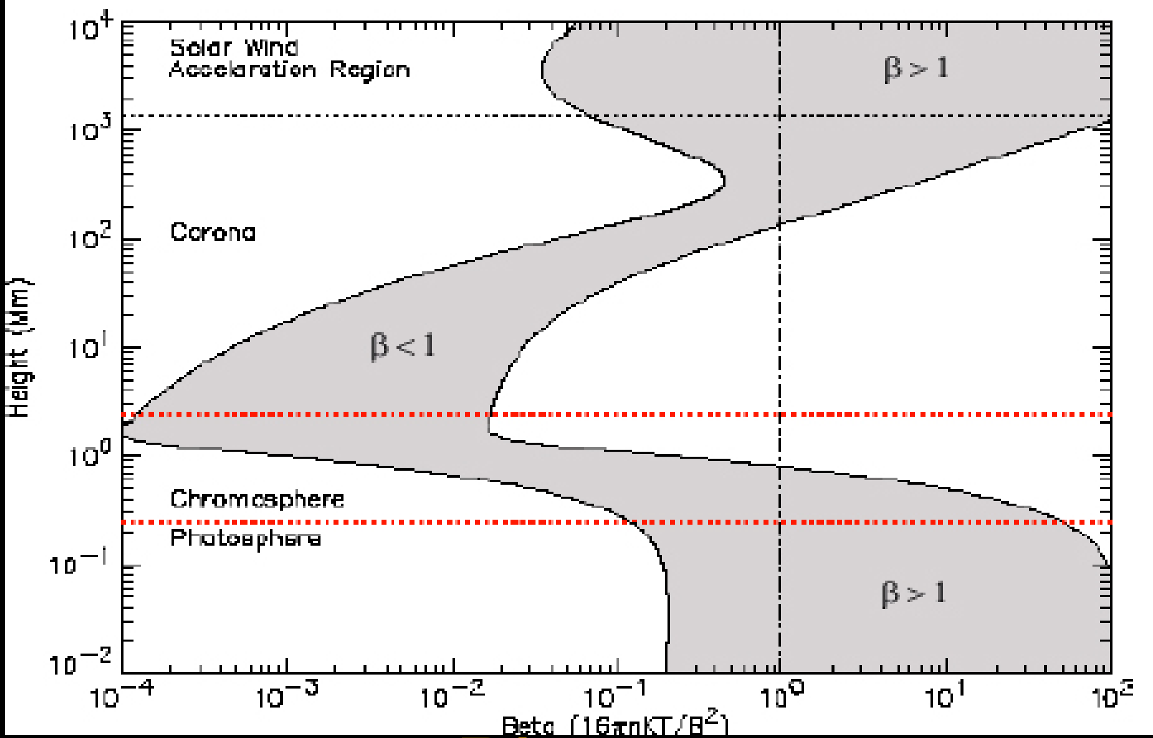

Plasma β

The goal is to measure:

- Magnetic fields
- Thermal properties
- Velocities
- Abundances

with high temporal and spatial resolution

Key parameters in NLTE are the electron density and the electron temperature

The SOHO Mission

- The Solar Heliospheric Observatory (SOHO) was a joint program between ESA and NASA
  - ESA: responsible for SOHO’s procurement, integration, and testing
  - NASA: provided launch and mission operations (at NASA/GSFC)
- Launched on December 2, 1995 from Cape Canaveral and still operative
- Special orbit around tha Lagrangian point L1 between Earth and Sun

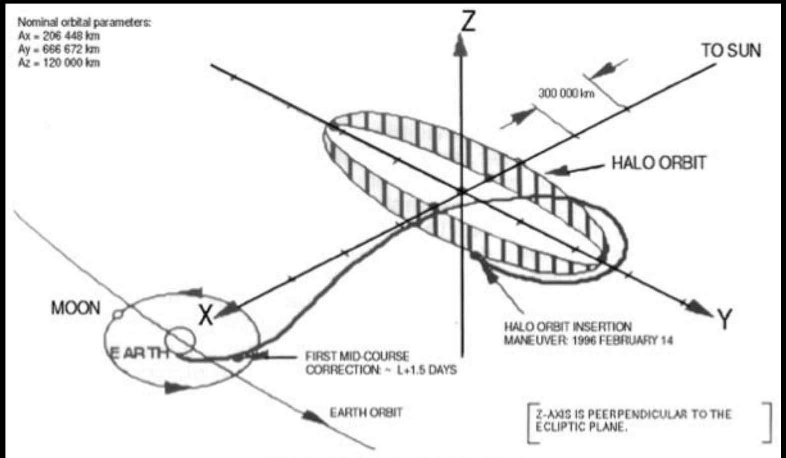

SOHO orbit schematic

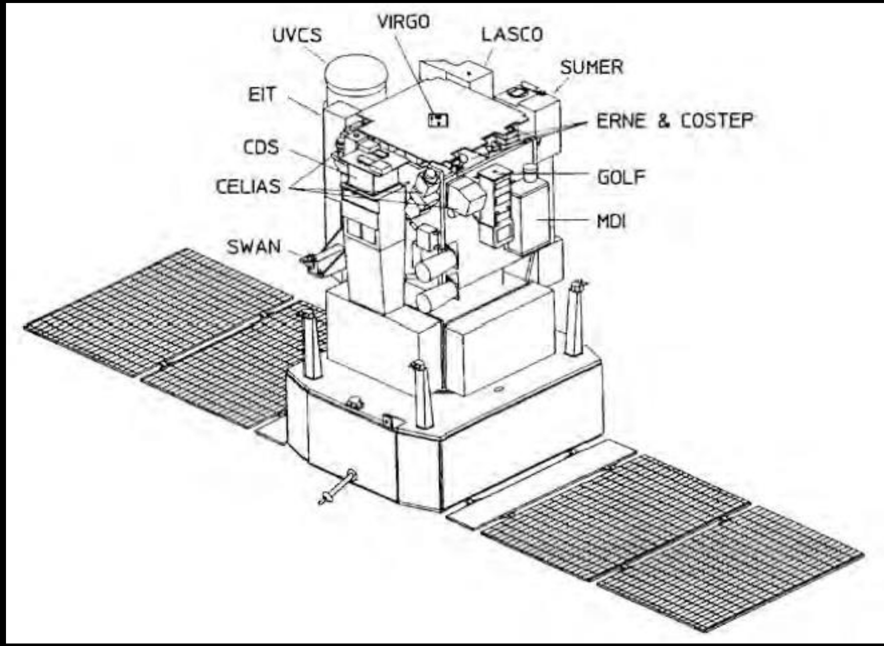

The SOHO Mission

- Largest solar observatory ever flown,
- Payload:
    - 3 helioseismology instruments (GOLF, VIRGO, MDI)
    - 6 remote sensing instruments (SUMER, CDS, EIT, UVCS, LASCO, SWAN)
    - 3 in situ instruments (CELIAS, COSTEP, ERNE)

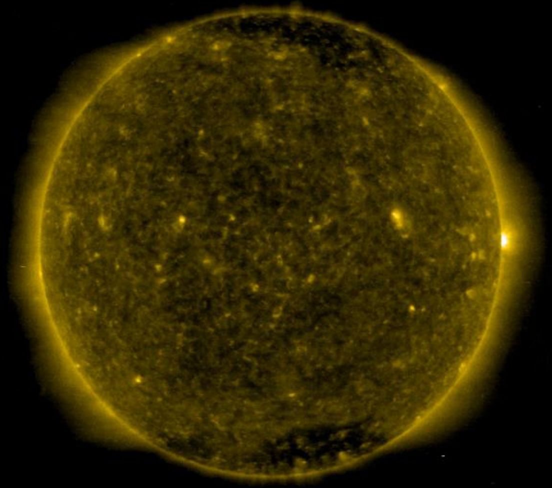

1996

Investigation	PI	Measurements	Technique	Bit rate (kb/s)
HELIOSEISMOLOGY				
GOLF	A.Gabriel, IAS, Orsay, F	Global Sun velocity oscillations (ℓ=0-3)	Na-vapour resonant scattering cell Doppler shift and circular polarization	0.160
VIRGO	C.Fröhlich, PMOD/WRC, Davos, CH	Low degree (ℓ=0-7) irradiance oscillations and solar constant	Global Sun and low resolution (12 pixels) imaging, active cavity radiometers	0.1
SOI/MDI	P.Scherrer, Stanford Univ., CA	Velocity oscillations with harmonic degree up to 4500	Doppler shift and magnetic field observed with Michelson Doppler Imager	5 (+160)
SOLAR ATMOSPHERE REMOTE SENSING				
SUMER	K.Wilhelm, MPAE, Lindau, D	Plasma flow characteristics: T, density, velocity in chrom. through corona	Normal incidence spectrometer: 50-160 nm spectral resolution 20000-40000, angular res.: 1.5"	10.5 (or 21)
CDS	R.Harrison, RAL, Chilton, UK	Temperature and density in transition region and corona	Normal and grazing incidence spectrom.: 15-80nm, spectr. res. 1000-10000 angular res. 3"	12 (or 22.5)
EIT	J.P.Delaboudinière IAS, Orsay, F	Evolution of chromospheric and coronal structures	Images (1024 x 1024 pixels in 42' x 42') in the lines of He II, Fe IX, Fe XII, Fe XV	1 (or 26.2)
UVCS	J.Kohl, SAO, Cambridge, Mass.	Electron and ion temp. densities, velocities in corona (1.3-10 $R_\odot$)	Profiles and/or intensity of several EUV lines (Ly α, O VI, etc.) between 1.3 and 10 $R_\odot$	5
LASCO	G.Brueckner, NRL, Washington, DC	Evolution, mass, momentum and energy trans. in corona (1.1-30 $R_\odot$)	1 internal and 2 externally occulted coronagraphs, Fabry-Perot spectrometer for 1.1-3 $R_\odot$	4.2 (or 26.2)
SWAN	J.L.Bertaux, SA, Verrières-le-Buisson,F	Solar wind mass flux aniso-atropies + temporal var.	2 scanning telescopes with hydrogen absorption cell for Ly-α light	0.2
SOLAR WIND 'IN SITU'				
CELIAS	D.Hovestadt, MPE, Garching, D	Energy distribution and composition (mass, charge, ionic charge) of ions (0.1-1000 keV/e)	Electrostatic deflection system, Time-of-Flight measurements, solid state detectors	1.5
COSTEP	H.Kunow, Univ. of Kiel, D	Energy distribution of ions (p, He) 0.04-53 MeV/n and electrons 0.04-5 MeV	Solid state and plastic scintillator detector telescopes	0.3
ERNE	J.Torsti, Univ. of Turku, SF	Energy distribution and isotopic composition of ions (p - Ni) 1.4-540 MeV/n and electrons 5-60 MeV	Solid state and scintillator crystal detector telescopes	0.71

SOHO Mission highlights

Helioseismology

- Revealing the first images ever of a star's convection zone (its turbulent outer shell) and of the structure of sunspots below the surface. (MDI)

- Providing the most detailed and precise measurements of the temperature structure, the interior rotation, and gas flows in the solar interior. (MDI)

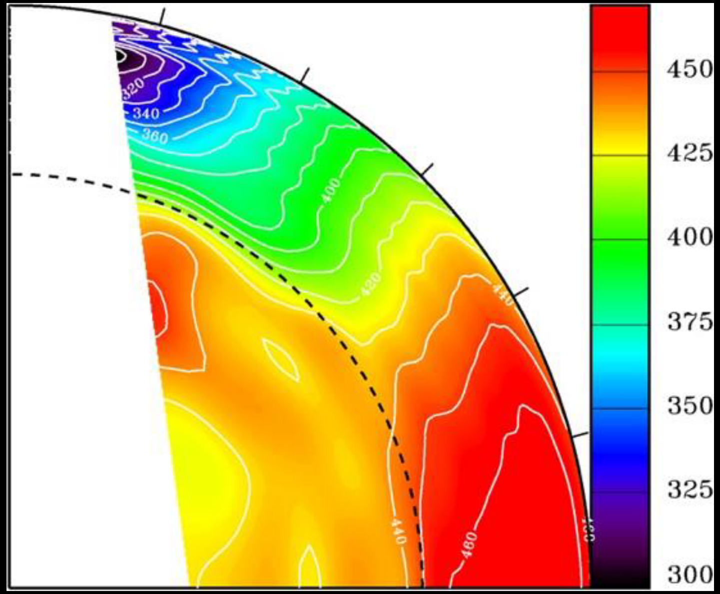

MDI - Schou+, 1998

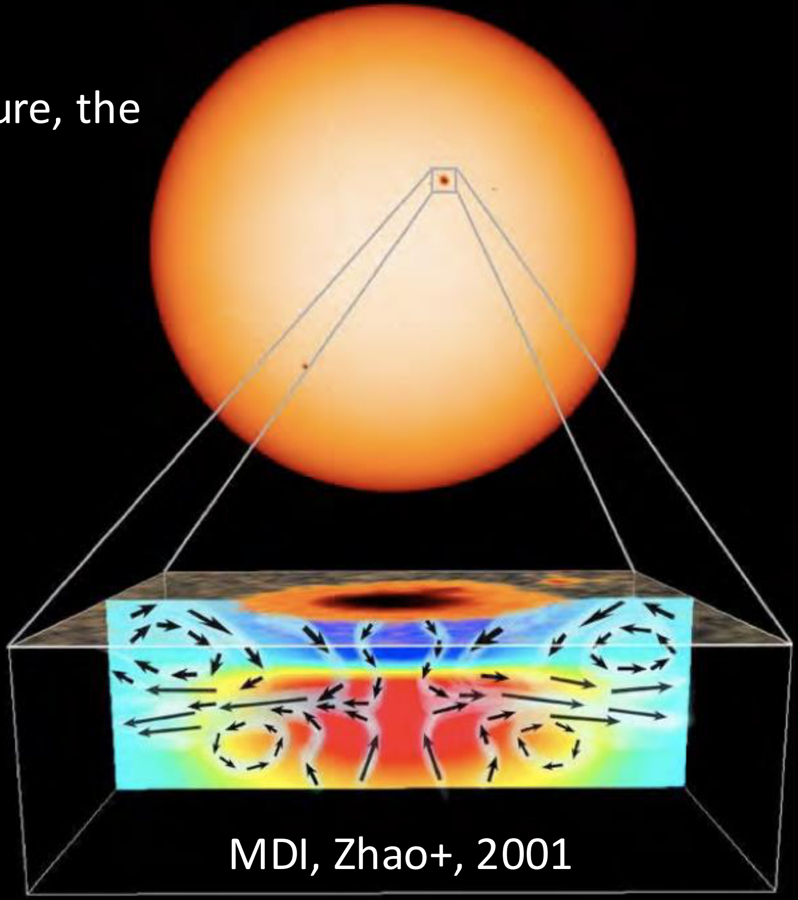

MDI, Zhao+, 2001

SOHO Mission highlights

Solar corona spectroscopy

- Measuring the acceleration of the slow and fast solar wind. (UVCS)
- Measuring the anisotropy of the ion's temperature distribution (UVCS)
- Identifying the source regions and acceleration mechanism of the fast solar wind in the magnetically "open" regions at the Sun's poles. (UVCS)

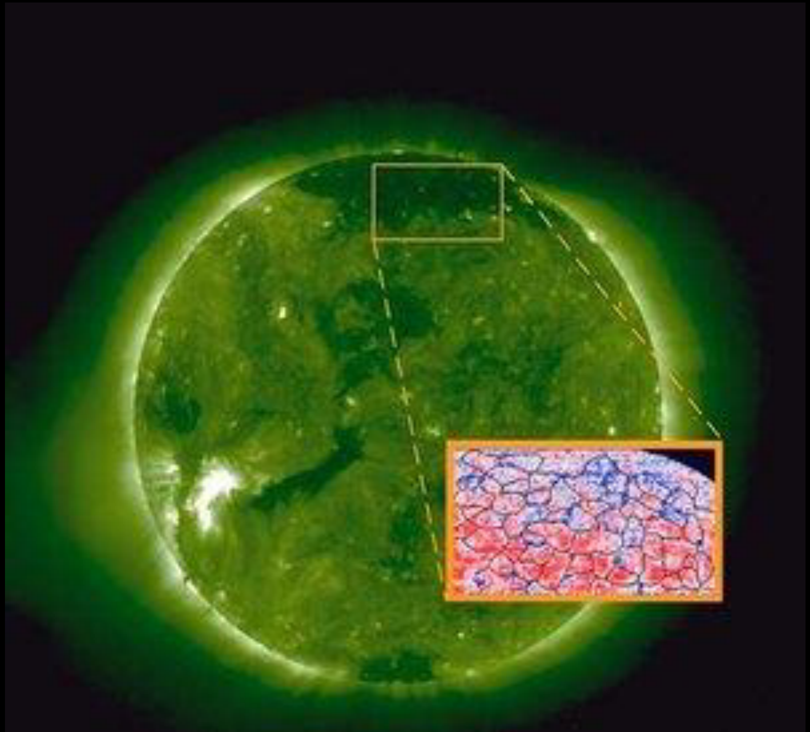

SUMER+EUI, Hassler+, 1999

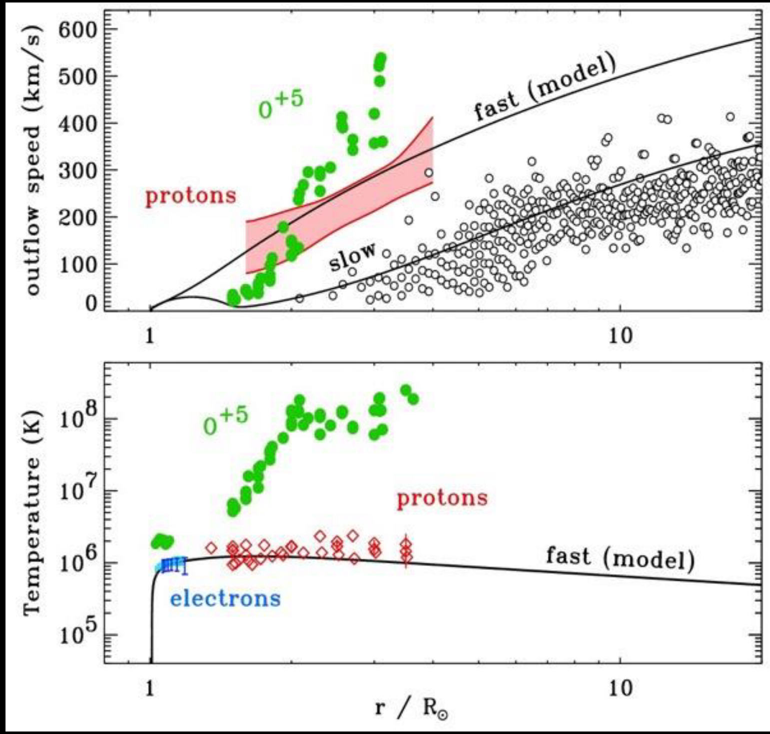

- UVCS/SOHO led to new views of the collisionless nature of the solar wind.
- Heavy ions are "minor ions," but they're valuable probes of the physics!
- In coronal holes, heavy ions (e.g., O^{+5}) both flow faster and are heated hundreds of times more strongly than protons and electrons, and have anisotropic velocity distributions.

(Kohl+. 1995, 2006; Cranmer+, 1999, 2008)

Remote sensing instruments

- **Vector magnetographs** (Photospheric mag field + helioseism.)
- **Disk imagers** (vertical temperature tomography of low corona)
- **X-ray imagers** (Flares)
- Spectrometers (Doppler shifts, temperatures and abundances)
- **Coronagraphs** (Extended corona)
- **Heliospheric imagers** (heliosphere)
- Total Solar Irradiance

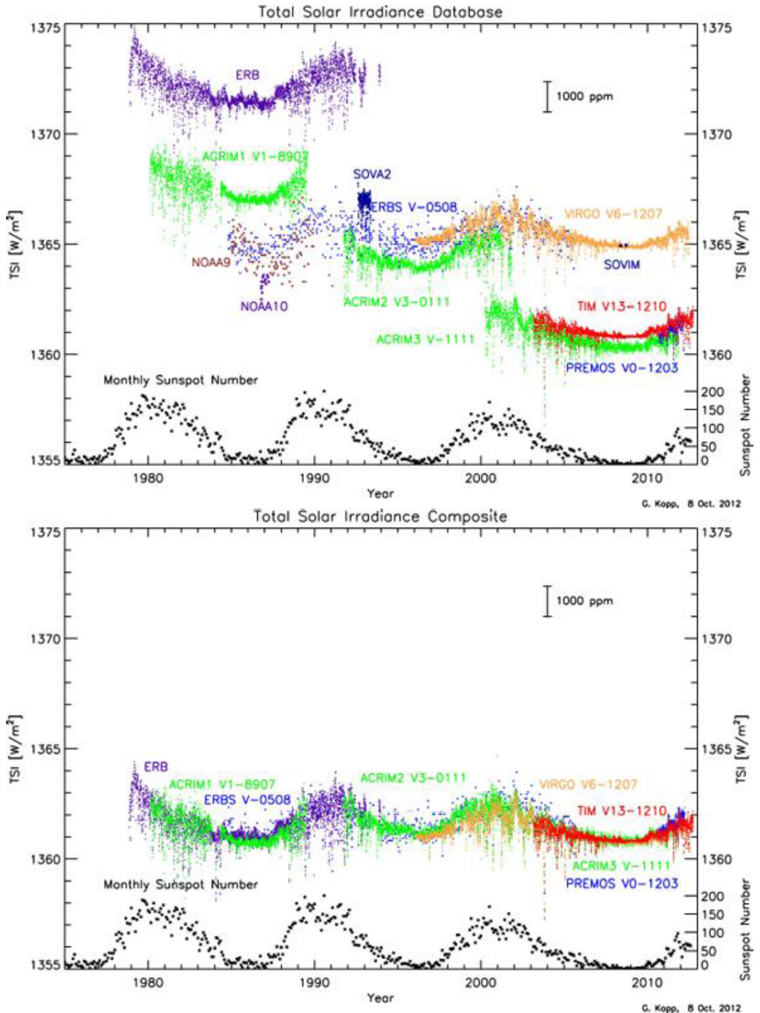

Solar Orbiter instrument descriptions in *The Solar Orbiter mission,* Special Issue, A&A

Operative missions and instrumentation

	Remote sensing						In situ				
Mission	Coronagraph	Heliospheric Imager	Disk imager	Magnetograph	Spectrometer	Irradiance	High Energy Particles	Solar Wind	Magnetic & Electric fields	Dust	Neutrons
SOHO (L1) 1995	LASCO (VL)	SWAN (UV)	EIT			GOLF VIRGO	ERNE COSTEP	CELIAS			
ACE (L1) 1997							CRIS SEPICA	SWEPAM SWICS SWIMS	MAG		
STEREO (Sun) 2006	COR1 (VL) COR2 (VL)	HI1 HI2	EUVI				IMPACT	PLASTIC	SWAVES		
HINODE (Earth) 2006			XRT	SOT	EIS						
SDO (Earth) 2010			AIA	HMI		EVE					
IRIS (Earth) 2013					IRIS						
PSP (Sun) 2018		WISPR					IS⊙IS	SWEAP (e, p, He)	FIELDS		
SolarOrbiter (Sun) 2020	Metis (VL,UV)	SOLOHI	EUI STIX (X)	PHI	SPICE		EPD	SWA	RPW MAG		
ASO-S (Earth) 2022	LST-SCI		LST-SDI LST-WST XDI (X)	FDG							
Aditya-L1 (L1) 2023	VELC (VL)		SUIT		SOLEX HEL1OS		PAPA	ASPEX			

Vector magnetograph

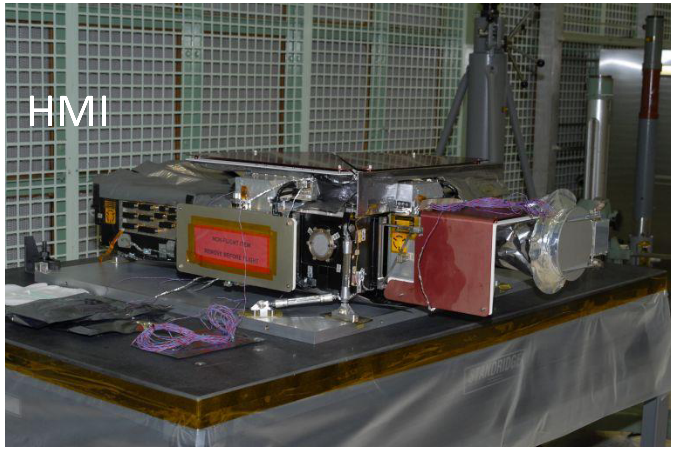

A vector magnetograph is a type of imaging telescope that can estimate the 3-D vector of the magnetic field with a specific solar spectrum line. The instrument measures wavelength of the line, its **Doppler shift** and by using polarization optics, its **Zeeman splitting**.

All recent space **dopplergraphs** and **magnetographs** are based on this type of instrument.

- **SOHO/MDI** (Michelson Doppler Interferometer) [1995-2015] NiI 676.8nm
- **SDO/HMI** (Helioseismic and Magnetic Imager) [2008-present] FeI 617.3nm
- **HINODE/SOT-NFI** (Narrowband Filter Imager) [2006 – present] FeI D1 630.15/630.25 nm
- **SolO/PHI** (Polarimetric and Helioseismic Imager) [from 2020] FeI 617.3nm
- **ASO-S/FMG** (Full disk vector MagnetoGraph) [from 2022] Fe I 532.4 nm

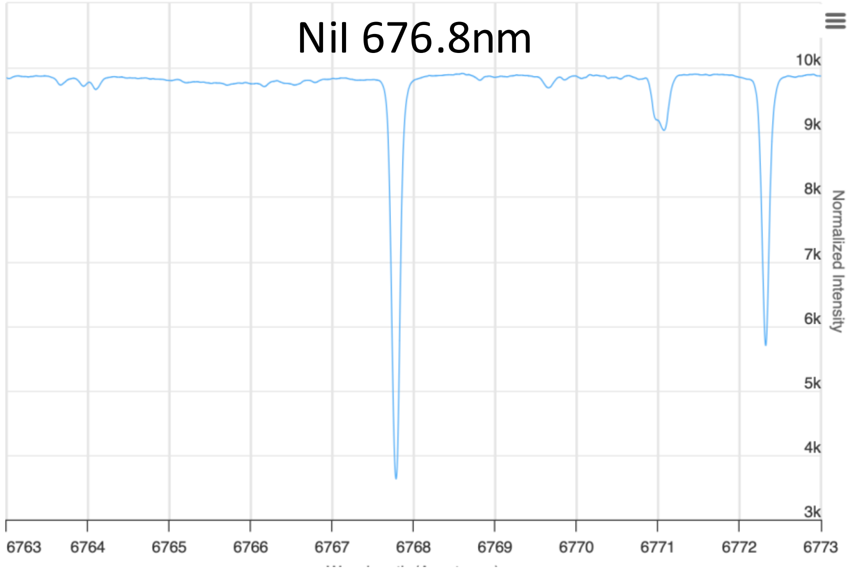

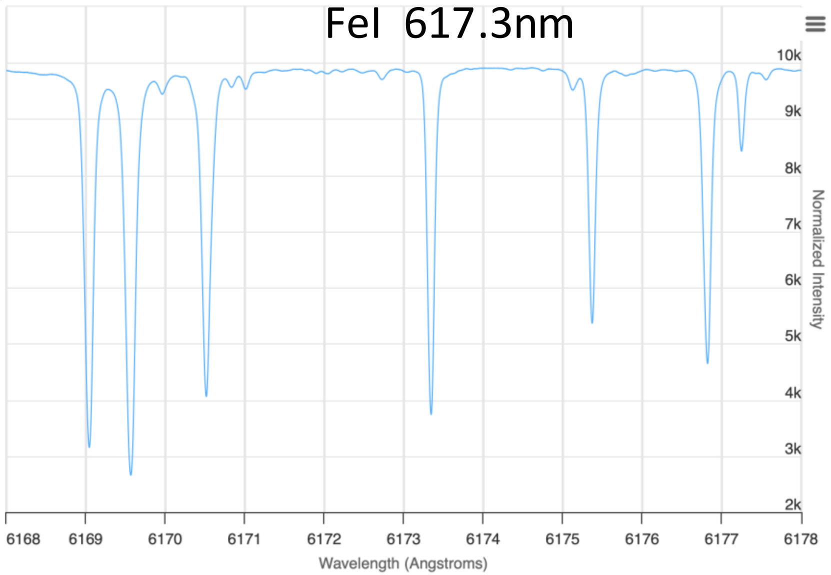

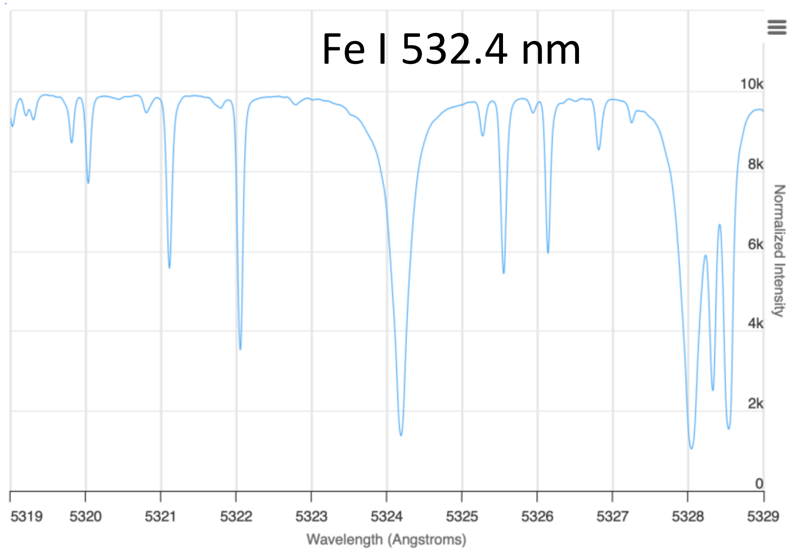

The Polarimetric and Helioseismic Imager (SO/PHI)

- SO/PHI is an imaging vector-spectro-polarimeter with two telescopes
- Full Disk Telescope:
  - 17.5mm refractor
  - images the entire Sun at all orbital positions

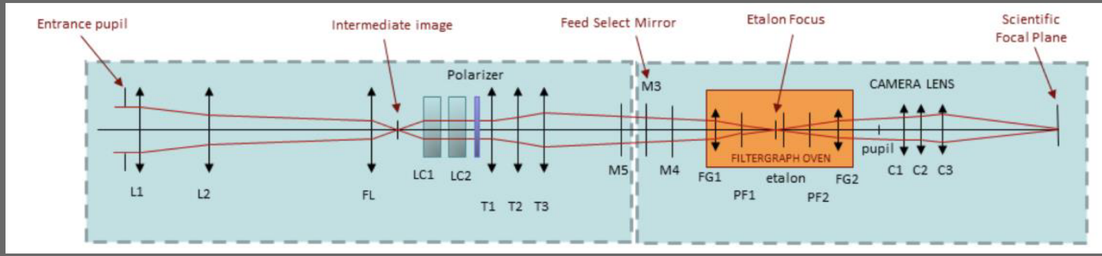

- High Resolution Telescope:
  - 140mm Ritchey-Chrétien
  - max resolution (@0.28 AU): 200km

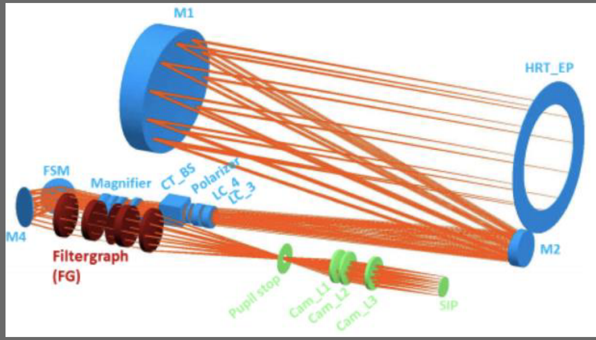

- Working wavelength: Fe I 617.3nm (same as SDO/HMI)
- Detector: 2k x 2k APS, 11fps
- Spectral FWHM: 106 mÅ

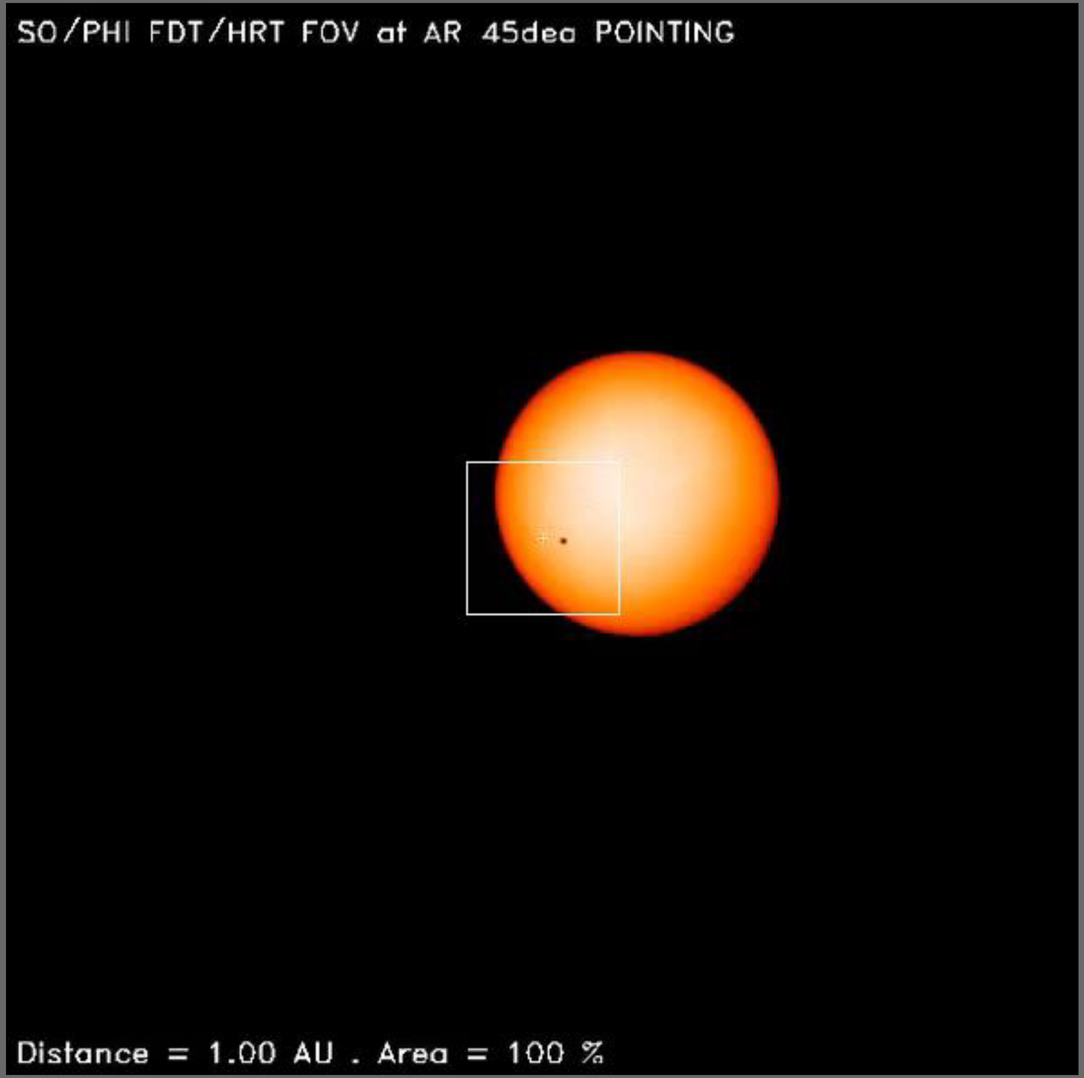

Solanki+, 2020

SO/PHI (measurement principle)

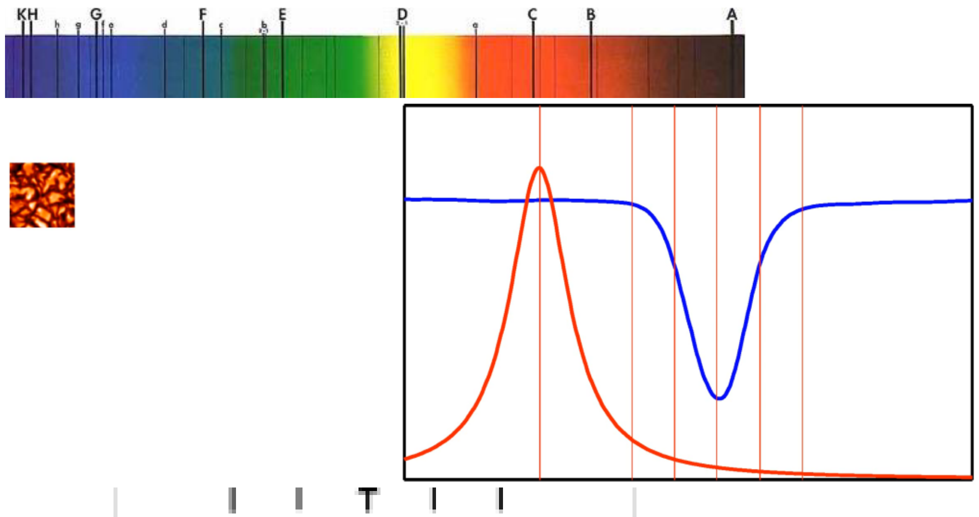

λ ≃ 617.3 nm; Δλ ≃ 10 nm

Polarized images in five plus one wavelengths

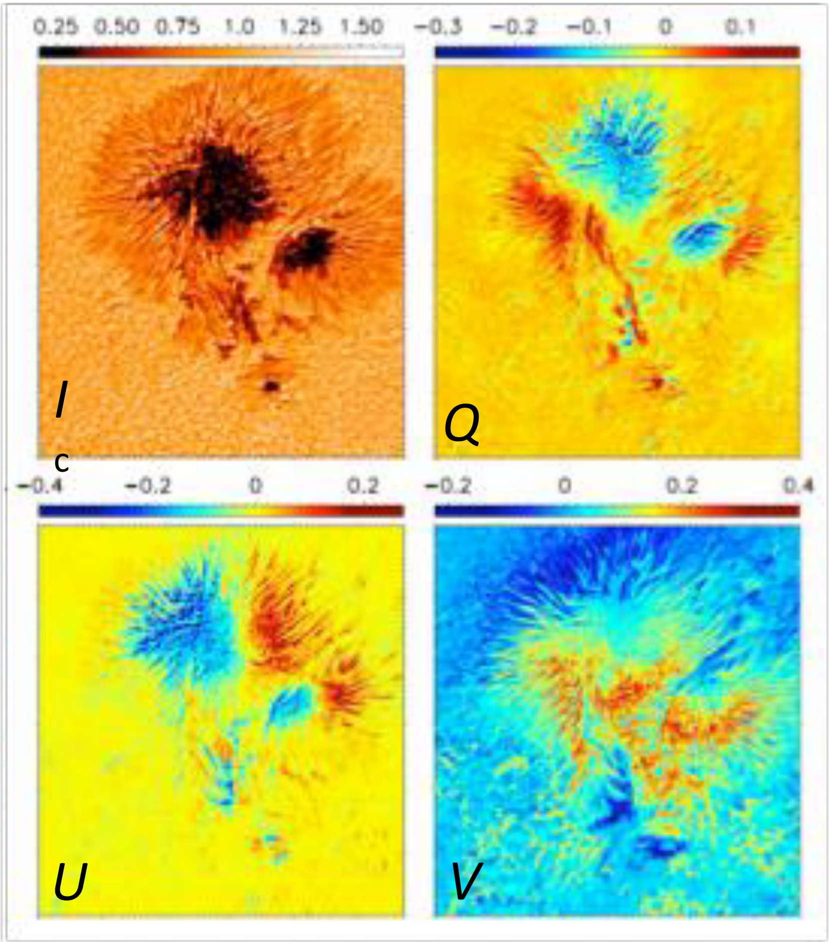

The polarization Stokes vector is obtained by a polarization analyser typically made of a rotating quarter wave plate and a linear polarizer (LP).
PHI makes use for the first time in space of a Liquid Crystal Retarder Plate + LP.
The vector magnetic field and the LOS velocity are inferred by inverting the RTE on board via the Zeeman Effect

SO/PHI Data Products

SO/PHI data products:

	Dynamic range	Noise
continuum intensity, I_c	-	≤ 10^{-3}
LOS velocity, v_{LOS}	±5 km/s	≤ 40 m/s
LOS magnetic field strength, B_{LOS}	±3.5 kG	15 G
magnetic field inclination, γ	180°	1°
magnetic field azimuth, φ	±180°	2°

- Maximum possible cadence:
  - During RS windows: 1 data set per minute
  - Outside RS windows: 1-4 data sets per day
- Main limitation: telemetry!

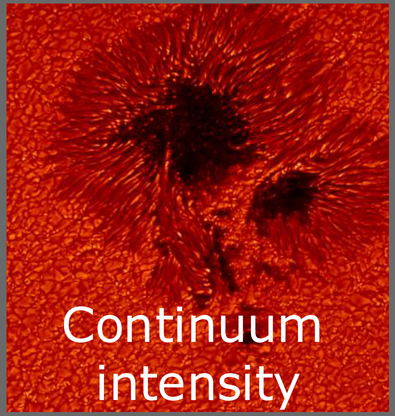

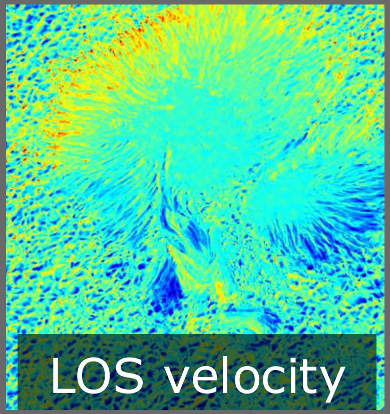

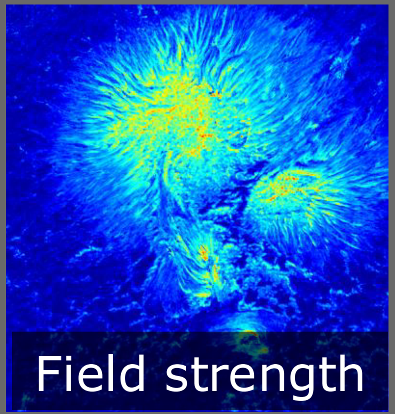

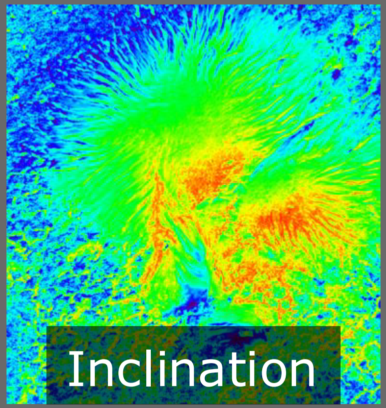

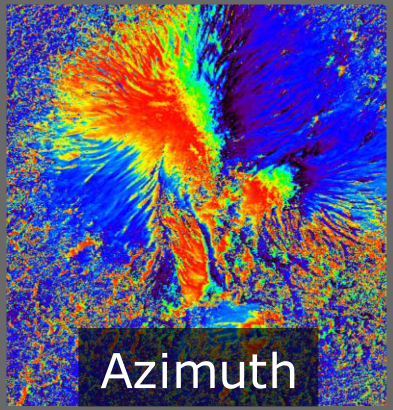

Examples of HRT science data

"Slow Wind" campaign on March 3-5, 2022: 3 HRT bursts at 3min cadence

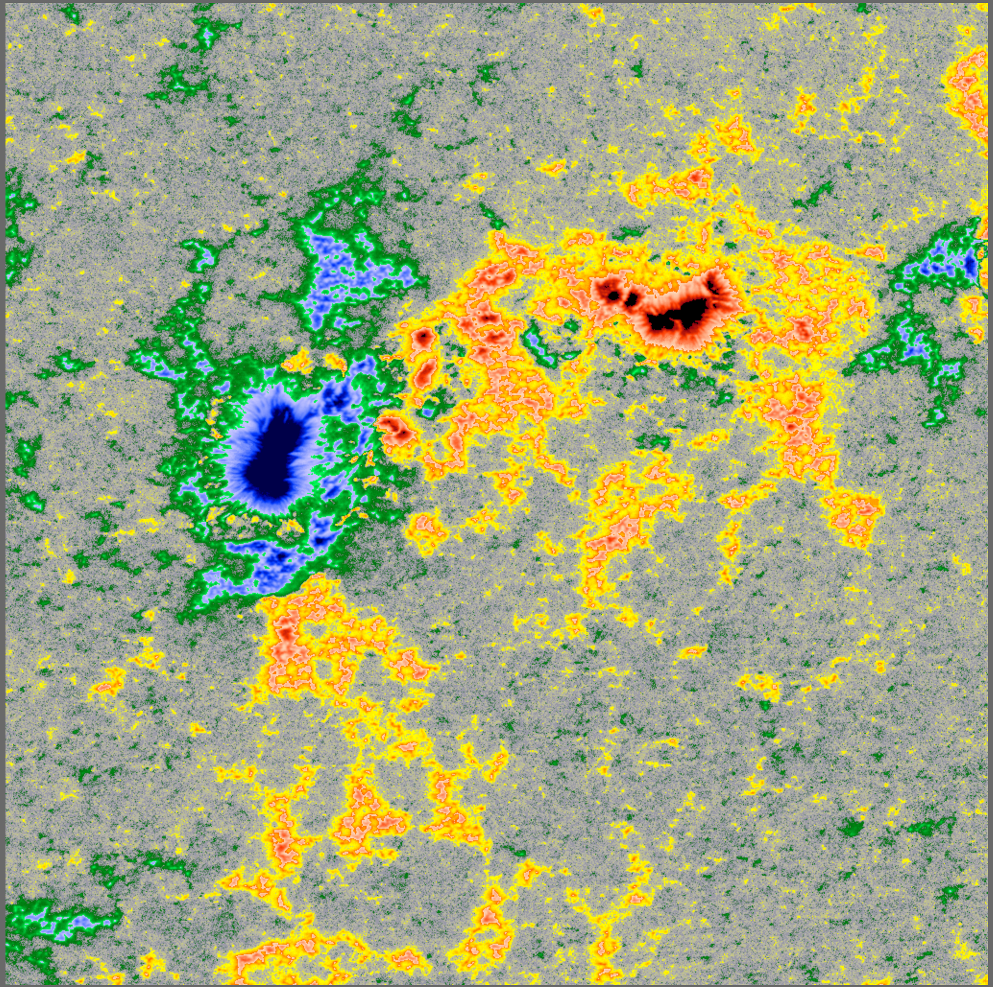

(line-of-sight) magnetogram scaled to ±1000G

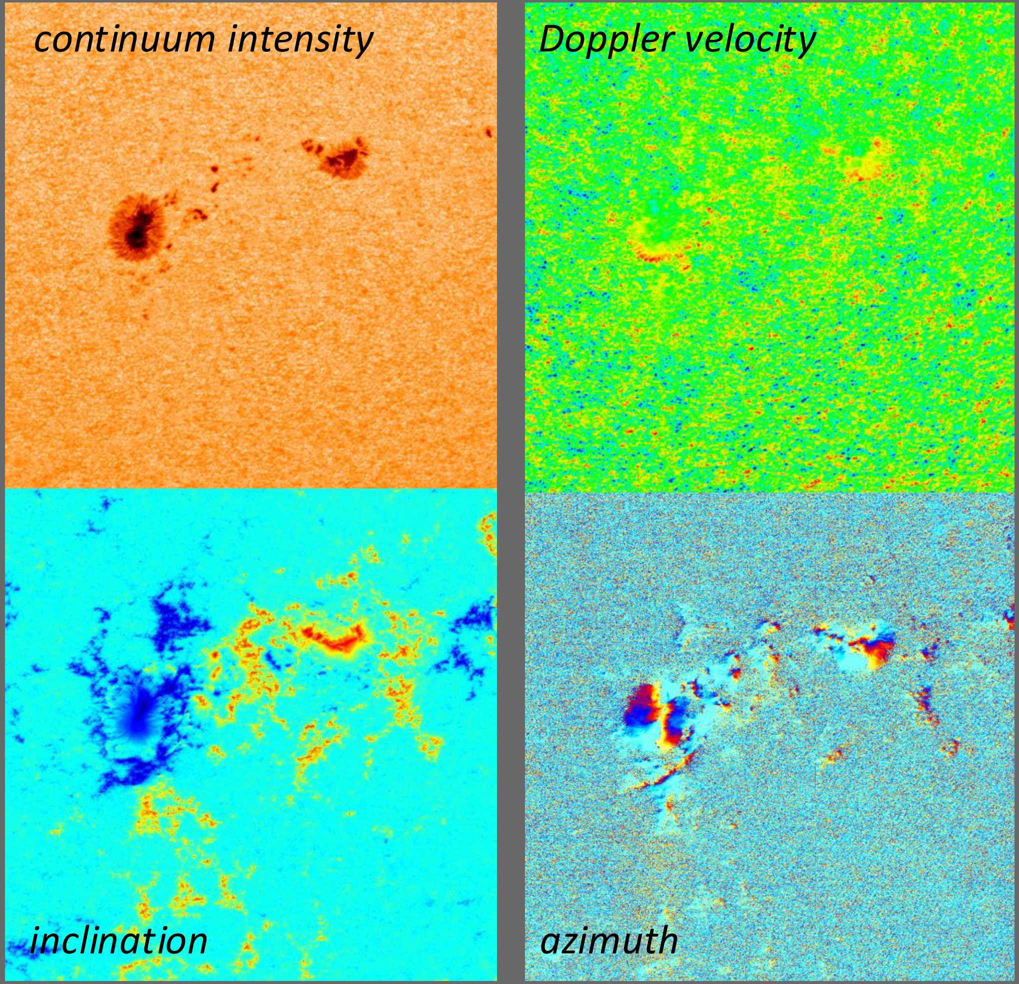

Stereoscopic disambiguation of vector magnetograms

Spectropolarimetric reconstructions of the photospheric vector magnetic field are intrinsically limited by the 180-ambiguity in the orientation of the transverse component. So far, the removal of such an ambiguity has required assumptions about the properties of the photospheric field, which makes disambiguation methods model-dependent.

The **Stereoscopic Disambiguation Method (SDM)** that solves the 180 ambiguity by combining information from two vantage points: SO/PHI, SDO/HMI.

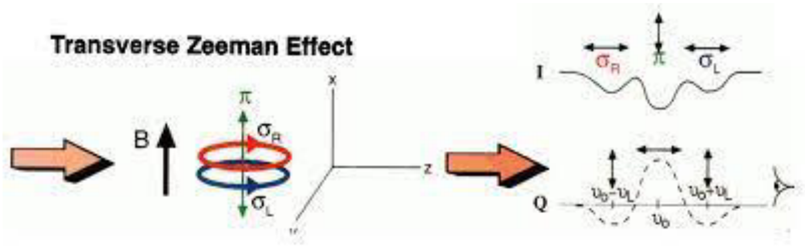

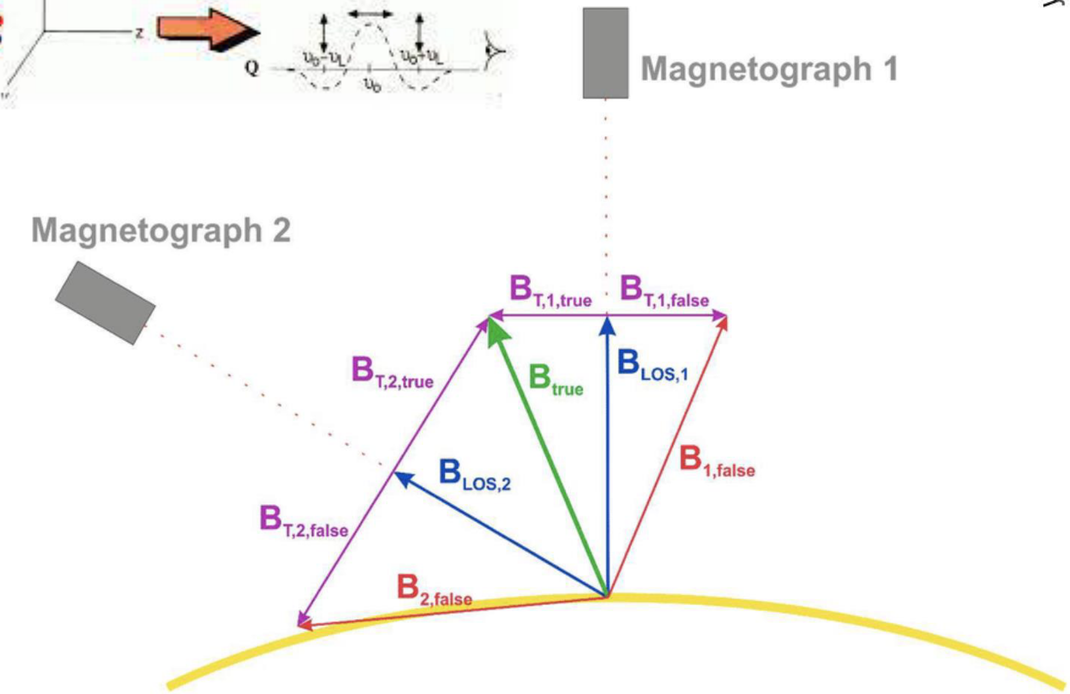

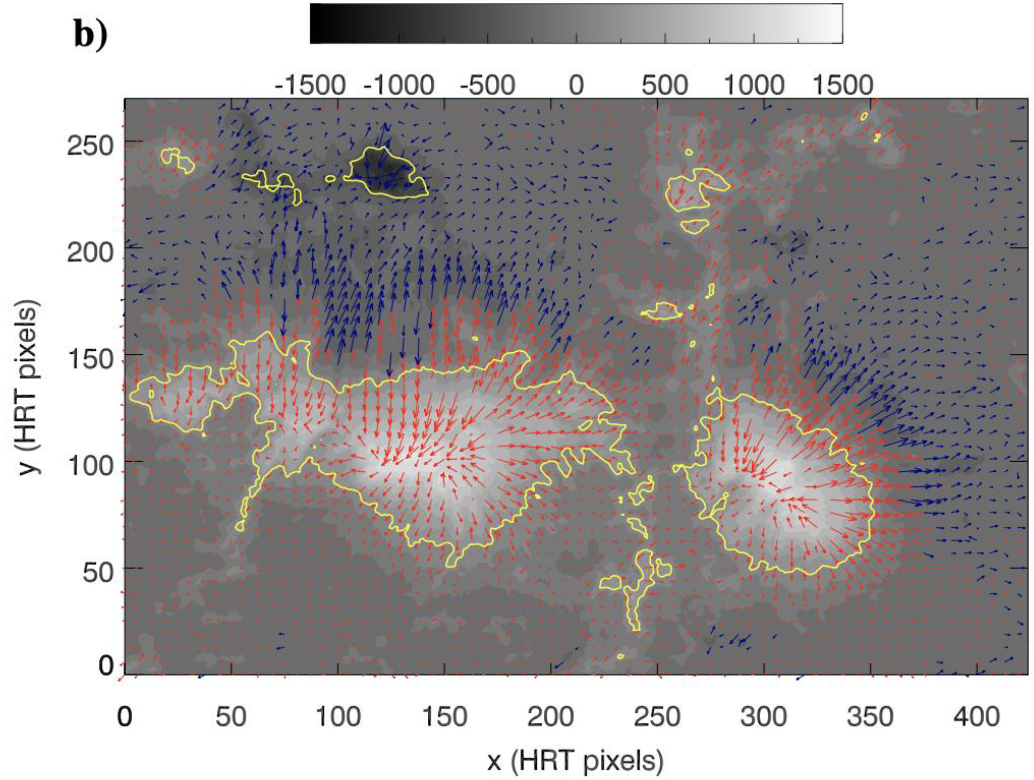

Valori+, Stereoscopic disambiguation of vector magnetograms: first applications to SO/PHI-HRT data, in preparation

[**Valori+, 2022, SolPhys, 297**]

Nanoflares

Kahil+, The magnetic drivers of campfires seen by the Polarimetric and Helioseismic Imager (PHI) on Solar Orbiter

The Extreme Ultraviolet Imager (EUI) on board the Solar Orbiter (SO) spacecraft observed small extreme ultraviolet (EUV) bursts, termed **campfires**, that have been proposed to be brightenings near the apexes of low-lying loops in the quiet-Sun atmosphere. The underlying magnetic processes driving these campfires are not understood.

In 71% of the 38 isolated events, campfires are confined between bipolar magnetic features, which seem to exhibit signatures of magnetic flux cancellation. The flux cancellation occurs either between the two main footpoints, or between one of the footpoints of the loop housing the campfire and a nearby opposite polarity patch.

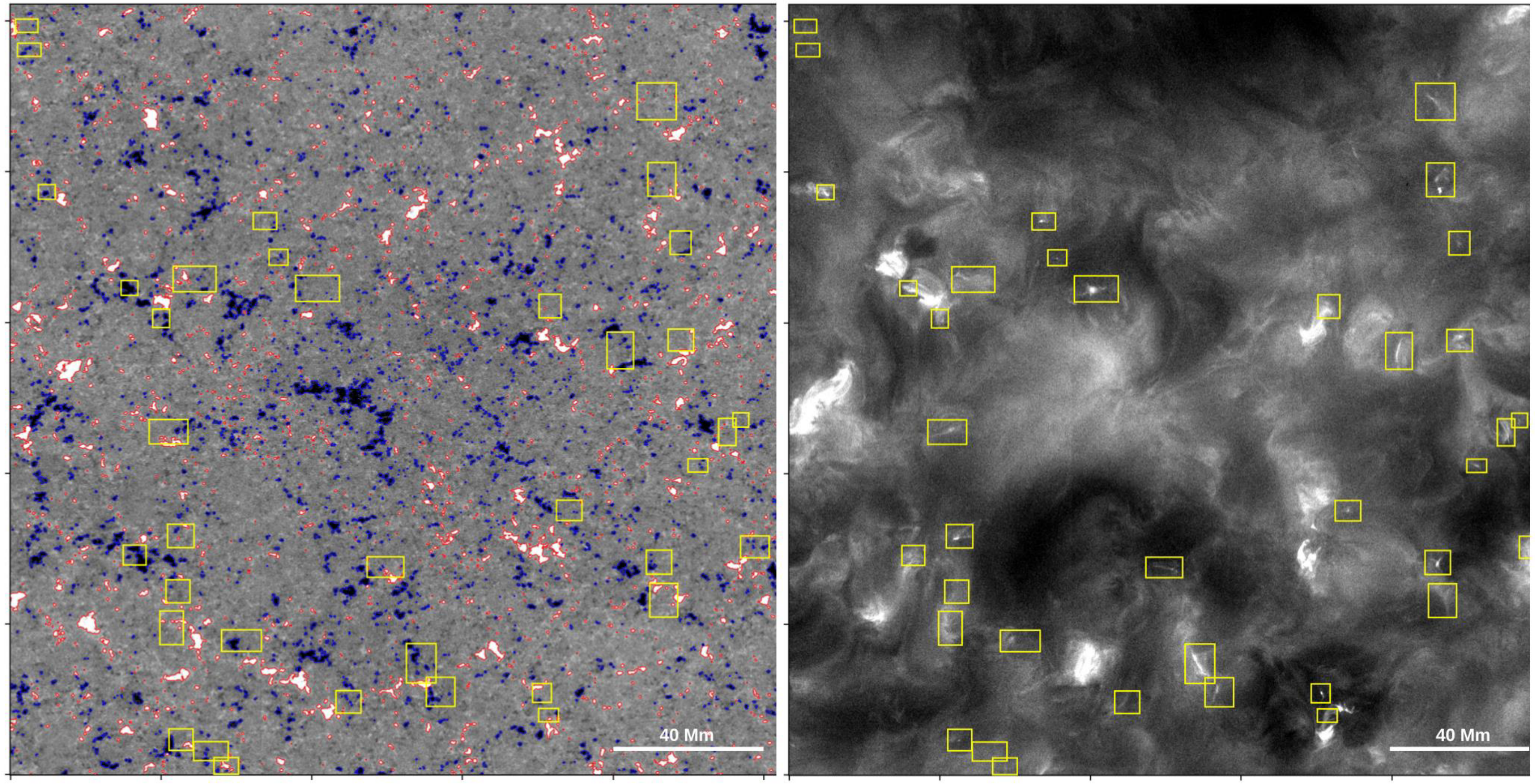

Fig. 3. Distribution of campfire events over the SO/PHI LOS magnetogram (left) and co-aligned HRI_{EUV} image (right). The contours on the magnetic field map enclose magnetic features with B_{LOS} above $3\sigma_B$ (21 G). Blue and red contours correspond to negative and positive flux, respectively. The yellow boxes in both figures enclose the studied campfire events which are located approximately in the centre of each box. The LOS magnetogram is saturated at ±40 G, and the size of the FOV is $512'' \times 512''$.

Far side helioseismology

Earth-side observations of solar p modes can be used to image and monitor magnetic activity on the Sun's far side. Here we use magnetograms of the far side obtained by the Polarimetric and Helioseismic Imager (PHI) onboard Solar Orbiter (SO) to directly assess – for the first time – the validity of far-side **helioseismic holography**

Yang+, [Direct assessment of SDO/HMI helioseismology of active regions on the Sun's far side using SO/PHI magnetograms]()

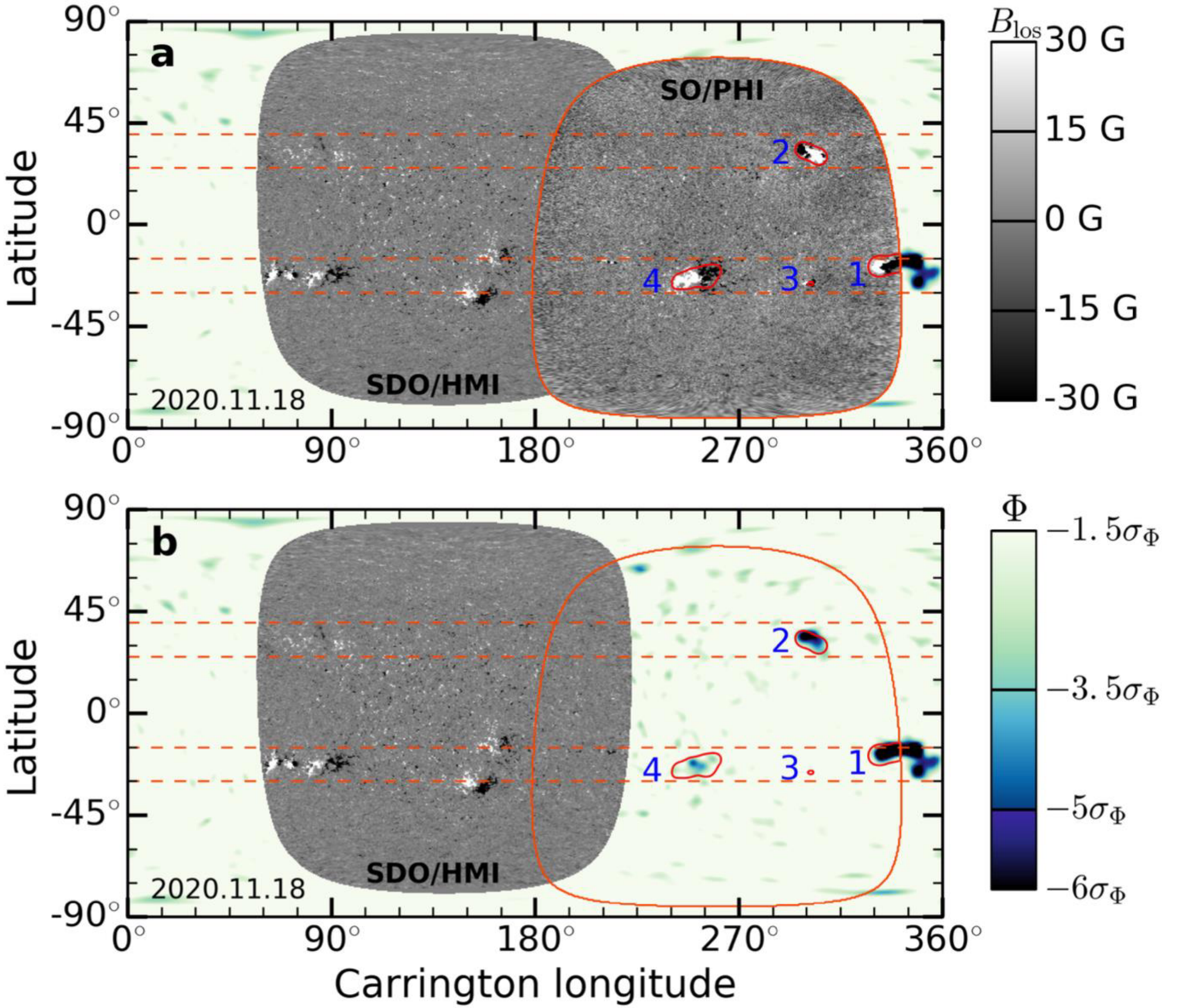

Fig. 2. Magnetic activity on the entire solar surface on 18 November 2020 during Carrington Rotation CR 2237. *Panel a*: The SO/PHI-FDT magnetogram covers a large fraction of the far side, while a 3-day averaged SDO/HMI magnetogram shows magnetic activity on the near side. Four active regions identified on the far side by SO/PHI are outlined by red contours (See Table 1). *Panel b*: The green/blue shades show the helioseismic phase Φ on the far side, deduced from acoustic oscillations observed on the near-side by SDO/HMI over 79 hours during 17–19 November. The seismic phase is shown over a range corresponding to 1.5–6 times the standard deviation of the noise in the quiet Sun ($\sigma_\Phi = 2.6°$).

Disk Imagers

- Disk imagers are telescopes used to image the solar corona in the UV and X
- Disk imagers have been flown in most of the solar space missions.
- Telescopes of the last decades make use of multilayer coatings, coupled with low bandpass aluminum filters to provide narrow band pass images at specific emission lines or group of lines, with normal incidence telescopes

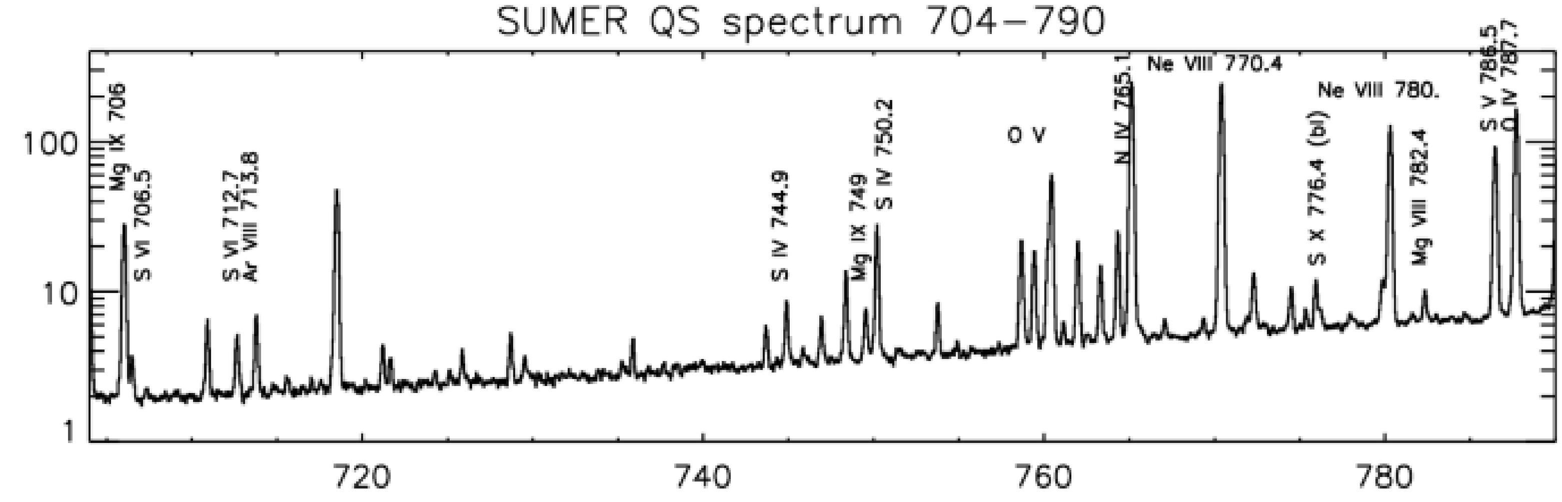

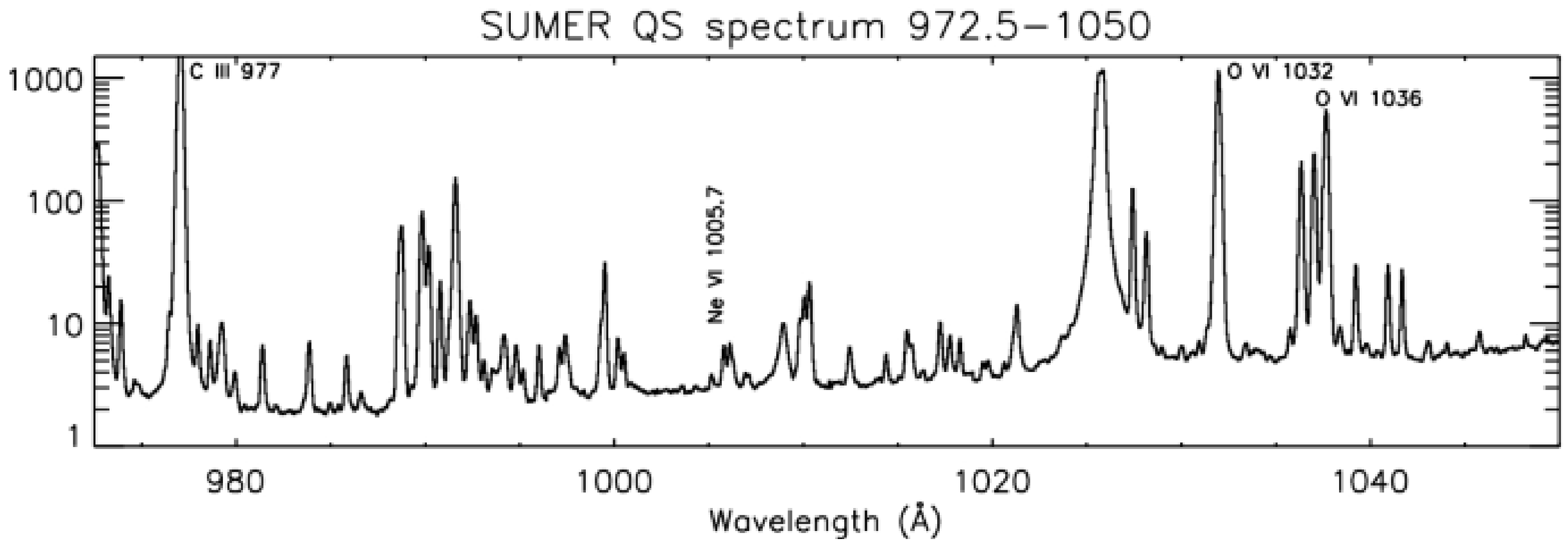

Del Zanna & Mason, LRSP (2018)
Curdt+, 2001,2004

Temperature of UV solar atmosphere line formation

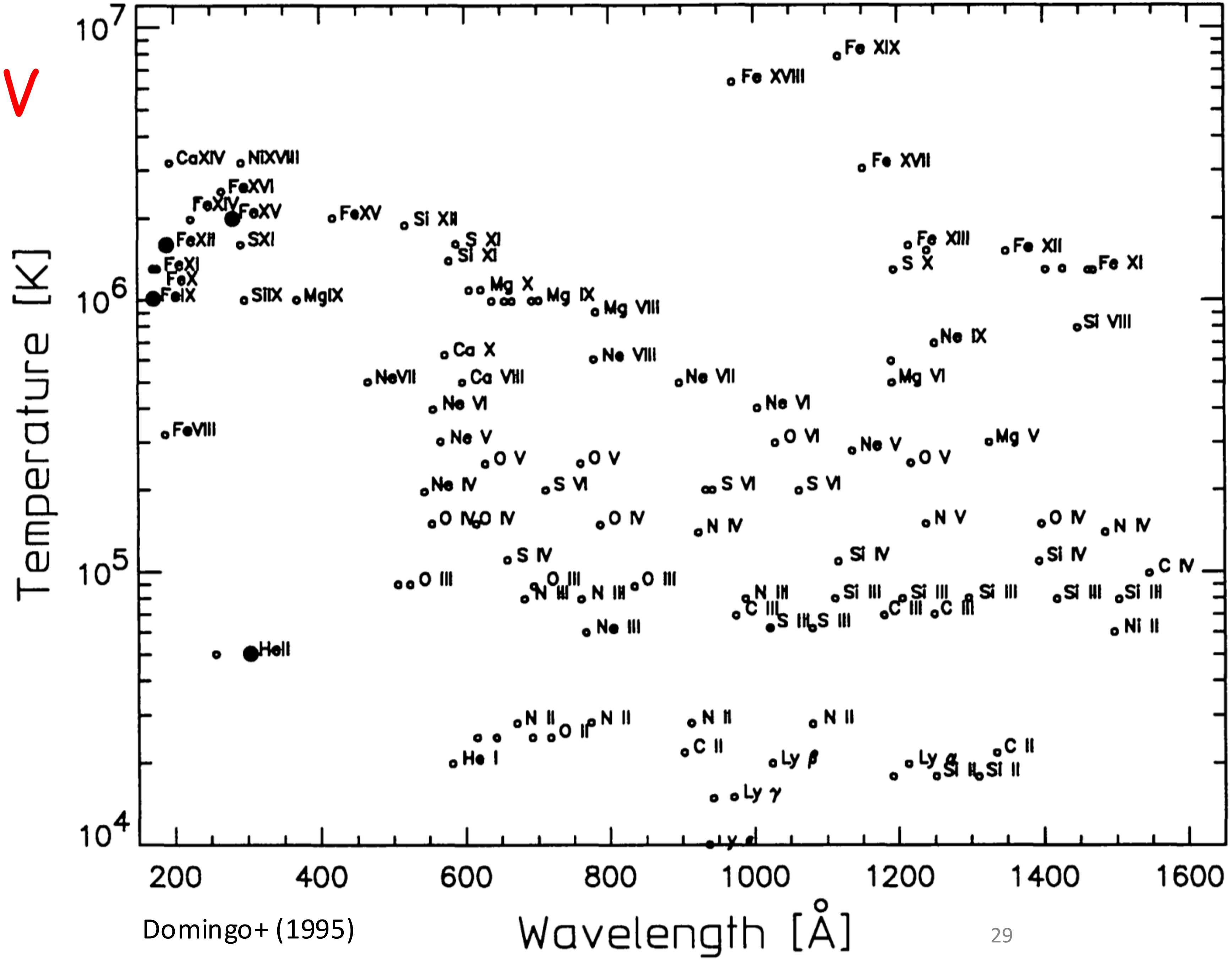

Domingo+ (1995)

Disk Imagers

AIA (Atmospheric Imaging Assembly) of SDO

Lemen, J.R., et al.,(2012), Solar Physics, DOI: 10.1007/s11207-011-9776-8

(36,000km Circular, 28.5° Geo Synch Inclined orbit).

Four telescopes → Ten wavelength band

AIA wavelength bands

Channel	Δλ††	Ion(s)	Region of Atmosphere*	Char. log(*T*)
Visible	-	Continuum	Photosphere	3.7
1700Å	-	Continuum	Temperature minimum, photosphere	3.7
304Å	12.7	He II	Chromosphere, transition region,	4.7
1600Å	-	C IV+cont.	Transition region + upper photosphere	5.0
171Å	4.7	Fe IX	Quiet corona, upper transition region	5.8
193Å	6.0	Fe XII, XXIV	Corona and hot flare plasma	6.1, 7.3
211Å	7.0	Fe XIV	Active-region corona	6.3
335Å	16.5	Fe XVI	Active-region corona	6.4
94Å	0.9	Fe XVIII	Flaring regions	6.8
133Å	4.4	Fe XX, XXIII	Flaring regions	7.0, 7.2

*Absorption allows imaging of chromospheric material within the corona;
††FWHM, in Å

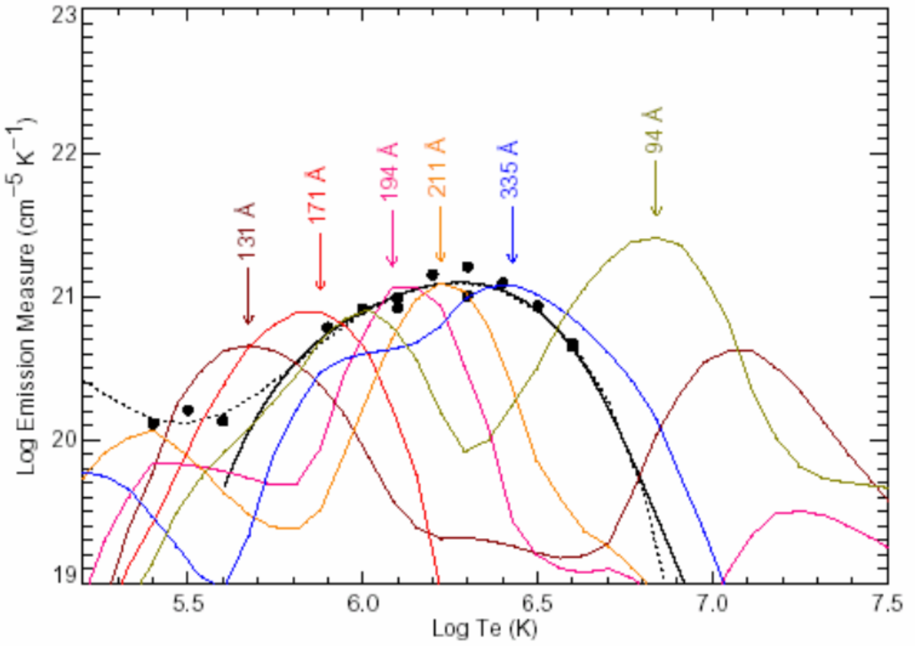

Disk Imagers (AIA)

Four Ritchey-Chretien Telescopes - 8 Science Channels

– 7 EUV Channels in a sequence of Fe line and He 304Å
– A UV Channel with 4500Å, 1600Å, 1700Å filters

- Active secondaries for image stabilization
- Four 4096 x 4096 thinned Back Illuminated CCD's (12μm pixel)

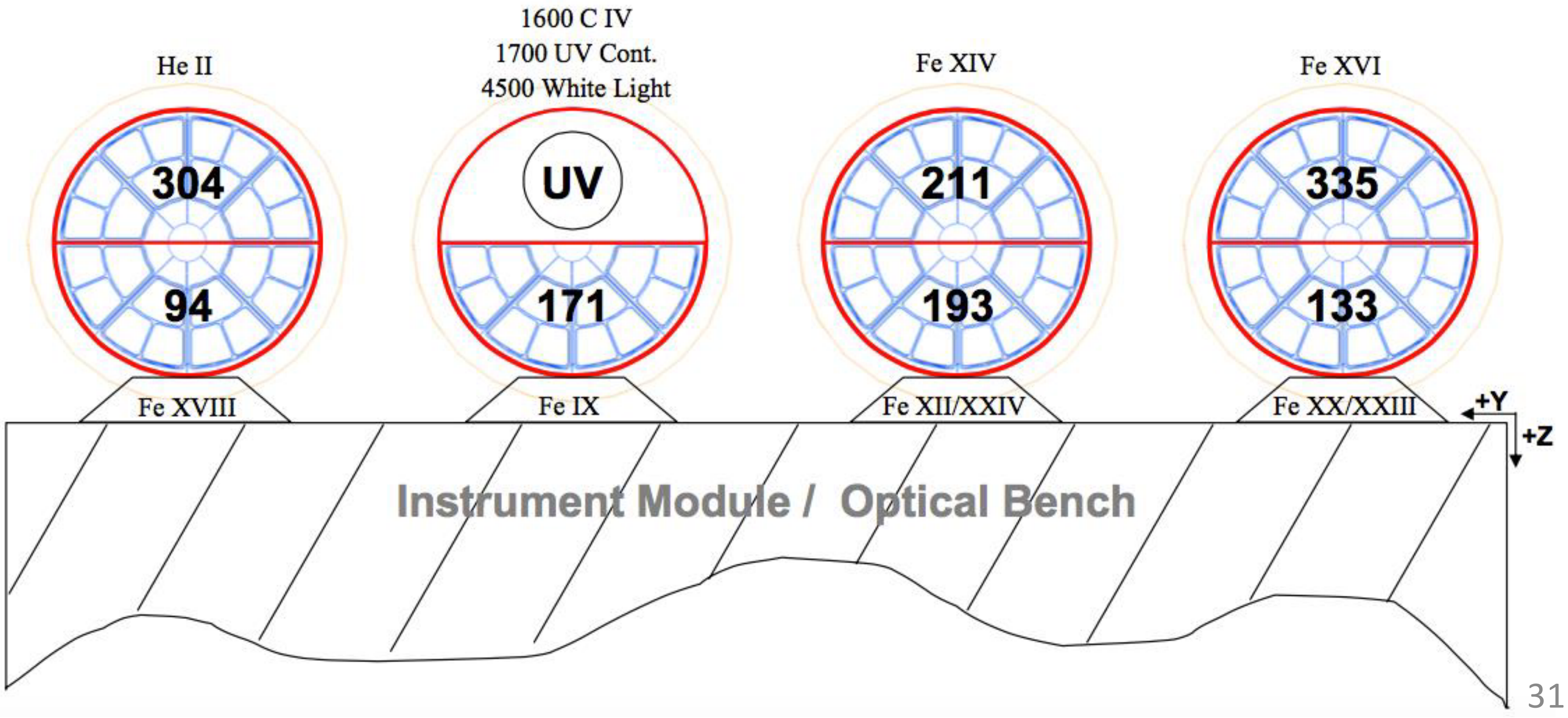

Multiband Sun

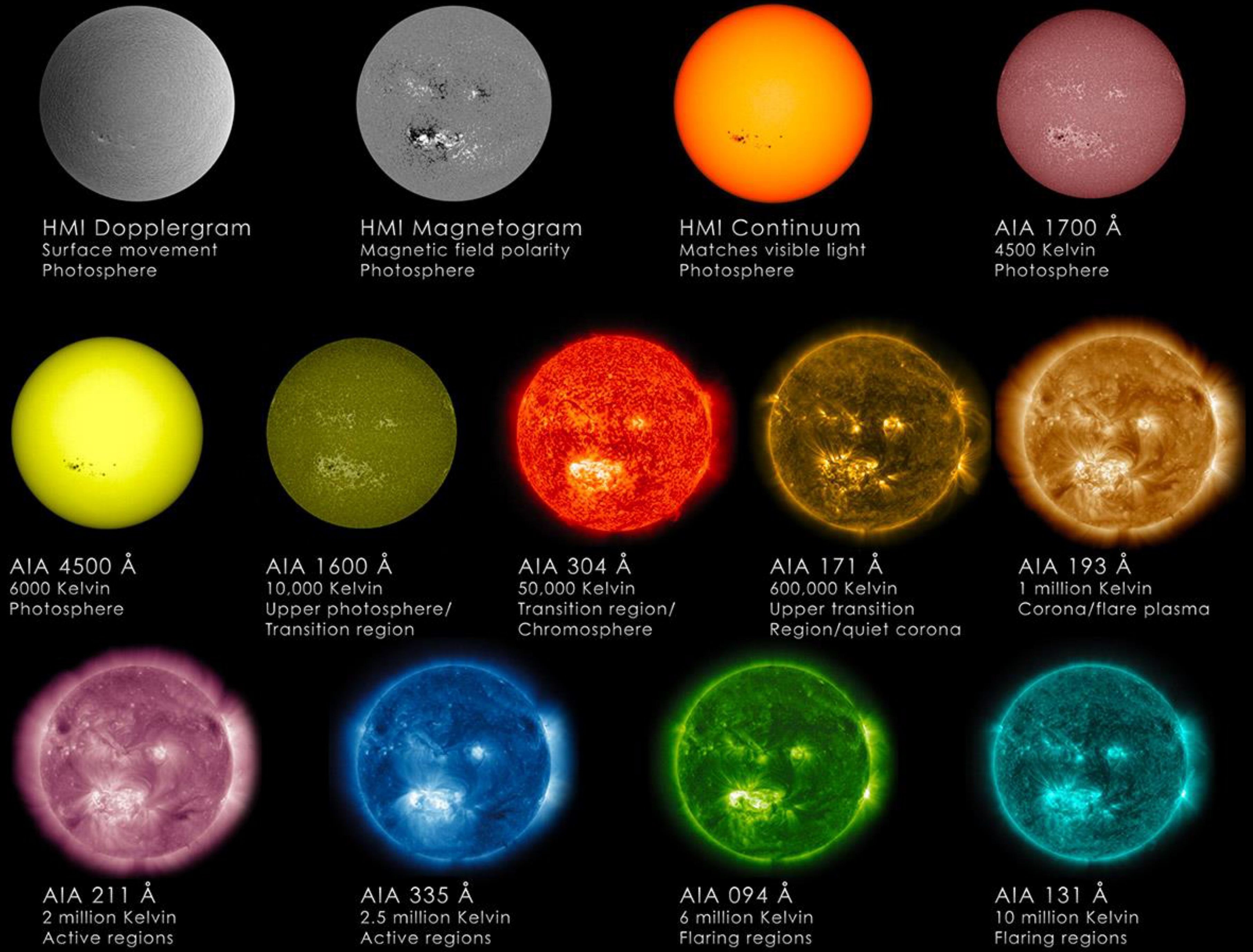

Solar Orbiter Extreme Ultraviolet Imager (EUI)

3 telescopes:

- Full Sun Imager (Fe X, HeII)
- High Resolution Imager (Lya)
- High Resolution Imager (FeX)

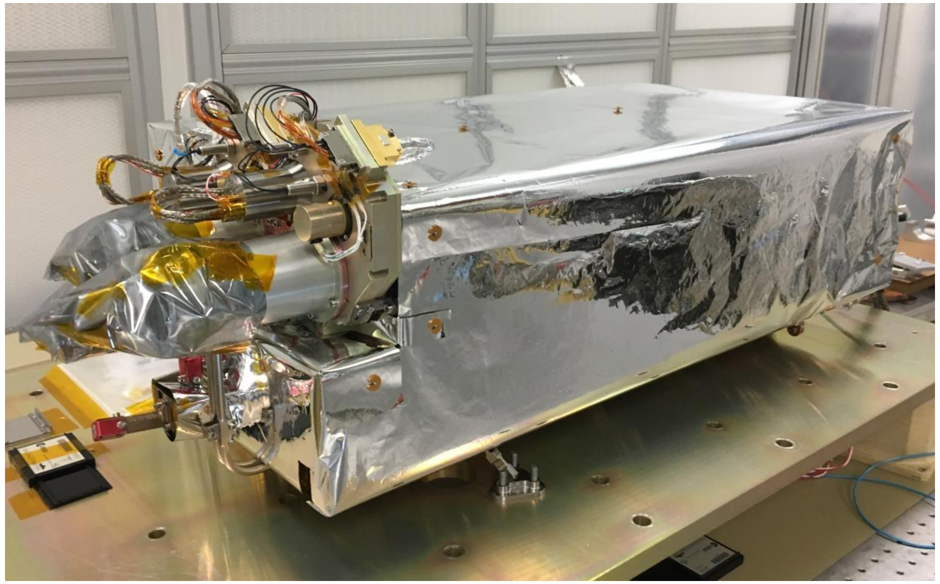

FSI Bandpass

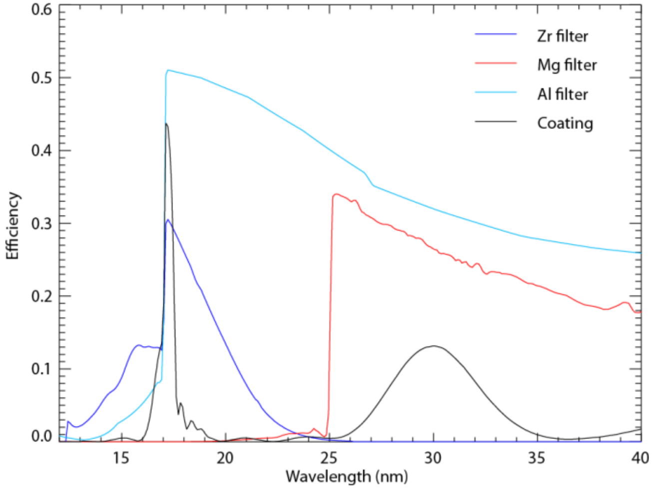

FSI dual EUV	Passband centre	174 Å and 304 Å alternatively
	Field of View	3.8 arcdeg × 3.8 arcdeg
	Resolution (2 px)	9 arcsec
	Typical cadence	600 s
HRI EUV	Passband centre	174 Å
	Field of View	1000 arc sec square
	Angular resolution (2 px)	1 arcsec
	Typical high cadence	2 s
HRI Lyman-α	Passband centre	1216 Å
	Field of View	1000 arcsec square
	Resolution (2 px)	1 arcsec
	Typical high cadence	Sub-second

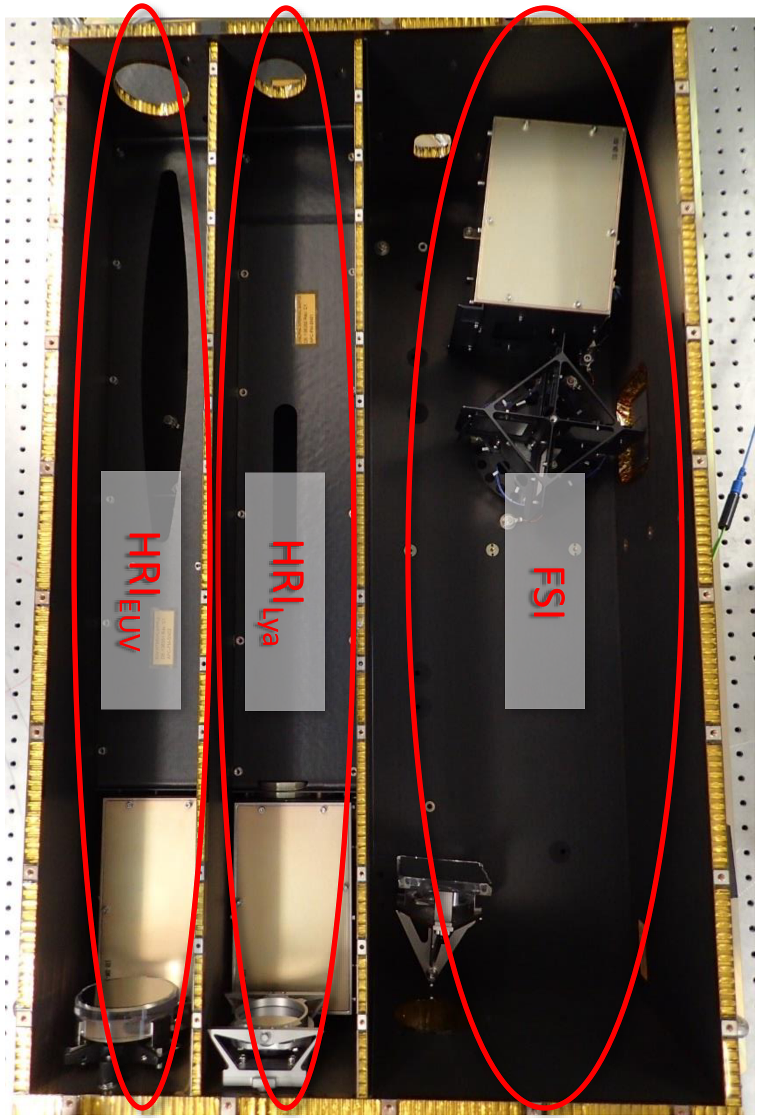

Rochus, Auchère, Berghmans, et al. 2021 A&A

Thermal response: FSI & HRI_{EUV}

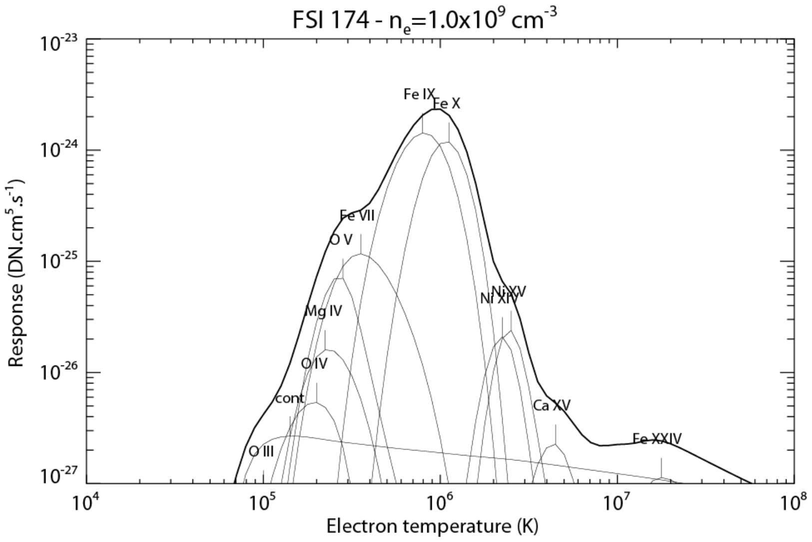

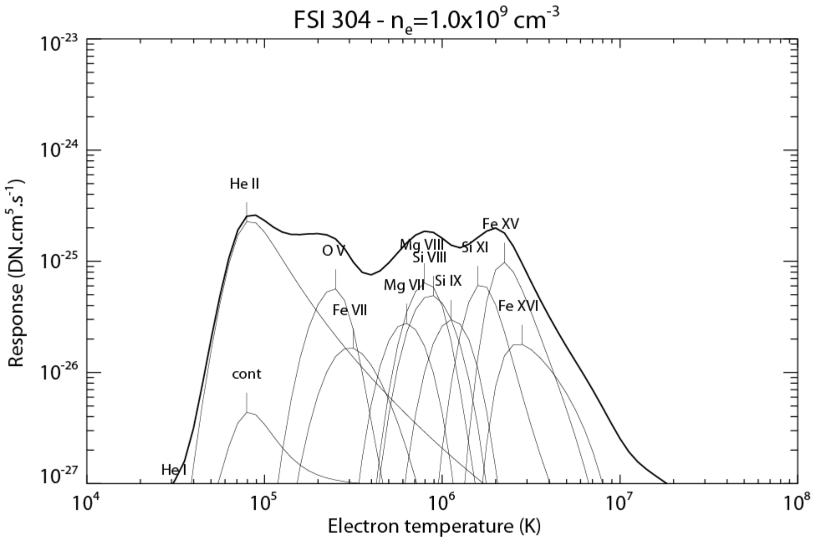

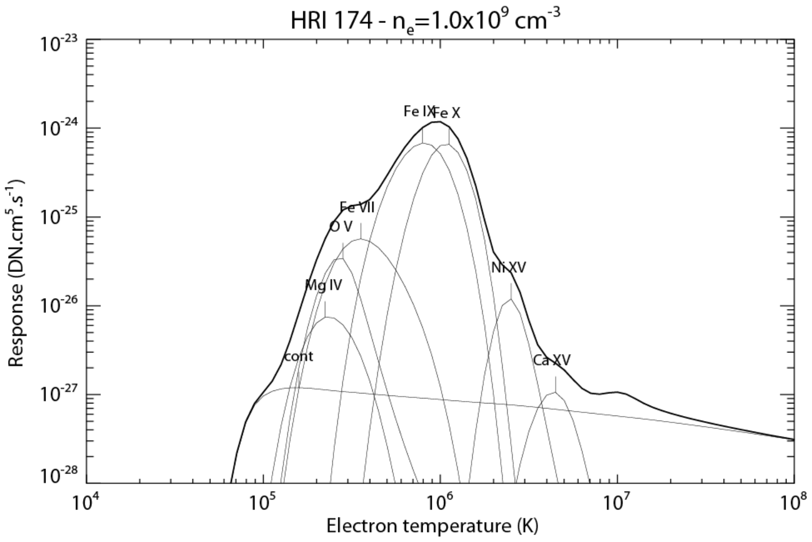

- Typical of 174 / 304 EUV imagers
- Based on pre-flight calibration
  - Subject to revisions …
- FSI_{174} & HRI_{EUV} similar
- Coronal contribution in FSI_{304}
  - Higher than in previous imagers
  - Due to single bounce design

FSI occulting disk

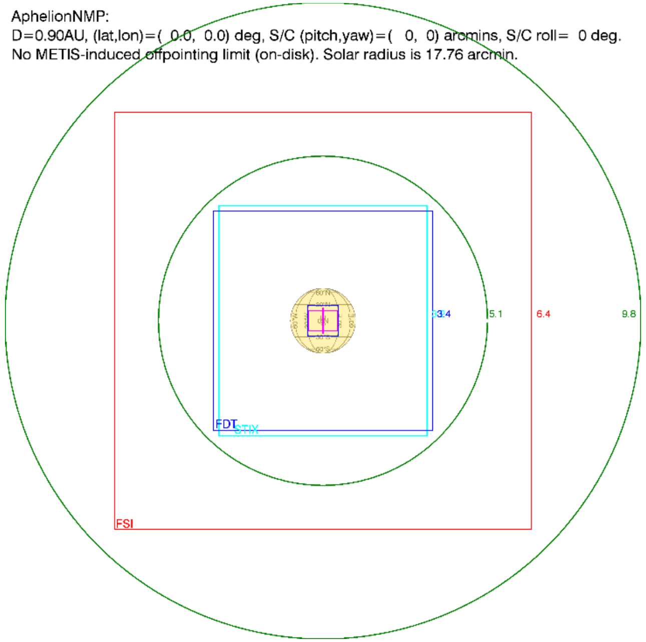

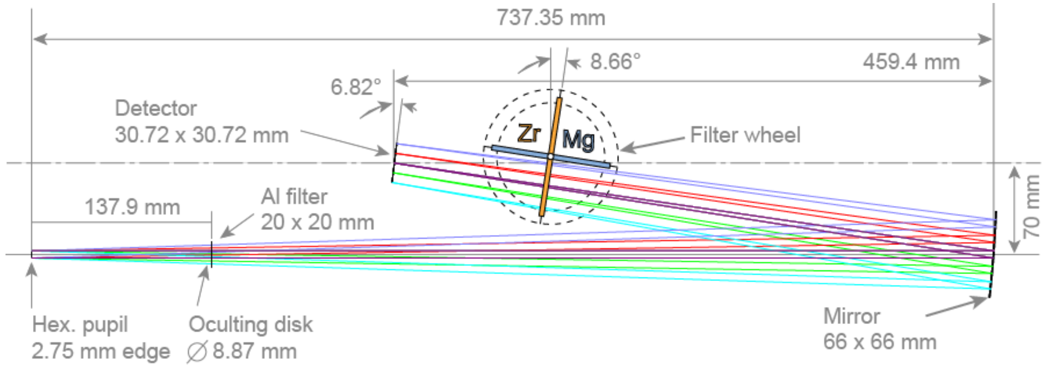

Auchere+, 2023

- 3.8°FOV: 4.1 Rs @ 0.56 AU
- Must run > 0.47au to occult disk
- Stray-light dominates above ~2Rs
- FSI can become a coronagraph
- Occulter mounted on internal door
  - Campaign mode only
  - Calibration under way

FeXI w/o occulter

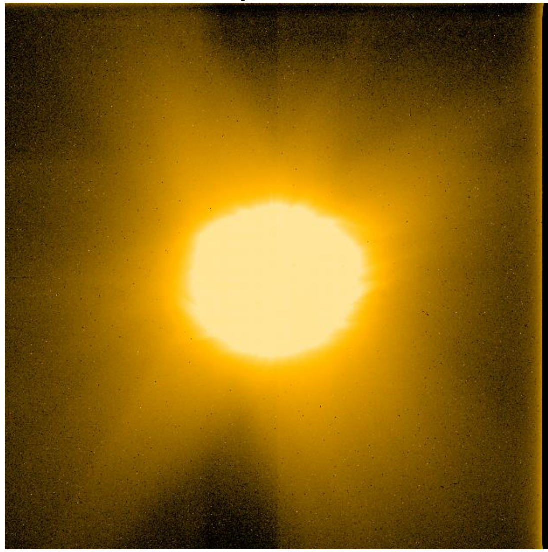

FeXI w occulter

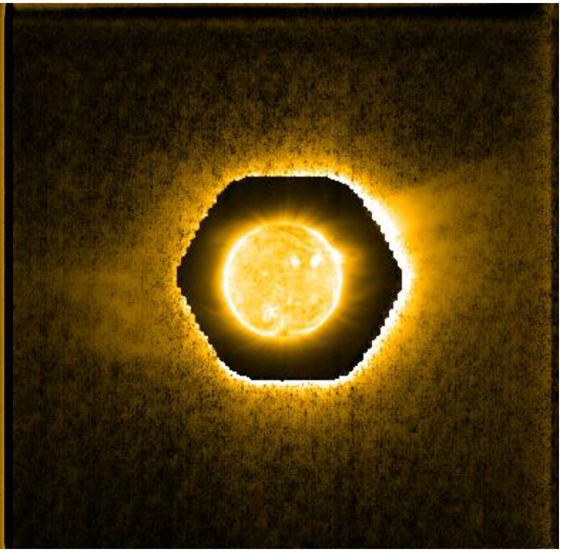

HeII

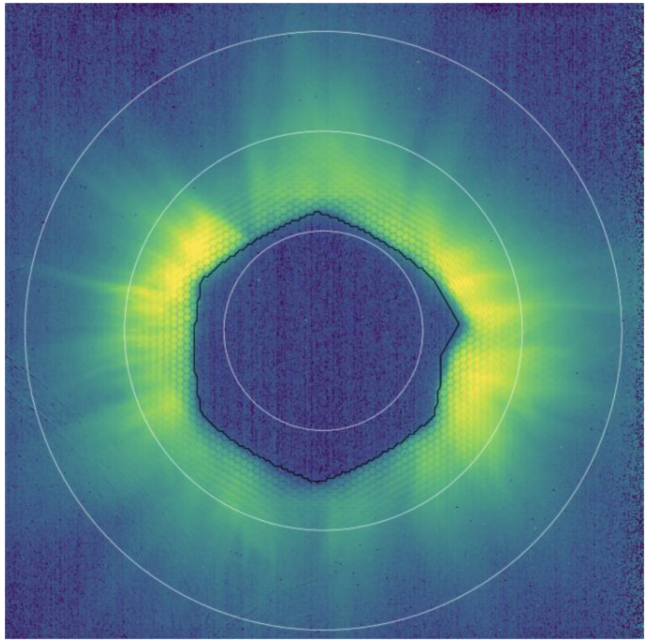

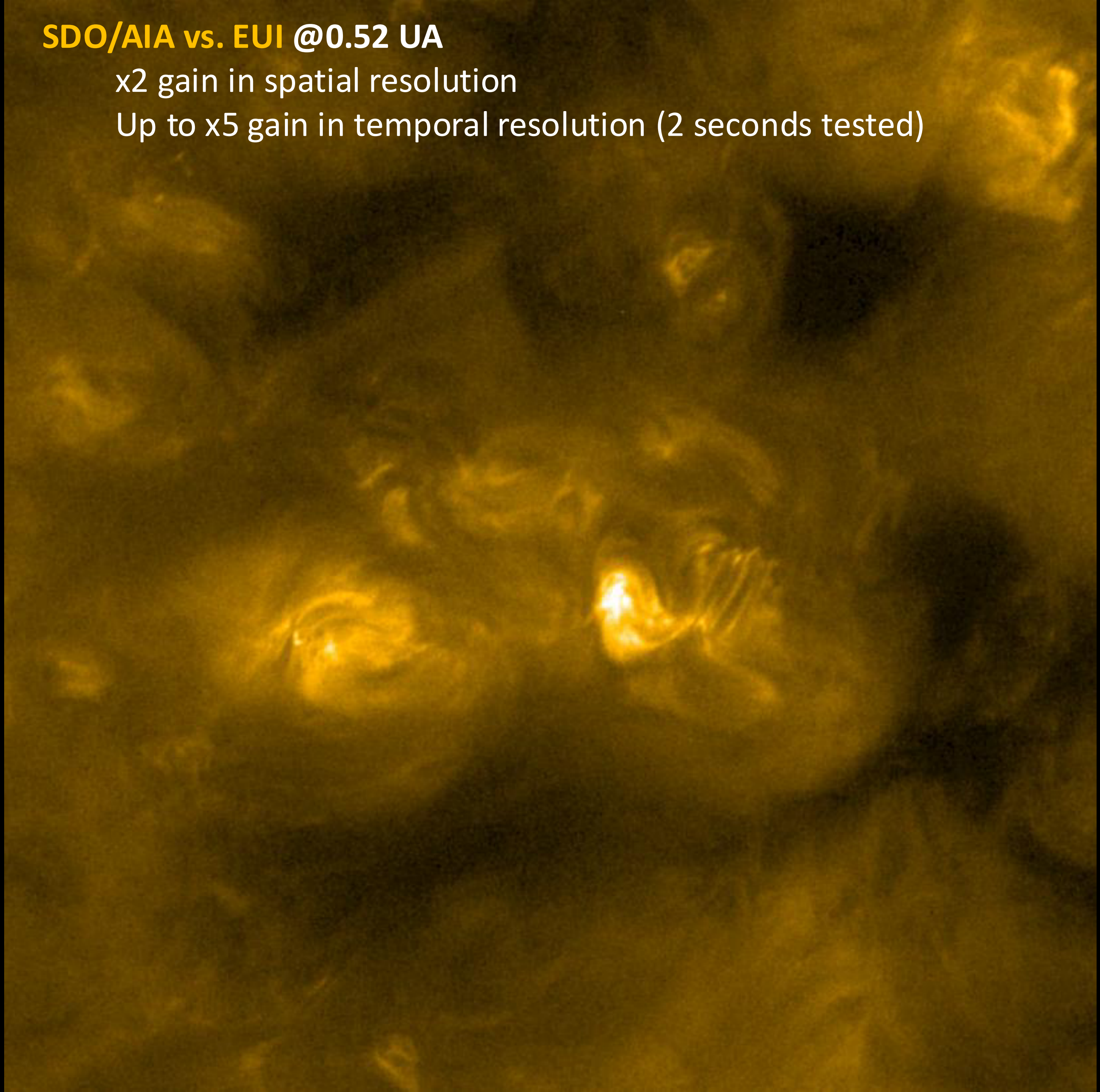
SDO/AIA vs. EUI @0.52 UA
x2 gain in spatial resolution
Up to x5 gain in temporal resolution (2 seconds tested)

Campfires!

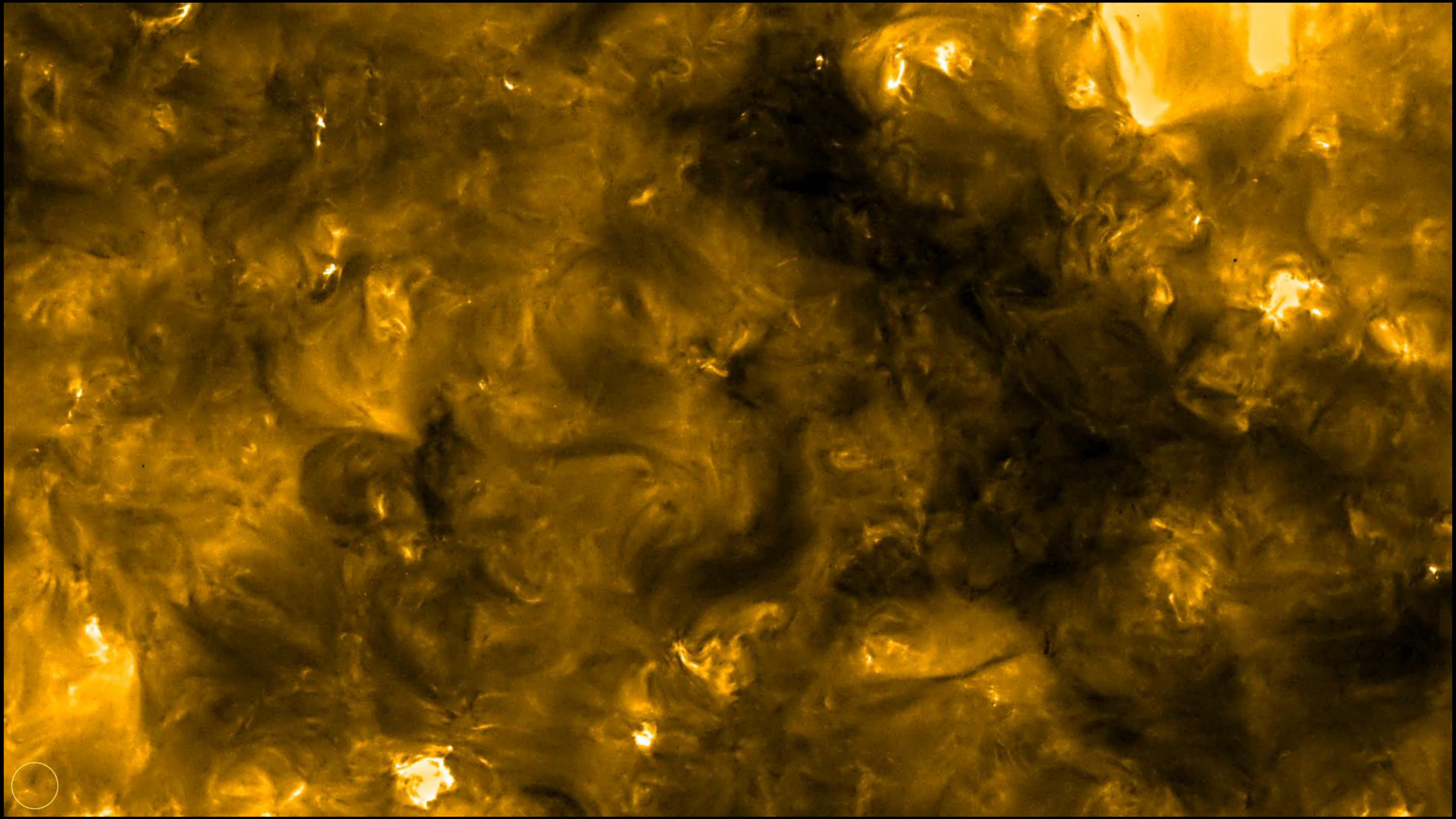

Berghmans, Auchère, Long et al. 2021 A&A

High resolution @0.31au Perihelion

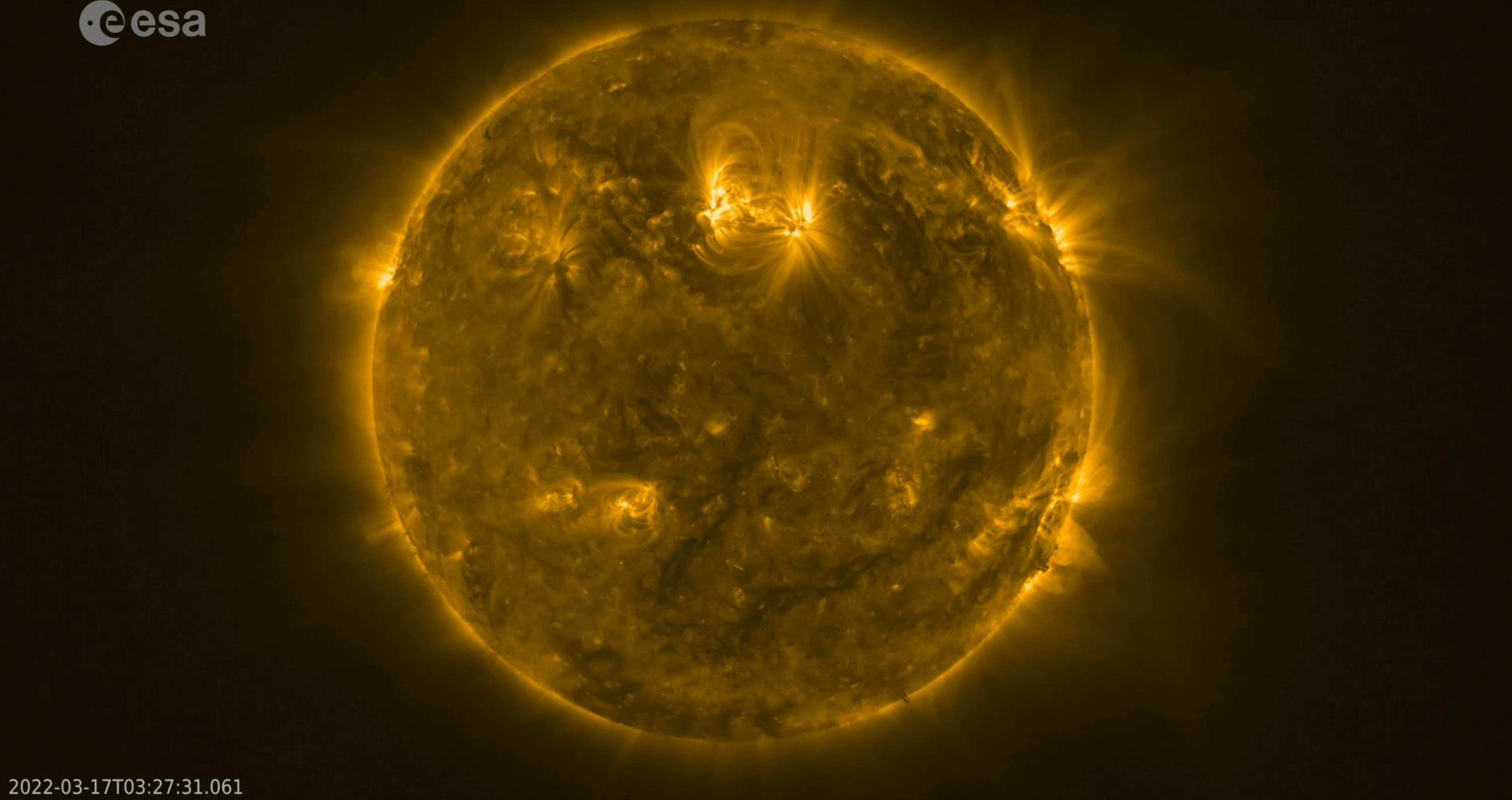

In-situ/ remote connection: slow wind sources

Coordinated observation campaigns were conducted by Hinode and IRIS. The **magnetic connectivity tool** was used, along with low latency in situ data, and full-disk remote sensing observations, to guide the target pointing of Solar Orbiter.
Solar Orbiter targeted with EUI, PHI and SPICE an active region complex, the boundary of a coronal hole, and the periphery of a decayed active region.
Post-observation analysis, using the magnetic connectivity tool along with in situ measurements from MAG and SWA/PAS, shows that slow solar wind, with velocities between ~210 and 600 km/s, arrived at the spacecraft originating from two out of three of the target regions.

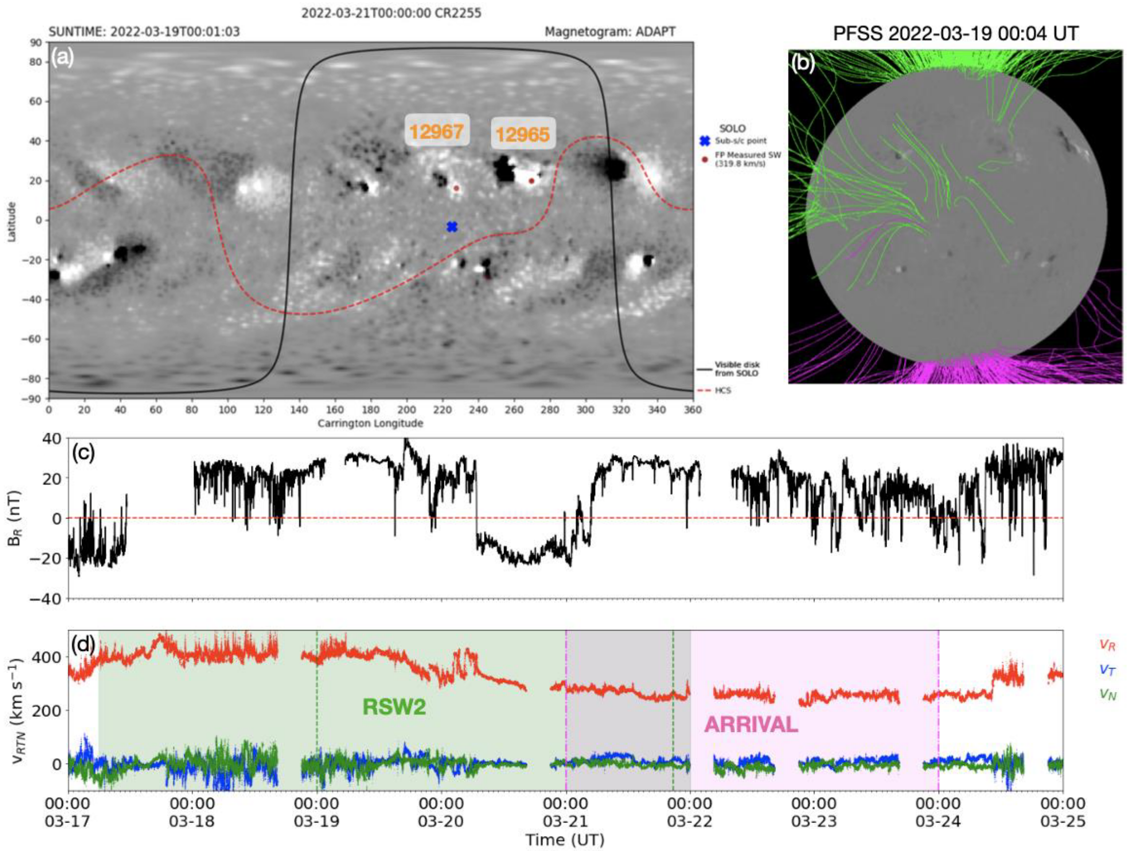

Figure 10. The SWA/PAS and MAG data taken by Solar Orbiter during the time period of 2022 March 17 to 25, along with the connectivity tool and the PFSS model taken in the middle of RSW2. Panel a shows the ADAPT magnetic field map from 2022 March 19 at 00:01:03 UT used to calculate the connectivity of Solar Orbiter on 2022 March 21 at 00:00 UT. The connectivity points (red circles) are determined by using a solar wind speed of 320 km s^{-1} measured by SWA/PAS. The online animation of panel a shows a movie of the magnetic connectivity between 2022 March 16 00:00 UT until March 26 00:00 UT(in situ time) with a cadence of 6 hr. Panel b shows an SDO/HMI magnetogram with open field lines taken from the PFSS model (created using the PFSS module from SSW developed by (Schrijver & De Rosa 2003)) taken at a similar time. Panel c shows the radial magnetic field measured by MAG and panel d shows the 3D velocity distribution functions measured by SWA/PAS. The green shaded region indicates the time period of RSW2 whereas the pink shows the corresponding solar wind arrival period taken from the connectivity tool. The first and last solar wind arrival (pink dash-dot lines) correspond to the Sun time (green dashed lines) determined from the connectivity tool, when Solar Orbiter is connected to the positive polarity of AR 12967 i.e. the second target of RSW2.

Yardley+, Slow Solar Wind Connection Science during Solar Orbiter's First Close Perihelion Passage

Magnetic connectivity tool http://connect-tool.irap.omp.eu

Hard X-ray diagnostics

The remote-sensing X-ray measurements determine intensity, spectrum, timing, and location of accelerated electrons near the Sun. In this way, STIX, together with RPW and EPD, is able to magnetically link the heliospheric region observed at the spacecraft back to regions on the Sun where the electrons are accelerated.

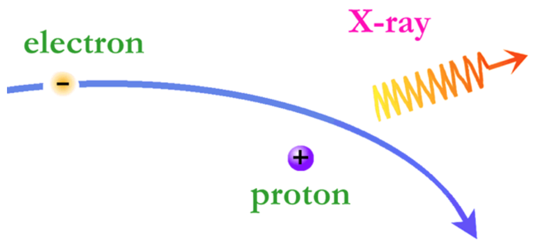

Bremsstrahlung
plus a few lines (Fe/Ni)

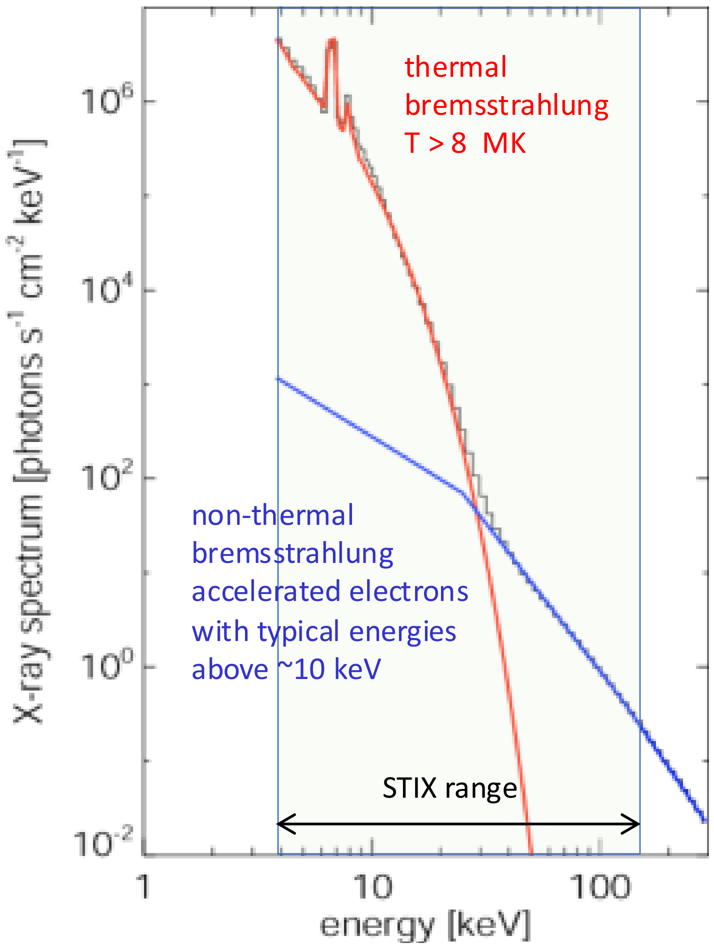

Typical X-ray spectrum of a solar flare: the red curve shows the spectrum of the hot flare loop. The blue spectrum is produced by high energetic electrons accelerated during the flare near the solar surface

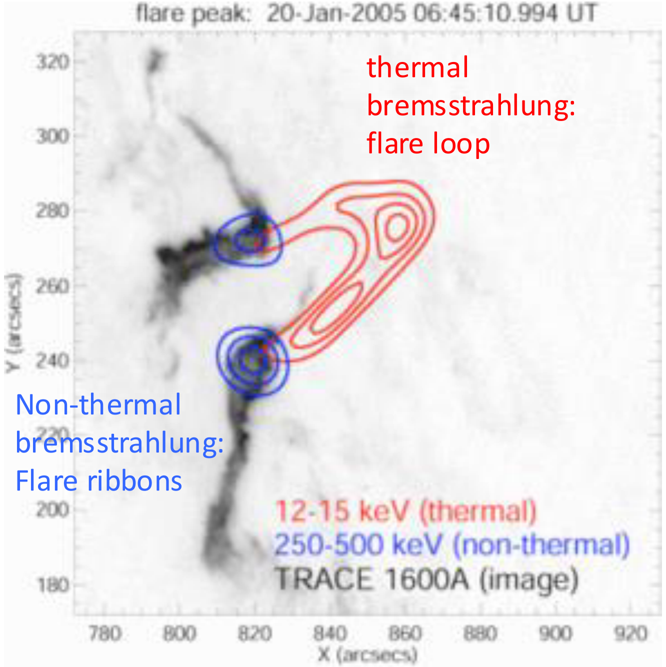

The image of the same event shows the flare loop in red with high-energy emission from the location where the flare loop is rooted in the photosphere.

Spectrometer Telescope for Imaging X-rays (STIX)

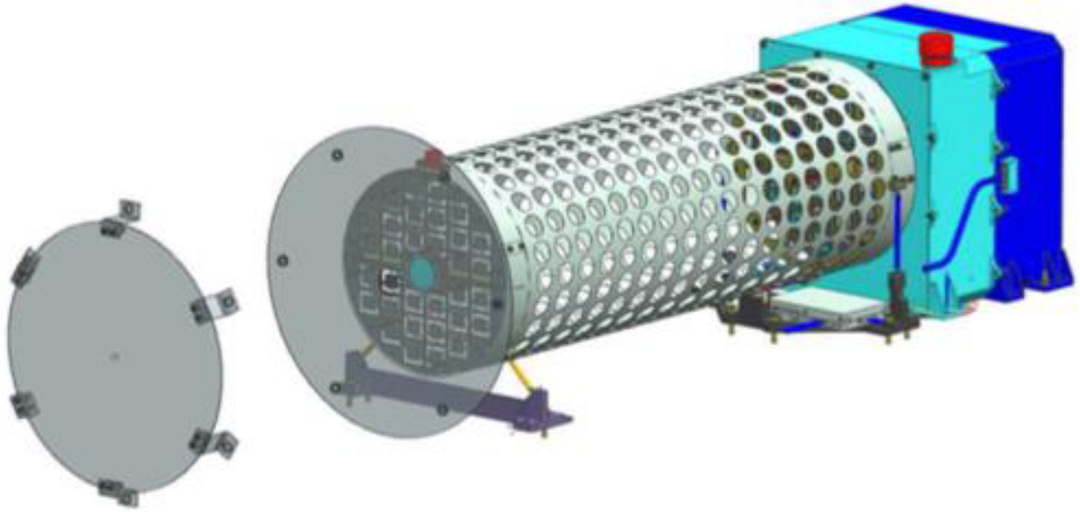

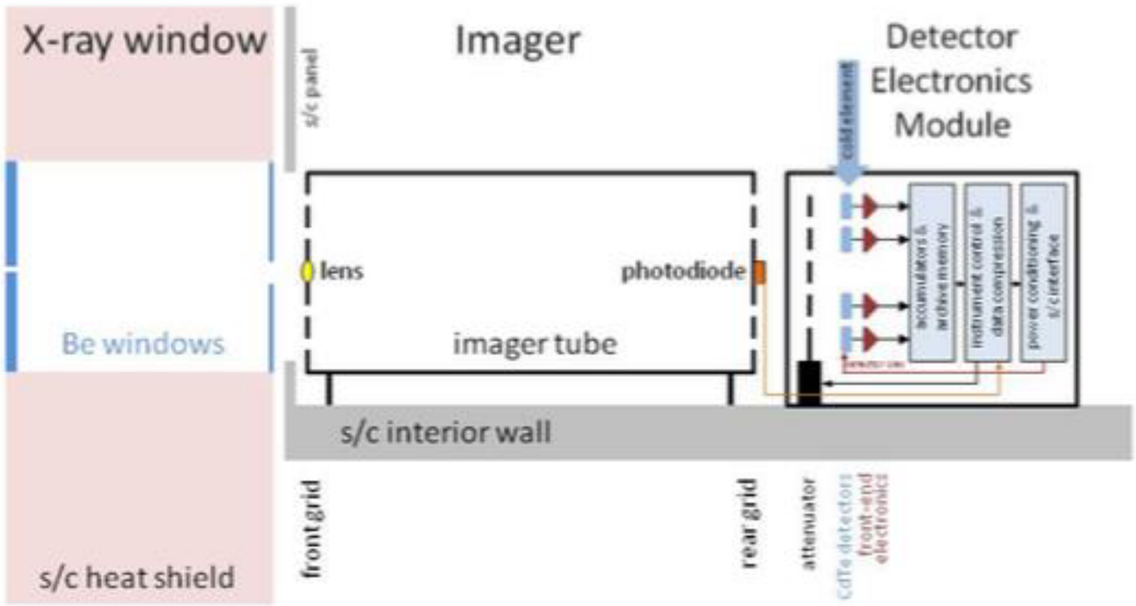

Since the use of focusing optics to achieve arcsec-class imaging over the 4-150 keV energy range is not feasible, STIX uses collimator-based, indirect imaging, similar to that used by Yohkoh/HXT and RHESSI to measure Fourier components of the source distribution.

Krucker+, 2020

STIX

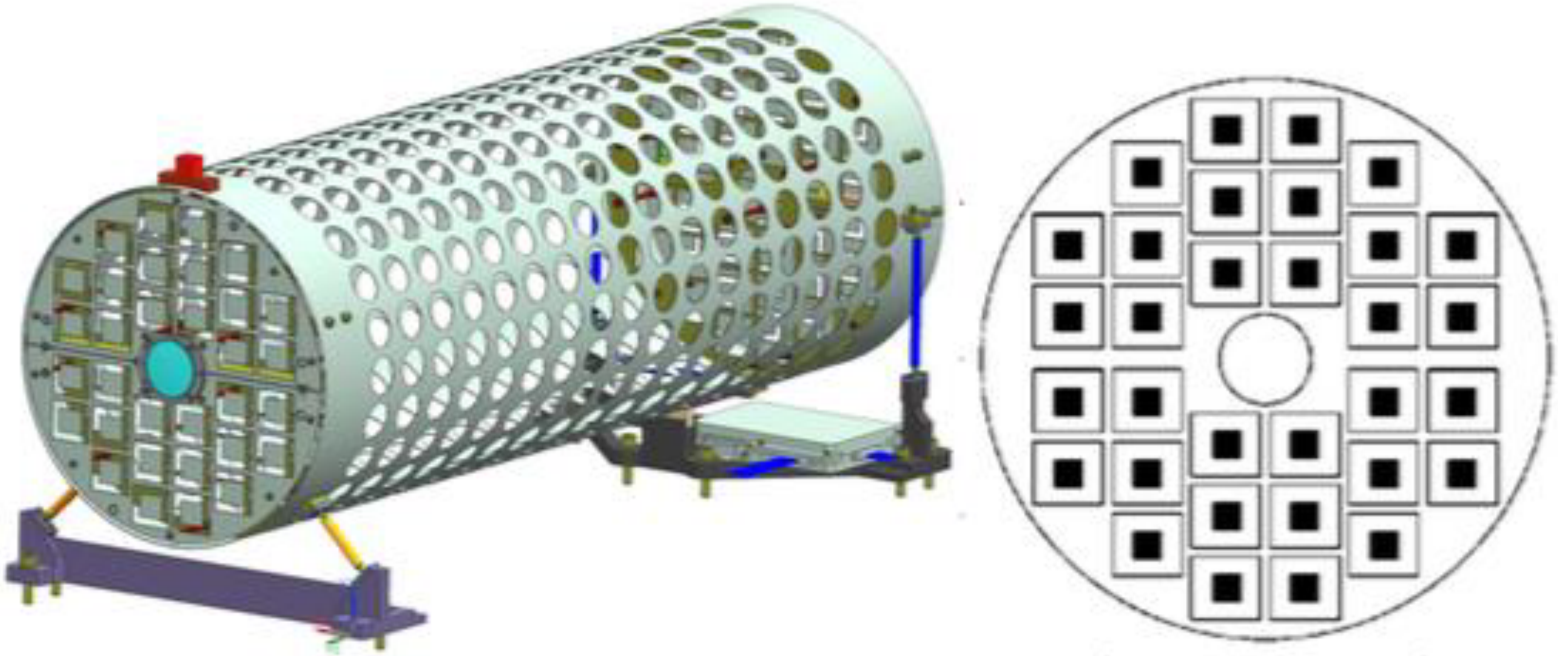

Figure 4. *Left:* The STIX Imager. *Right:* Layout of the front grid assembly. Its 180 mm diameter contains thirty-two 22 mm × 20 mm subcollimators (open rectangles) as well as room for an aspect lens at its center. The rear grid assembly is similar except that there is no lens and the subcollimators dimensions are only 15 mm × 15 mm. The solid squares represent the 10 mm × 10 mm^2 detectors located in the DEM behind the grids.

Energy Range	4 – 150 keV
Energy Resolution (FWHM)	1-15 keV (energy dependent)
Effective area	6 cm^2
Finest angular resolution	7 arcsec
Field of view	2°
Image placement accuracy	~4 arcsec
Time resolution (statistics limited)	≥ 0.1 s

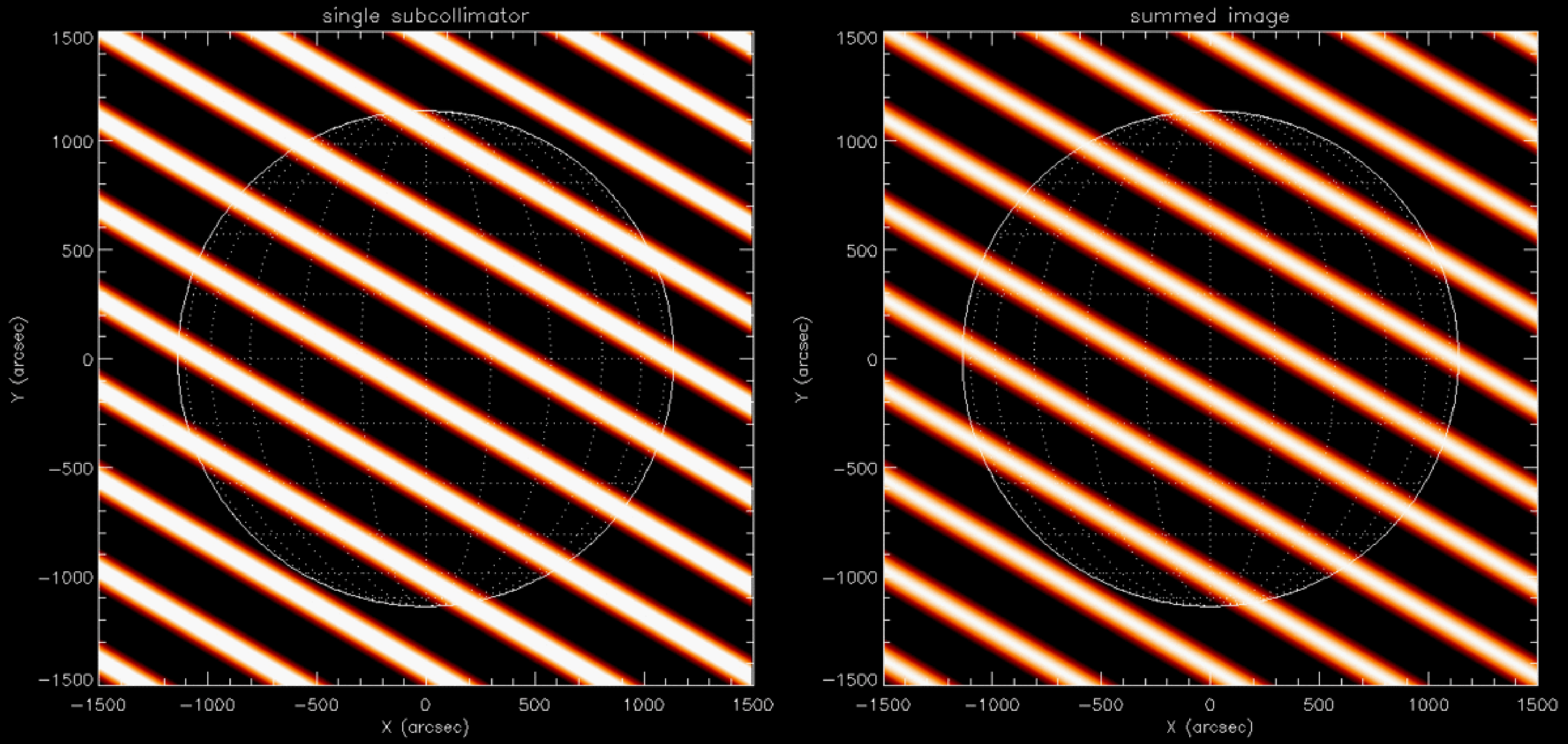

Flare of April 17, 2021

EUI + STIX captured a solar flare erupting from an active region on the face of the Sun on 2 March 2022.

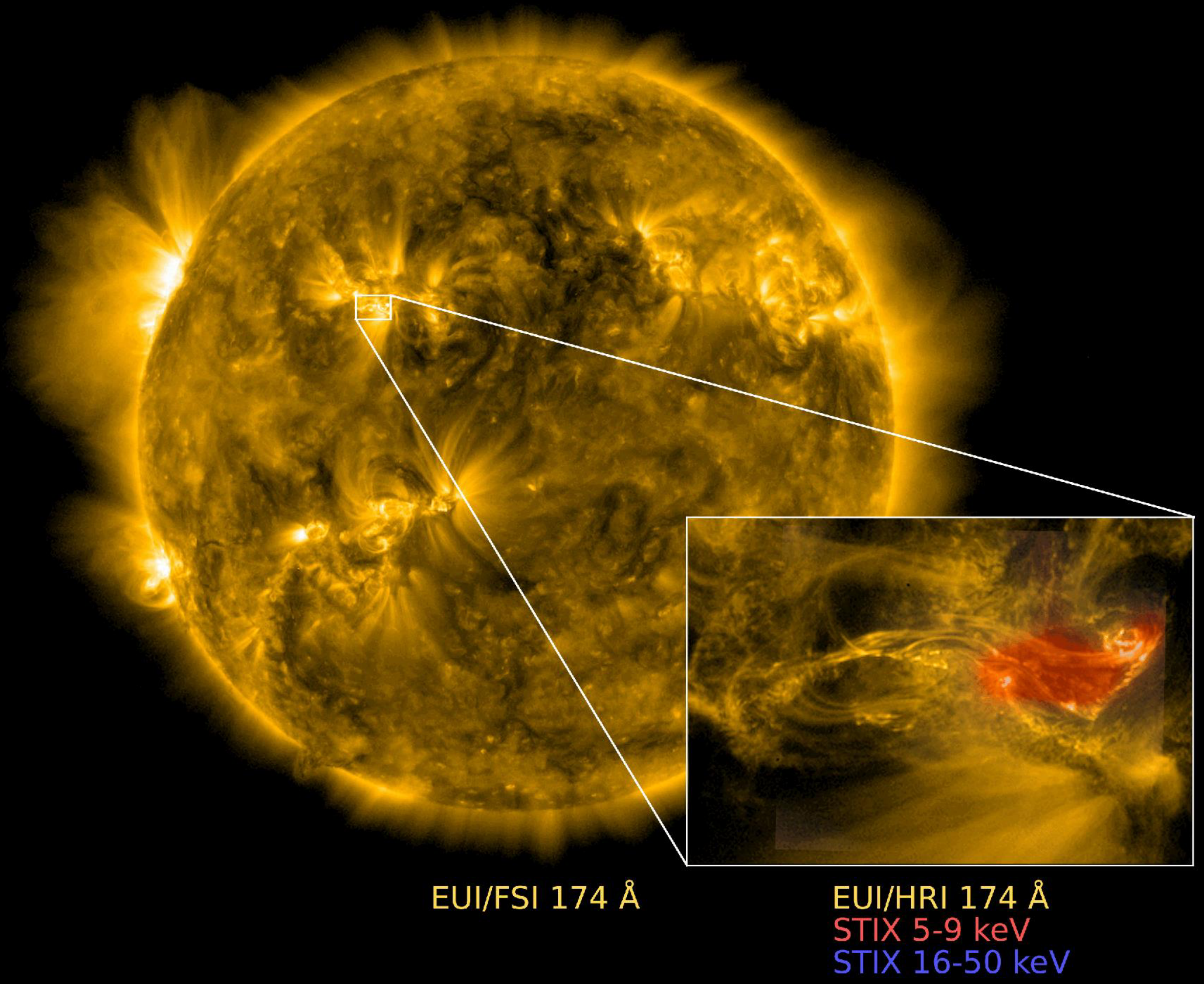

A. Battaglia, FHNW/ETH

Coronagraphs

A coronagraph is a telescope that by means of an occulting disk performs an artificial eclipse of the Sun.
Two main configurations are used:

- Internally occulted coronagraph (Lyot coronagraph)
- Externally occulted coronagraph

- Internally occulted coronagraphs:
    - constant pupil aperture
    - Necessary to observe the corona close to the limb
    - All ground based coronagraphs are internally occulted

- Externally occulted coronagraphs
    - Variable entrance pupil (vignetting)
    - Necessary to observe the extended corona
    - Almost all space coronagraphs are externally occulted

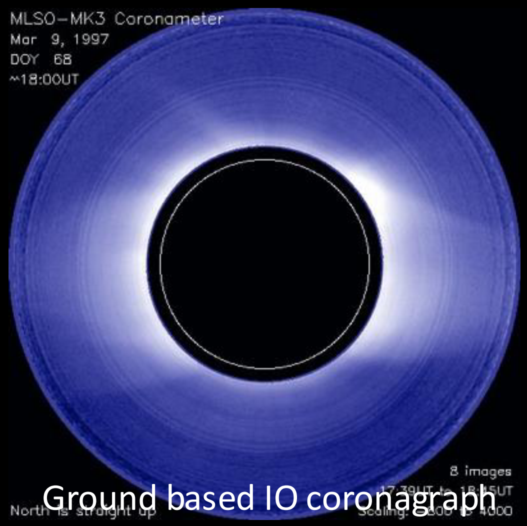

Ground based IO coronagraph

Eclipse
Eclipse
Eclipse


Space EO coronagraph
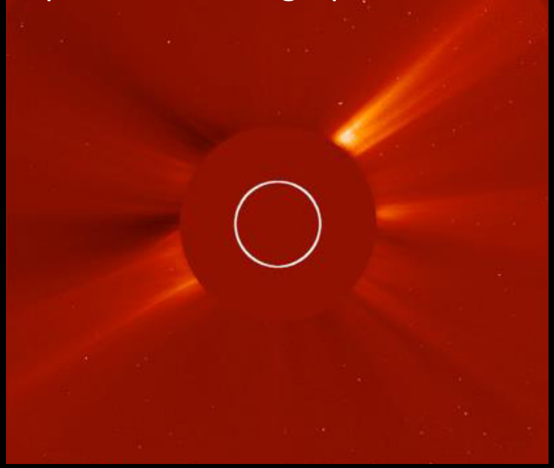

Space heliospheric imager
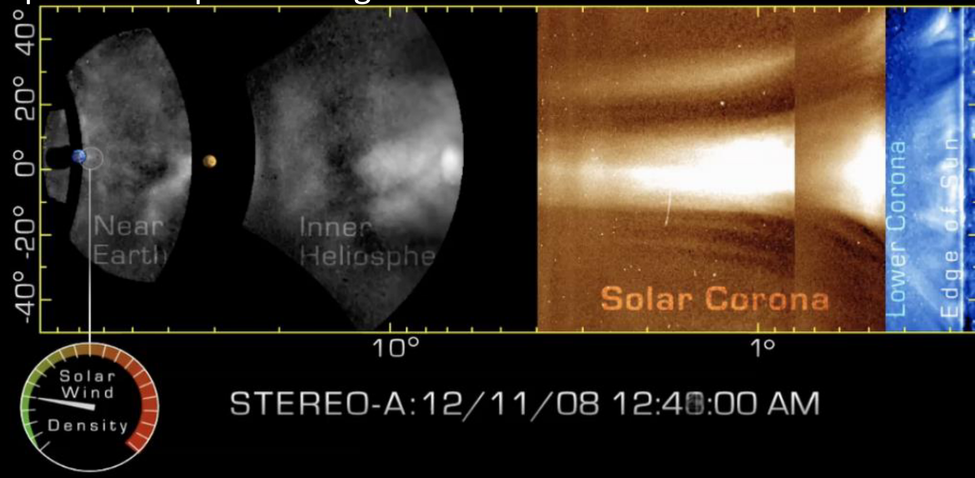

Lyot coronagraph

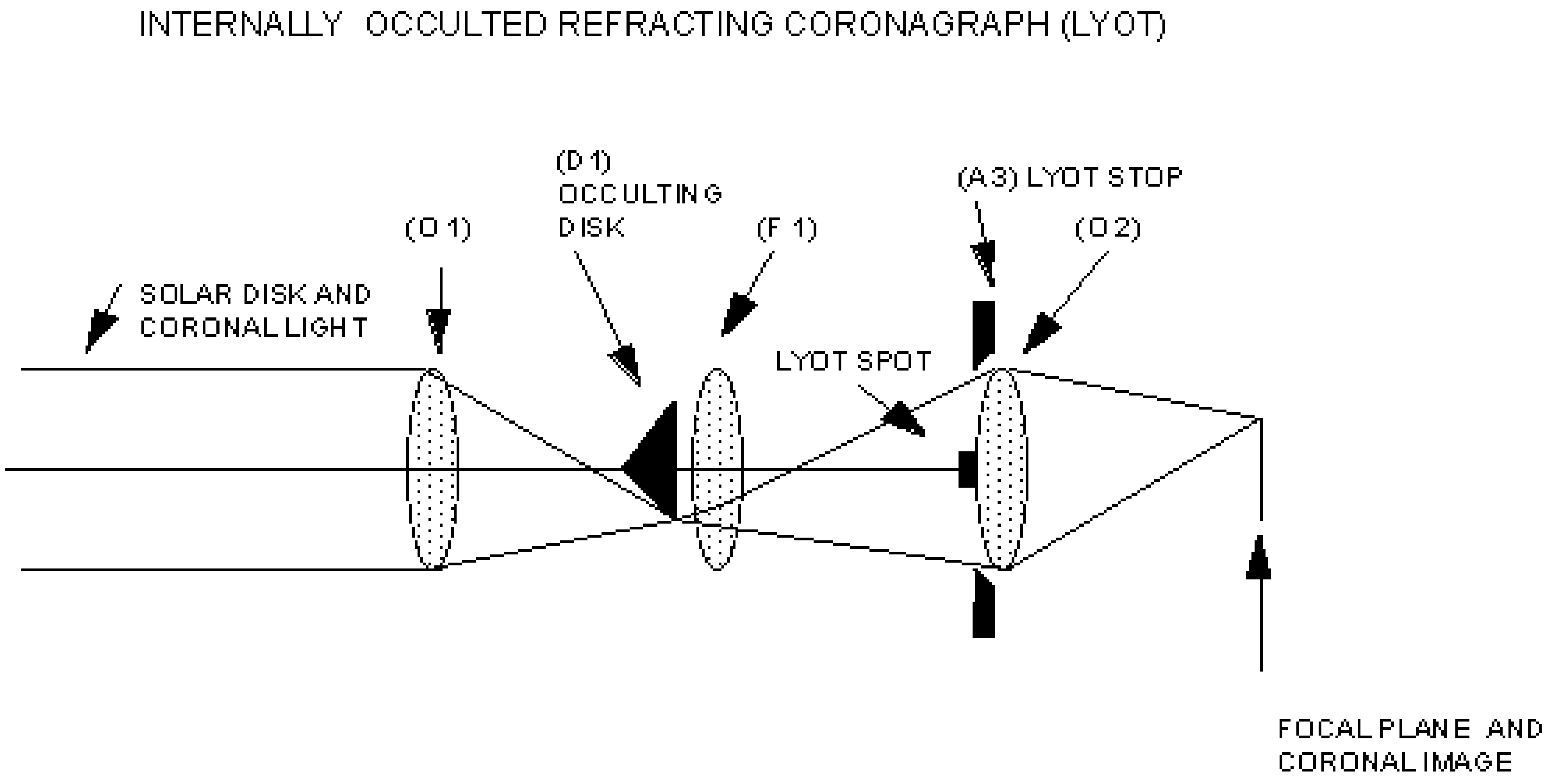

Space internally occulted coronagraph

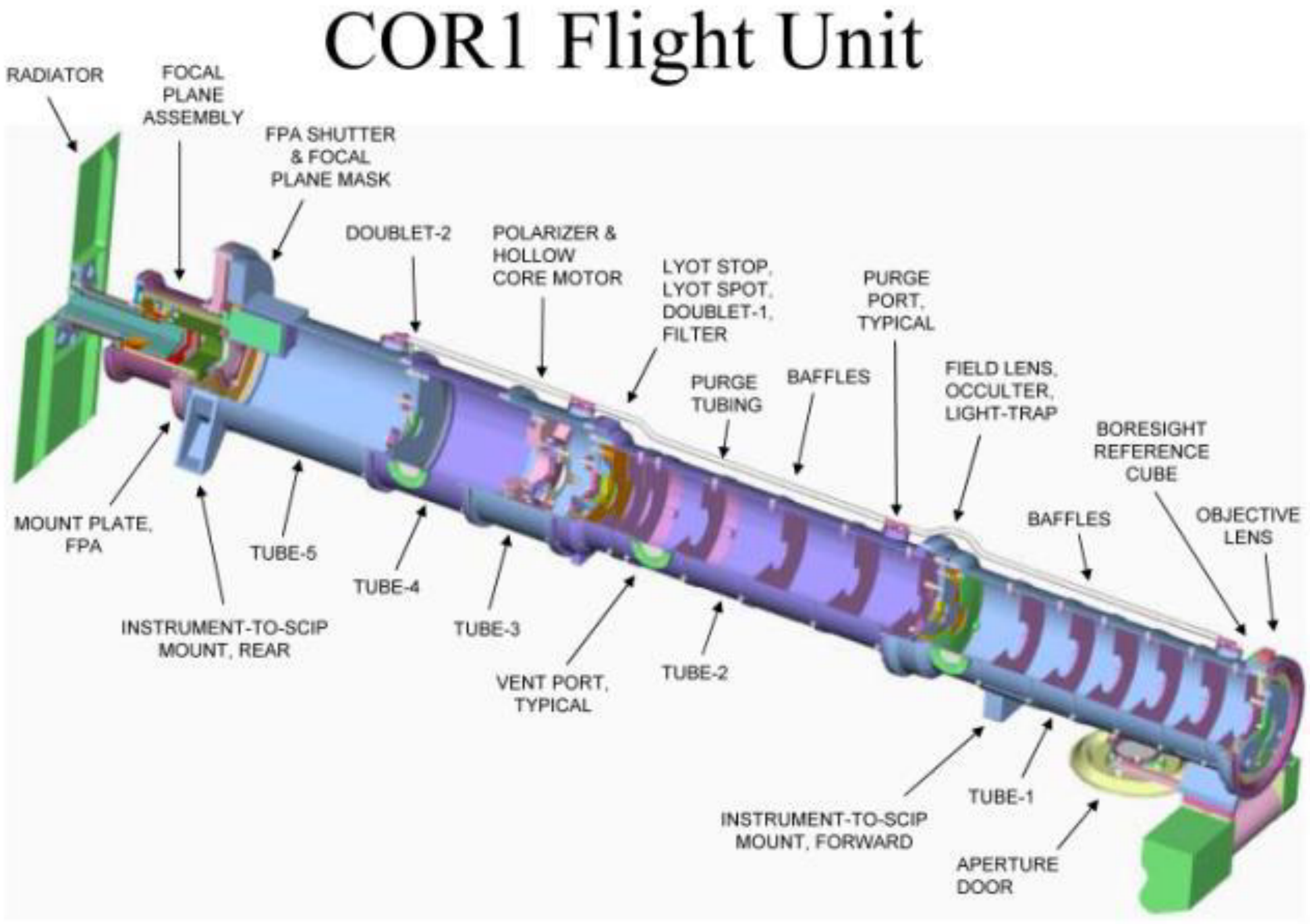

Stereo-Cor1 (1.3 – 4 Rs)
and LASCO/C1 (1.1 – 3 Rs)
are the only internally occulted space coronagraphs
(Now LST on board of ASO-S)

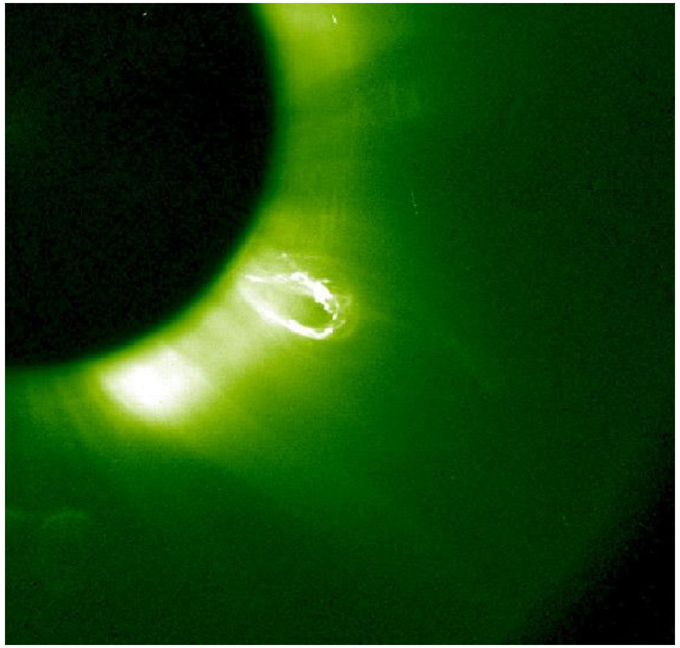

Externally occulted coronagraph

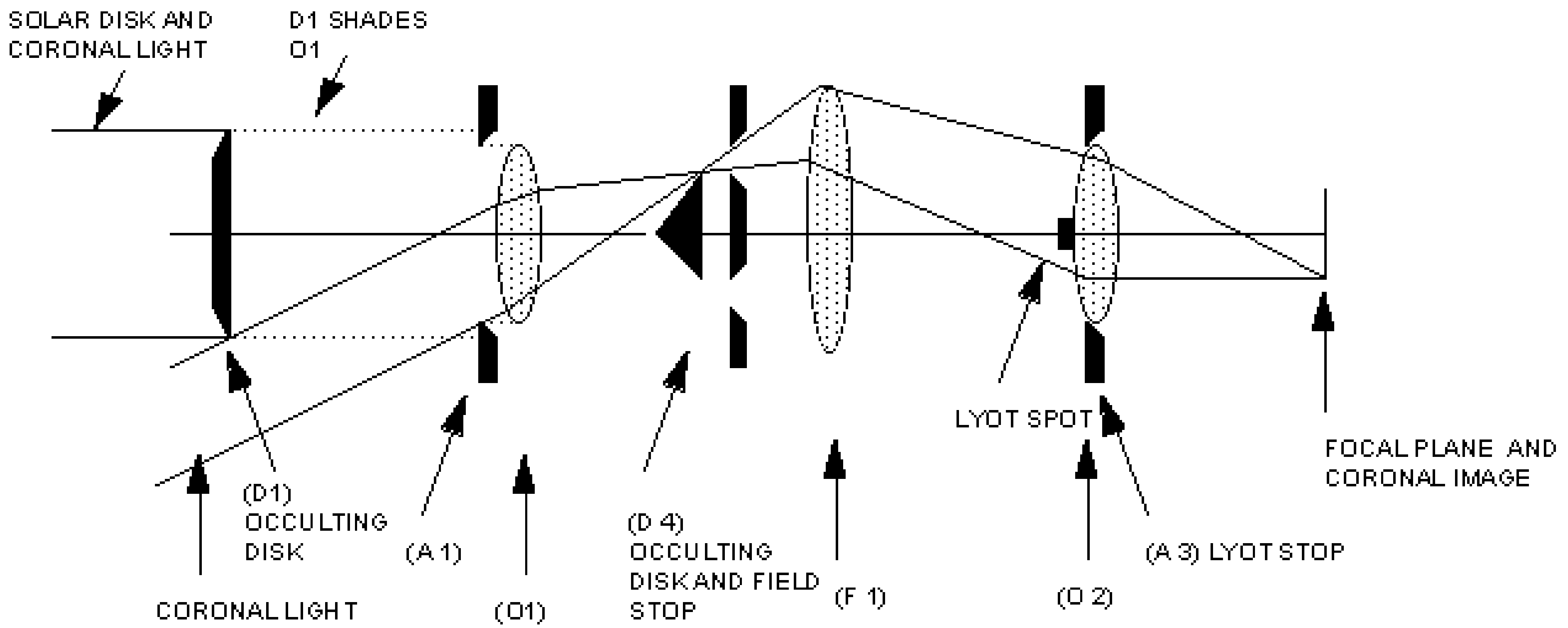

EXTERNALLY OCCULTED REFRACTING CORONAGRAPH (NEWKIRK)

Metis: the Solar Orbiter coronagraph

Antonucci+, 2020

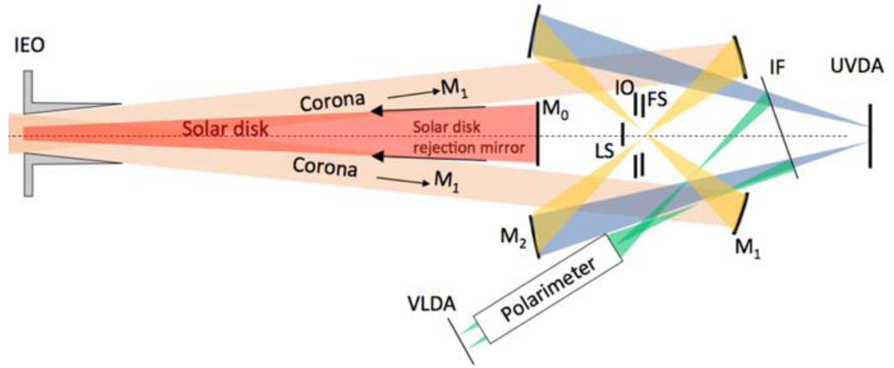

Metis is an externally-occulted coronagraph designed to provide full imaging of the extended corona (~ 1.7-9 $R_\odot$) in:

- **total and polarised visible-light brightness** (580-640 nm) and
- **UV HI Lyman-α line** (121.6 ± 10 nm)

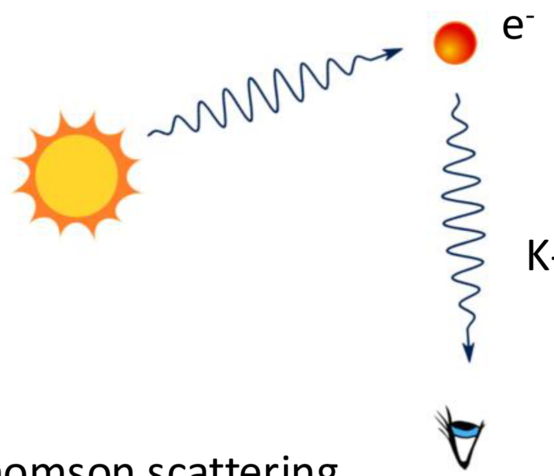

Thomson scattering

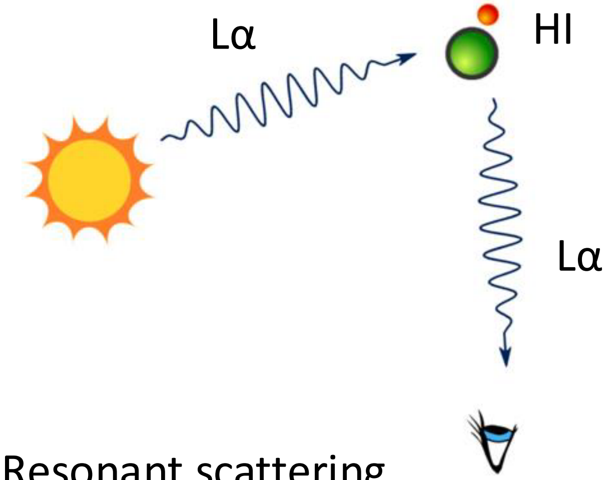

Resonant scattering

Inverted occultation principle

Classical external occultation

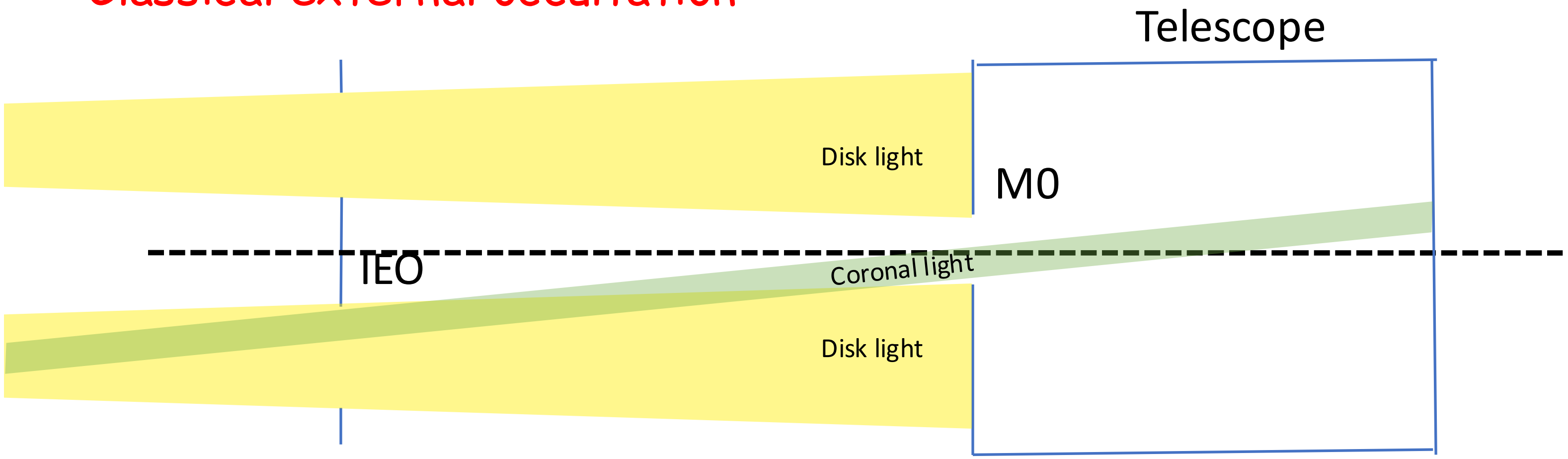

Inverted external occultation

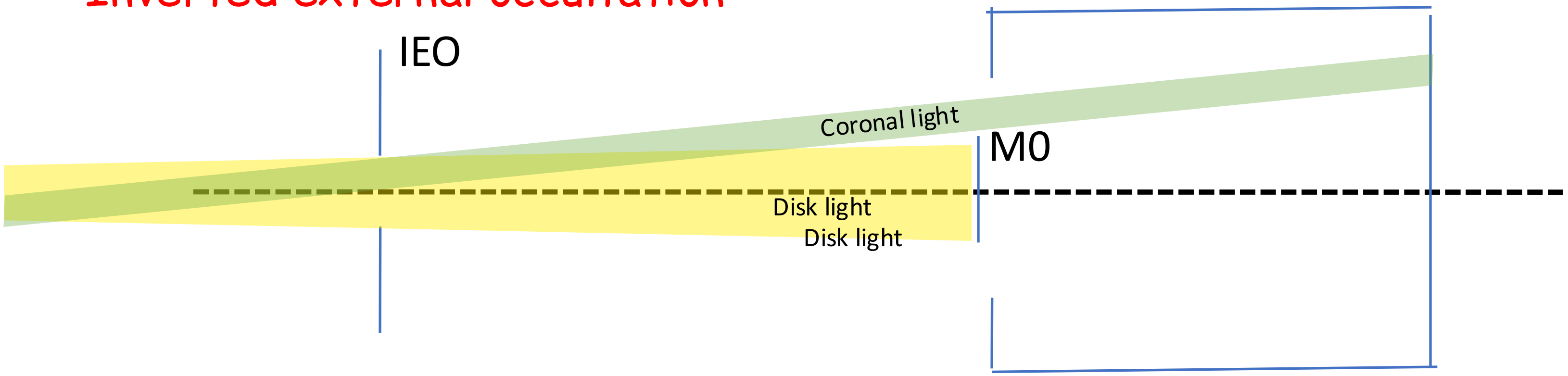

Metis: the Solar Orbiter coronagraph

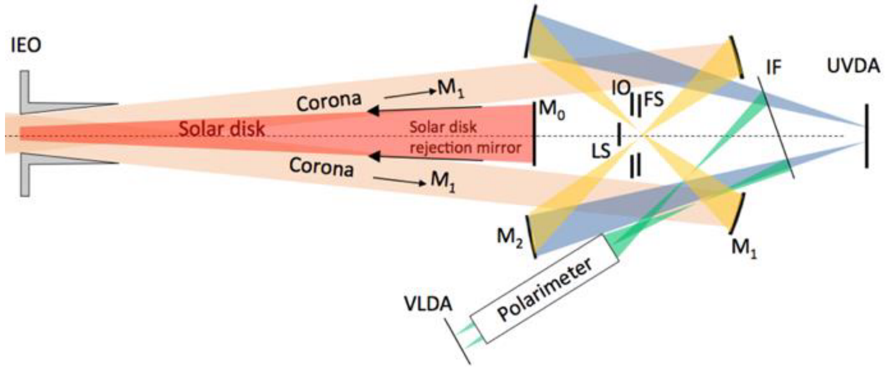

Metis is an externally-occulted coronagraph designed to provide full imaging of the extended corona ($\sim$ 1.7-9 $R_\odot$) in:

- **total and polarised visible-light brightness** (580-640 nm) and
- **UV HI Lyman-α line** (121.6 ± 10 nm)

Metis observations allow the investigation of the:

- density distribution of coronal e^- and HI atoms (protons)
- 2D solar-wind outflow (HI/proton component)
- large-scale dynamics of e^- and HI in CMEs and other solar transients

Doppler dimming

- The coronal radiation is mainly produced by collisions with free electrons and through resonant scattering of chromospheric photons by coronal atoms/ions (dominant in the case of the Lyα emission). The observed radiation reduction is linked to the Doppler shift of chromospheric photons as seen by the flowing coronal atoms/ions (e.g., see Withbroe et al. 1982; Noci et al. 1987).

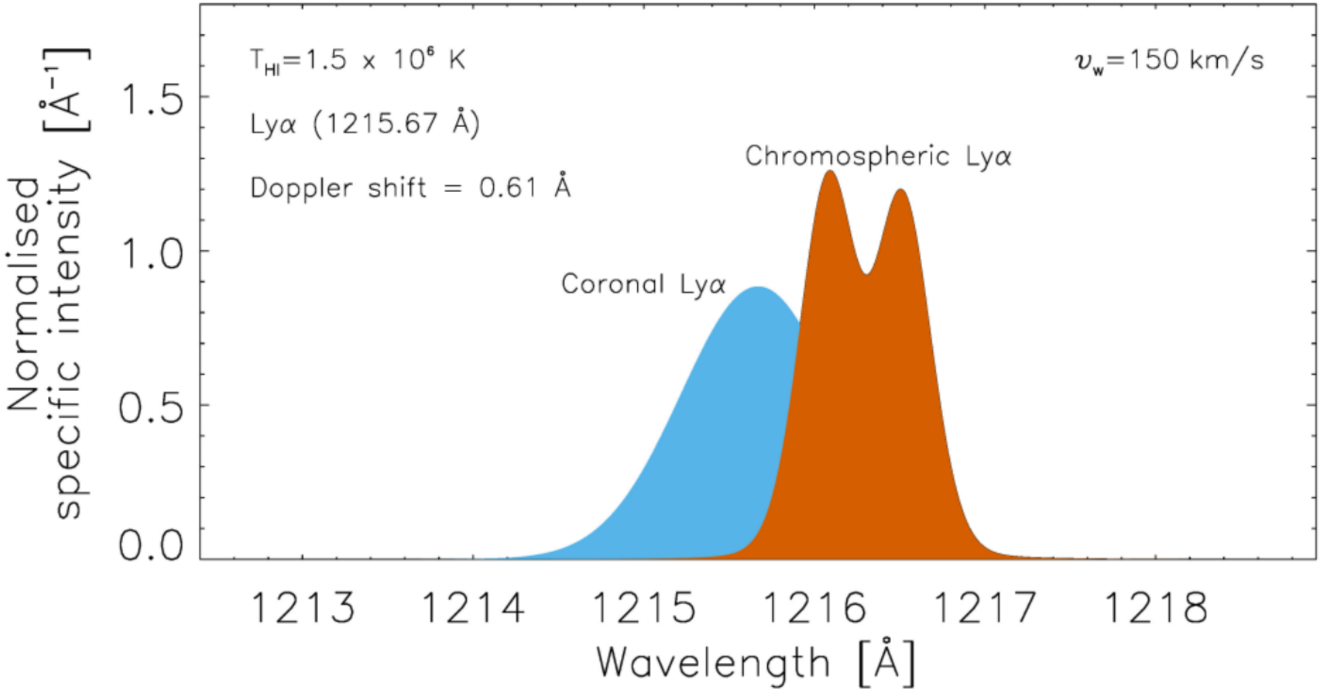

- The scattered intensity depends on the expanding corona velocity: the higher is the outflow velocity, the lower is the scattered coronal intensity.

$$F(\mathbf{n}', v_w, \theta) = \int_{-\infty}^{+\infty} I(\lambda' - \lambda_0 - \delta\lambda, \mathbf{n}')\, \Phi(\lambda' - \lambda_0)\, d\lambda'$$

$$I_{rad} = \frac{0.833\, h\, B_{12}}{4\pi\lambda_0} \int_{-\infty}^{+\infty} n_e\, R_{\mathrm{H\,I}}(T_e)\, dl \int_{\Omega} \frac{11 + 3(\mathbf{n}\cdot\mathbf{n}')^2}{12}\, F(\mathbf{n}', v_w, \theta)\, d\Omega$$

Wind speed diagnostics

Analysis of the first images acquired by Metis in May 2020 using the Doppler dimming technique:

From the comparison *of* **coronal UV HI Lyα** emission **dimmed** due to **coronal expansion** with UV HI Lyα emission for **a static corona** (no dimming) synthesized on the basis of electron density from VL pB **2D maps** of the coronal plasma **wind speed** are generated. (Dolei+ 2018; Dolei+ 2019)

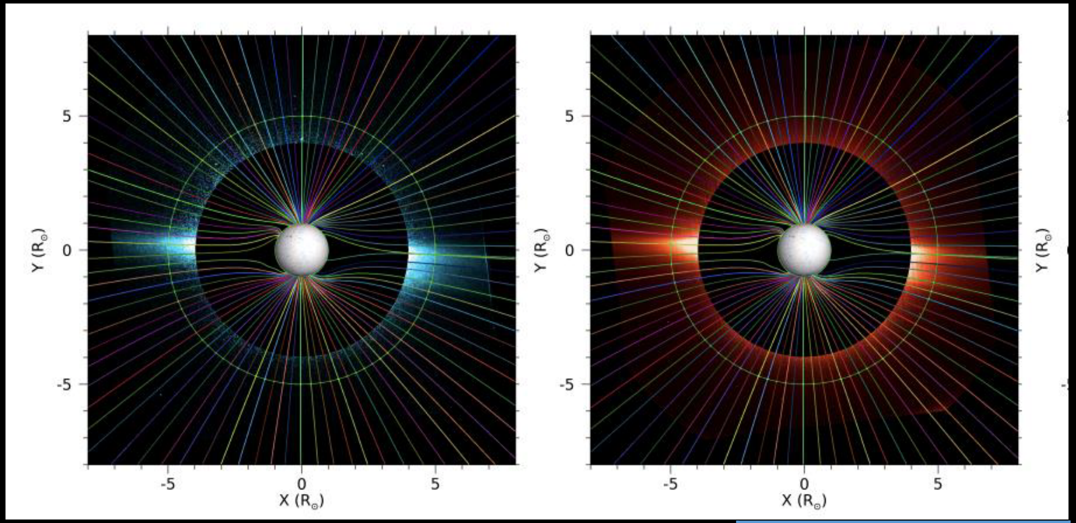

- Identification of a high-density layer centred on the extension of a quiet equatorial streamer -- the coronal origin of the heliospheric current sheet
- The slow wind is found to flow along the axis of the equatorial streamer at ~160 km/s from 4 $R_\odot$ to 6 $R_\odot$
- The wind velocity rapidly increases beyond this layer, marking the transition between slow and fast wind in the corona

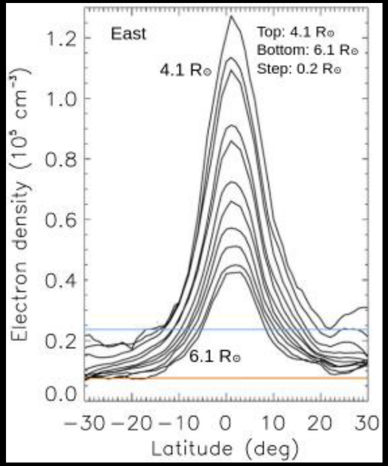

Romoli+ 2021

Antonucci+ 2023

0.64 AU heliodistance
11° heliolongitude
FOV ~ 4-7 $R_\odot$

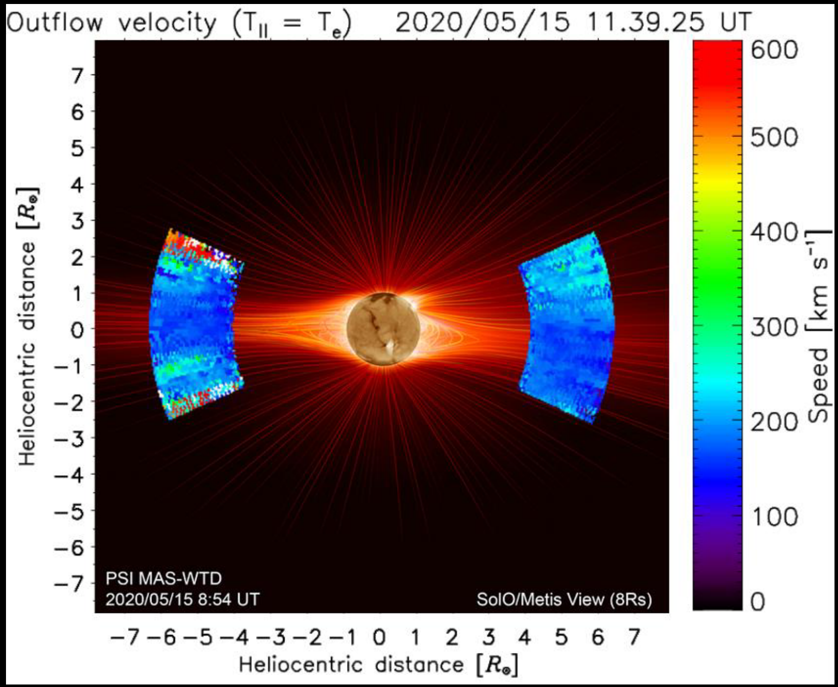

- A first estimate of the polar fast solar wind using Metis data is in Telloni+ 2023

High cadence observations in VL

Metis high cadence observations provide a new window on the dynamics of the solar corona in a range of physical parameters never explored before.

Metis design permits unprecedented observations at high temporal cadence:

- down to 1 s per frame, in single polarization mode (FP)
- down to 20 s per frame in total brightness mode (tB)
- and down to 1 polarized brightness (pB) image per minute

High cadence observations at perihelion take also advantage of the high spatial resolution

Upflows and downflows in a loop region – J-maps

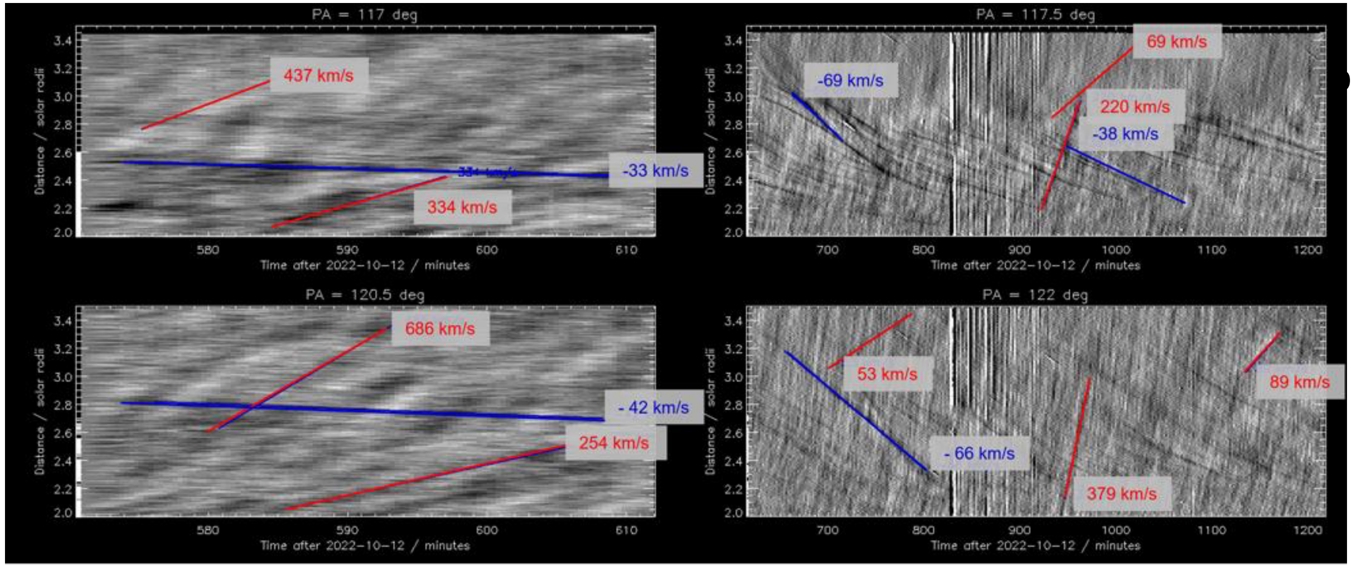

Cadence: 20s

Cadence: 1 min

Abbo+, 2024, in preparation

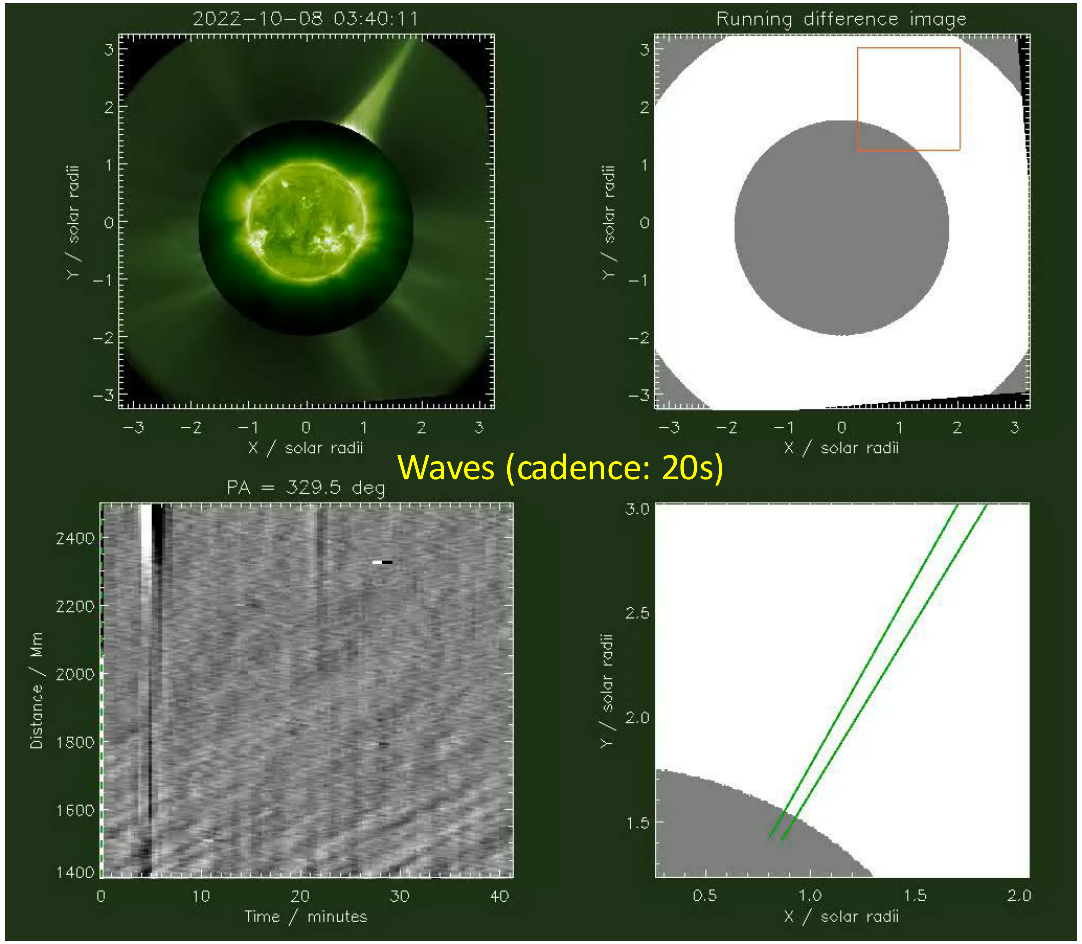

Andretta+ 2025, submitted

High cadence VL observations (< 1 min) open to a new type of coronal investigation

UV and VL extended corona diagnostics

	VL imaging	UV imaging	UV spectroscopy	
			Line intensity	Line profile
Velocity	POS velocity (rising features)	POS velocity (rising features Doppler dimming)	POS velocity (Doppler dimming)	LOS velocity (line shift) Turbulence
Density	Electrons (pB)	Hydrogen Maps	Hydrogen	Hydrogen
Abundance		Elemental Maps (He, Fe, O, etc.)	Elemental (He, Fe, O, etc.)	Elemental (He, Fe, O, etc.)
Temperature			Electron Temp. (line ratio)	Kinetic (H, ions) Electron temp.
Magnetic Field	Morphology		Spectro-polarimetry needed for MagField intensity measurement through Hanle Effect	

Most of the diagnostics requires the knowledge of the electron density

Withbroe et al. (1982), Kohl et al. (2006)

STEREO (Solar TErrestrial RElations Observatory)

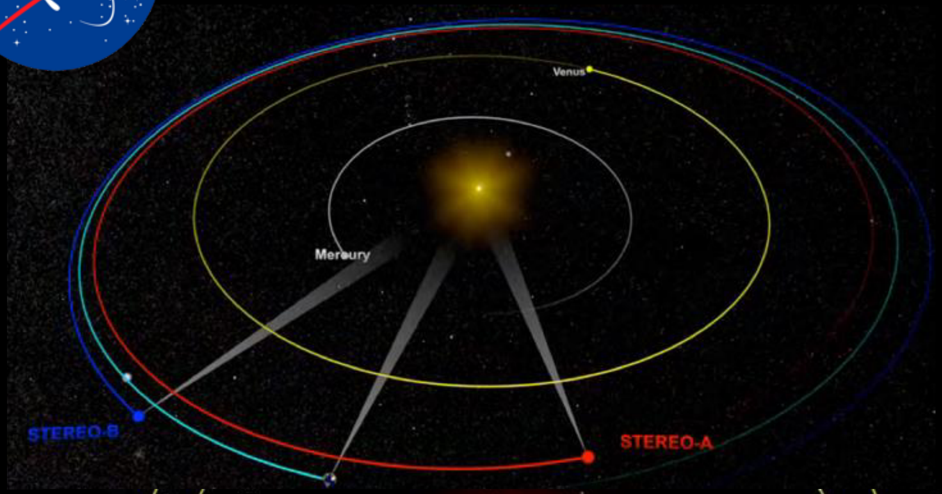

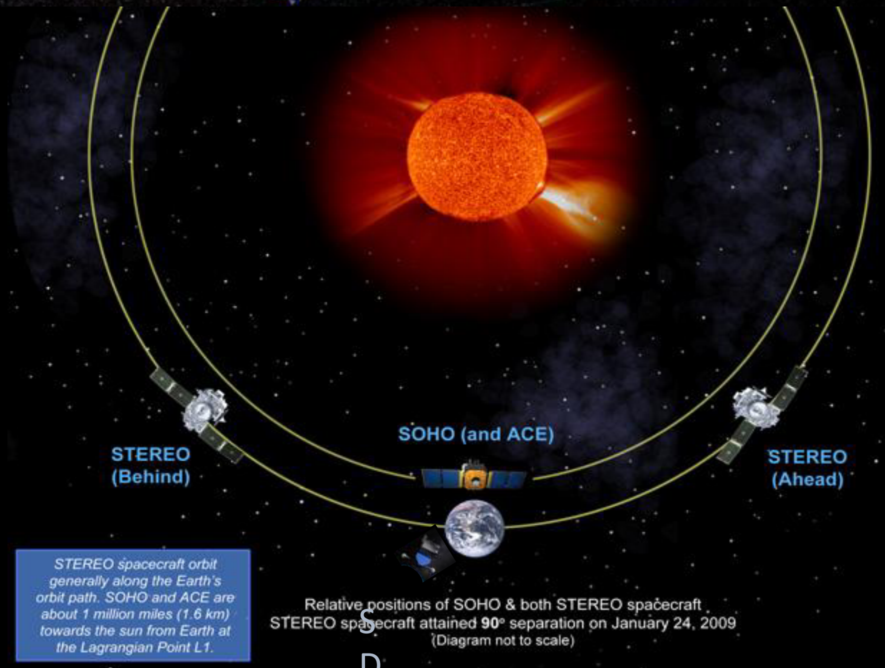

https://stereo.gsfc.nasa.gov/gallery/gallery.shtml

- Launched in October 2006

- STEREO consists of two nearly identical spacecrafts put into slightly different orbits around the sun - one moving faster than Earth (Ahead), one moving more slowly (Behind) - so they each have a different vantage point of the star.

- Payload:
  - SECCHI, coronagraph suite + disk imager
  - In-situ particles and radio waves instruments (IMPACT, PLASTIC, SWAVES)

- The STEREO mission was designed to provide the first-ever stereoscopic measurements of the sun, providing 3D views of the structure and evolution of eruptions on the sun - eruptions such as coronal mass ejections that can disrupt the space environment near Earth and interfere with radio communications and satellite electronics.

- Contact with STEREO-B was lost on October 1, 2014. Recovery attempts lasted until 2018, with no success except for a brief contact in 2016, that did not give time for the rescue.

STEREO Scientific results

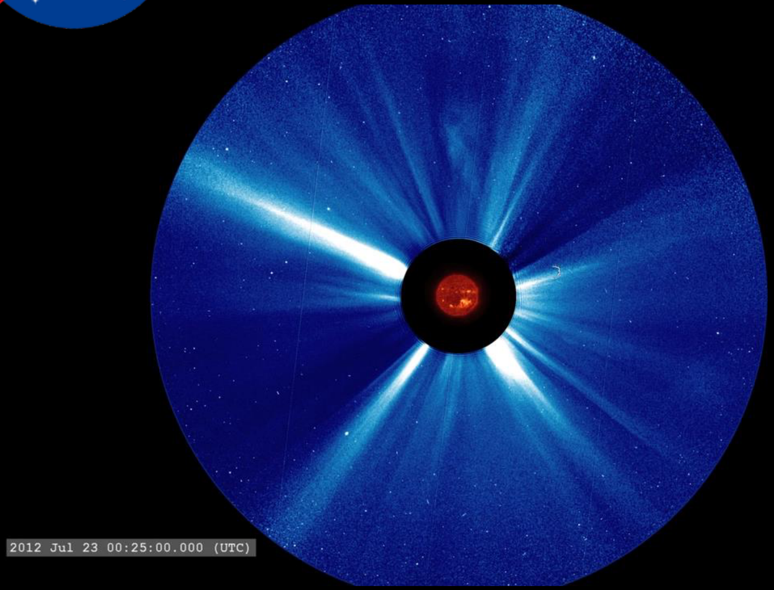

The Carrington-Class CME of July 23,2012

Heliospheric activity from the Sun out to the Earth

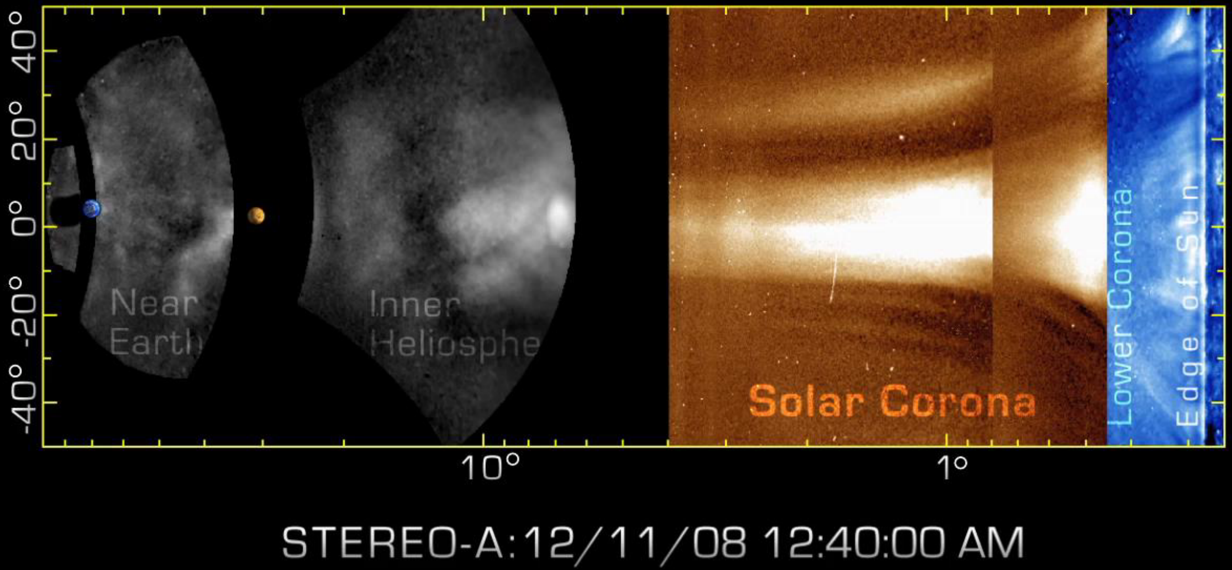

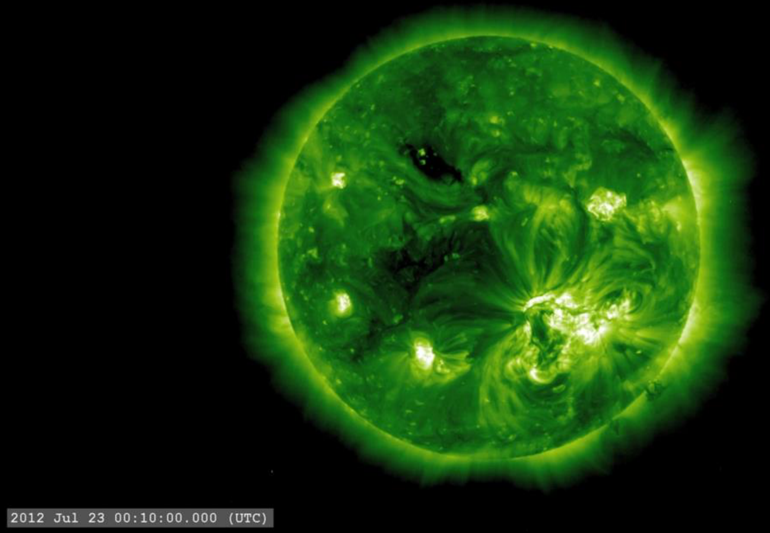

On July 23, 2012, STEREO-A was in the path of the CME of the solar storm of 2012. This CME, if it were to collide with Earth's magnetosphere, is estimated to have caused a geomagnetic storm of similar strength to the Carrington Event

STEREO Scientific results

Fine-scale structures in the outer corona at solar maximum, with deep-exposure campaign data from COR2 coronagraph coupled with postprocessing to further reduce noise and thereby improve effective spatial resolution.

The processed images reveal radial structure with high density contrast at all observable scales. Inferred density varies by an order of magnitude on spatial scales of 50 Mm.

They are inconsistent with a well-defined "Alfvén surface," indicating instead a broad trans-Alfvénic region rather than a simple boundary. We use these structures to track overall flow and acceleration, These results point toward a highly complex outer corona with far more structure and local dynamics than has been apparent.

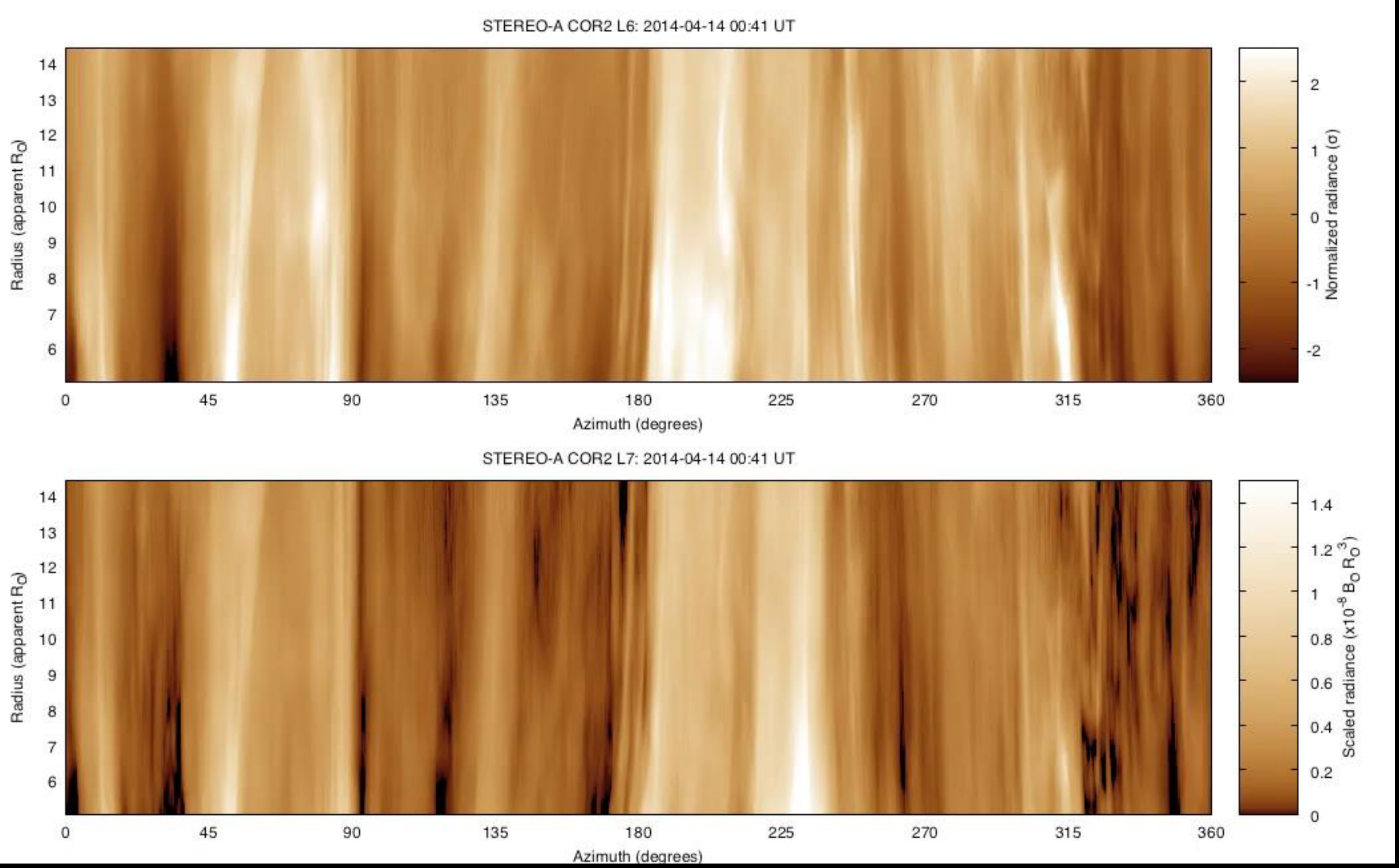

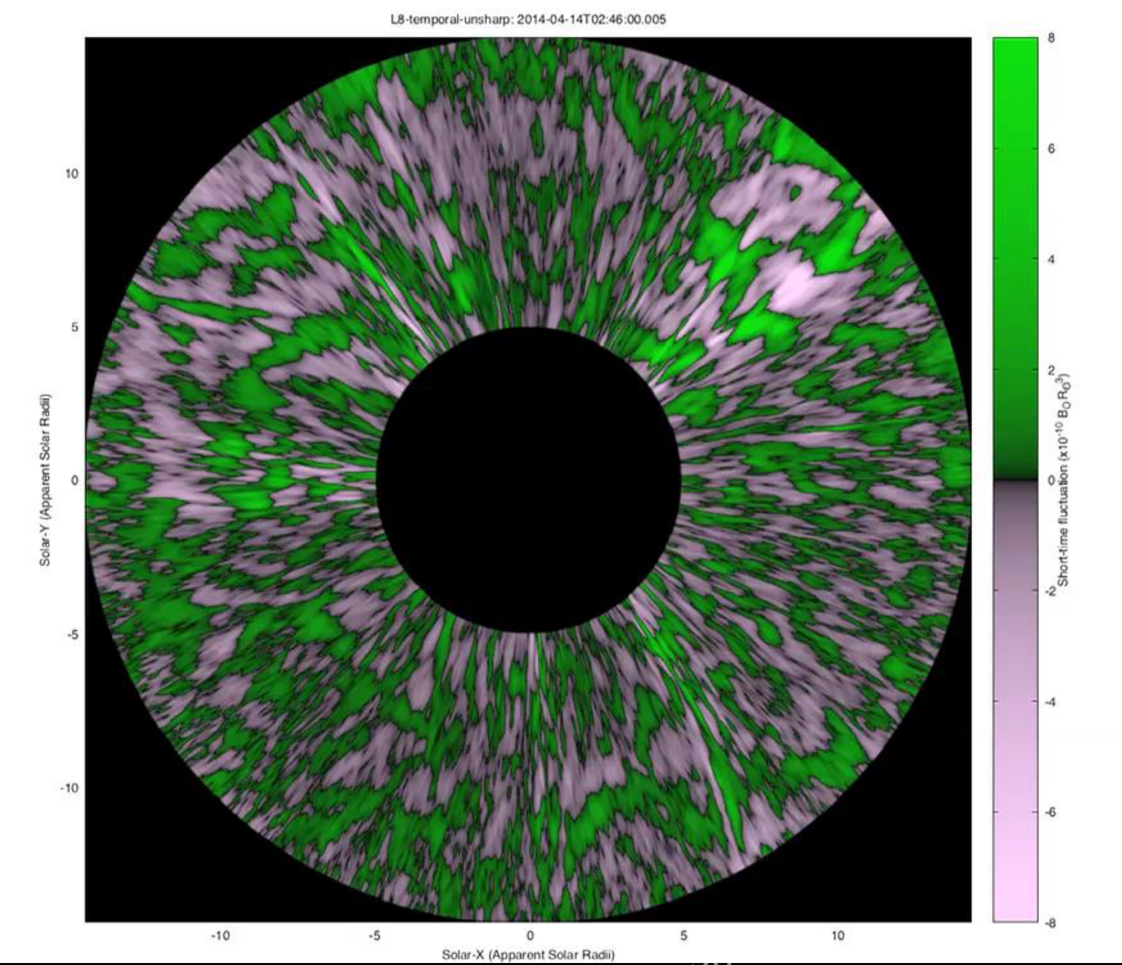

DeForest+, The Highly Structured Outer Solar Corona, ApJ, 2018, DOI: https://doi.org/10.3847/1538-4357/aac8e3

The ASO-S Mission

http://aso-s.pmo.ac.cn/en_index.jsp

- Advanced Space-based Solar Observatory
- Launched on October 9, 2022
- ASO-S has three payloads
  - Full-disk vector Magnetograph (FMG)
  - Lyman-alpha Solar Telescope (LST)
  - Solar Hard X-ray Imager (HXI)
- To
  - Measure the full-disk vector magnetic field
  - Observe the Sun and inner corona in both the Lyα line and WL waveband
  - Image the Sun in HXR (30 – 200 keV)
- Three main top-level scientific objectives
  - Simultaneously, to record non-thermal images of hard X-rays and observe the formation of CMEs to understand the relationships between flares and CMEs
  - Simultaneously, to observe the full disc vector magnetic field, the energy release of solar flares, and the initiation of CMEs, to understand the causality among them.

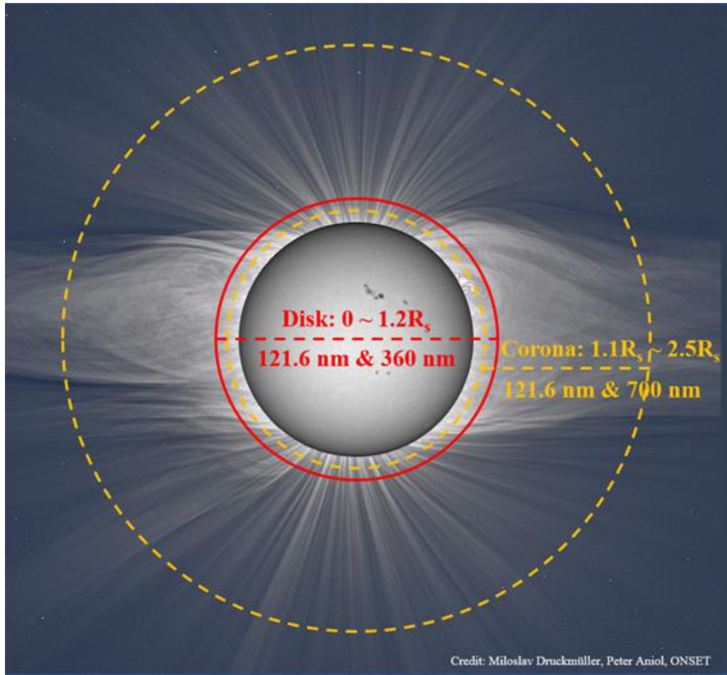

The Aditya-L1 Mission

https://www.isro.gov.in/Aditya_L1-MissionDetails.html

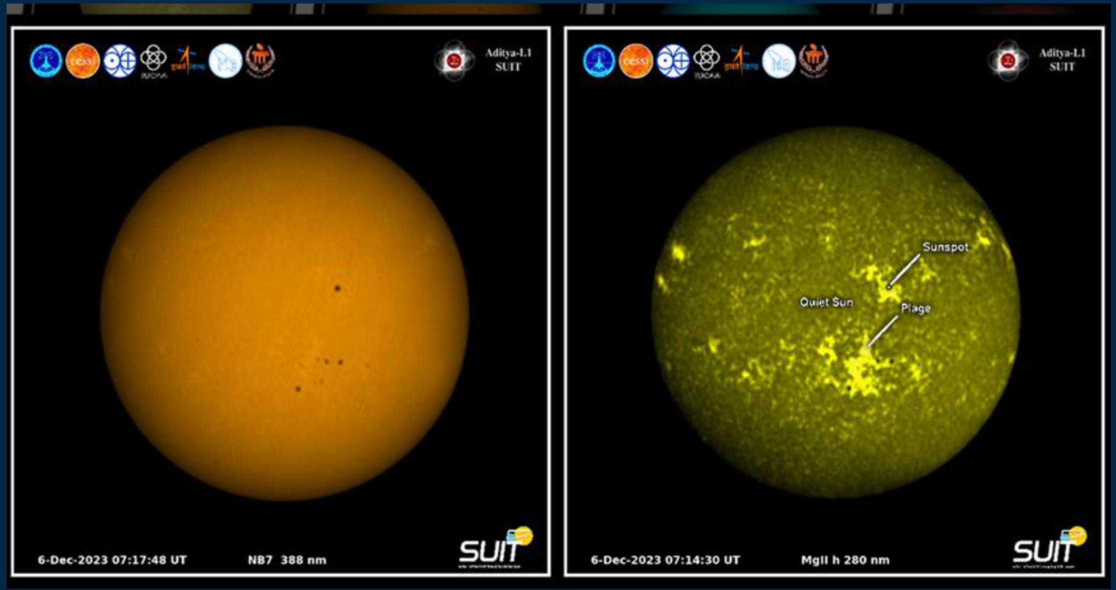

- Aditya-L1 is the first space-based observatory-class Indian solar mission to study the Sun.
- Launched on September 2, 2023, destination: L1
- Aditya-L1 payload
  - Visible Emission Line Coronagraph (VELC)
  - Solar UV Imaging Telescope (SUIT) near UV
  - Solar Low Energy X-ray Spectrometer and High Energy L1 Orbiting X-ray Spectrometer (SoLEXS – HEL1OS)
  - Aditya Solar wind Particle EXperiment and Plasma Analyser Package for Aditya (ASPEX – PAPA)
  - Magnetometer (MAG)

Seetha, Megala, 2018

- Uniqueness of Aditya-L1
  - First-time spatially resolved solar disk in the near UV band
  - CME dynamics close to the solar disk (~from 1.05 solar radius) thereby providing information in the acceleration regime of CME, which is not observed consistently
  - Onboard intelligence to detect CMEs and solar flares for optimised observations and data volume
  - Directional and energy anisotropy of solar wind using multi-direction observations

SOL INVICTUS

INAF
ISTITUTO NAZIONALE
DI ASTROFISICA

proba-3 esa

PROBA-3/ASPIICS Coronagraph

- Objective: Artificial eclipse-like observations of the corona
- Spacecraft: Formation-flying Coronagraph s/c & Occulting s/c
- Instrument: Visible-Light pB & FeXIV & HeI D3
- Corona Physical parameters: Electron density;
- Launch: December 4th, 2024
- Earth Orbit: Period: 20 hrs
  Apogee 60,000 km; Perigee 300 km
- Nominal mission: 2 years

- 5 channels: (1 white light, 4 polarised light, 1 narrow-band filter to be centered at the He I D3 line at 5876 Å).
- 2048x2048 pixels, 2.8 arc sec per pixel
- Outer edge of the field of view: 2.99 $R_\odot$ (4.20 $R_\odot$ in the corners)
- 60 s nominal cadence
- 2 s cadence if only a quarter of the field of view is used.

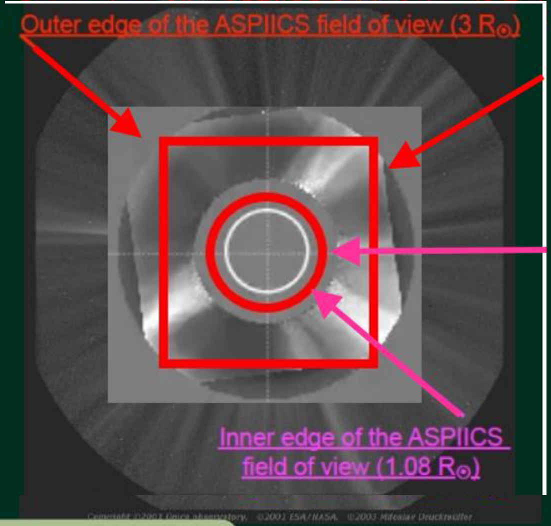

Metis outer edge of the field of view (3 $R_\odot$) with Solar Orbiter at 0.3 AU

Metis inner edge of the field of view (1.8 $R_\odot$) with Solar Orbiter at 0.3 AU

ASPIICS will cover The Gap between typical fields of view of EUV imagers and externally occulted coronagraphs!

Orbit:
HEO
around
the Earth

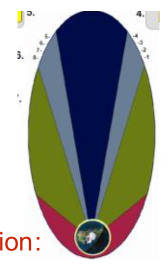

in dark blue:
formation
flying
(6 hours)

orbit duration:
19h 38min

The future

Out-of-Ecliptic science (Solar Orbiter and polar orbiters)

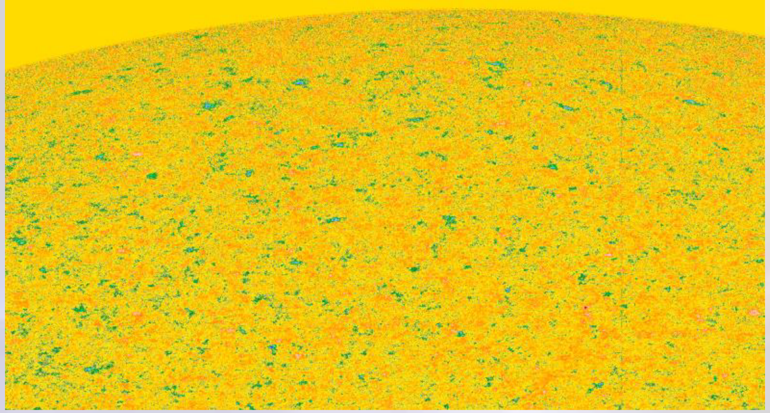

Solar Polar Observatory (CAS)

Space Weather Surveillance

Polarimeter to Unify the Corona and Heliosphere PUNCH

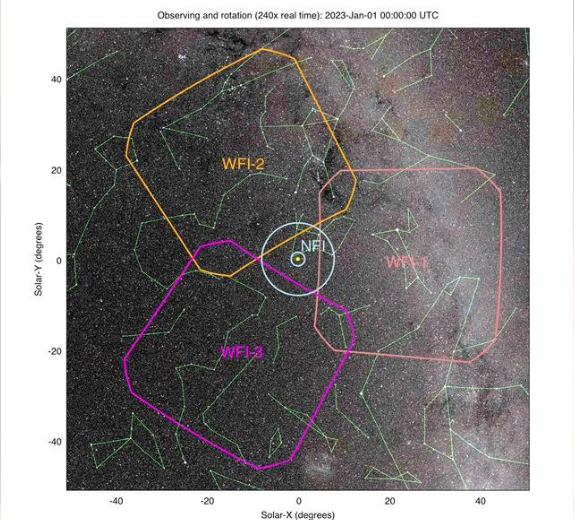

4π view of the Sun

FIREFLY

Solar News: https://solarnews.aas.org/

SPA newsletter: http://lists.igpp.ucla.edu/mailman/listinfo/spa

European Heliophysics community (EHC): https://spaceweather.gfz.de/helio-europe-mailing-list
https://www.heliophysics.eu/

Space Weather and Environment (SWEN): https://swe.ssa.esa.int/es-ES/web/guest/swen-newsletter

European Space Weather and Space Climate Association (E-SWAN): https://eswan.eu/index.php/newsletter

UK Solar Physics newletters: https://uksolphys.org/news/newsletter-archive/

MIST: https://www.mist.ac.uk/community/mist-mailing-list

SCOSTEP: https://scostep.org/